SSD Analyze for the Assessment of Long Term Thermal Effect of Urbanization on the Izmir City's Local Climate Change

OZSEN CORUMLUOGLU (ocorumlu@hotmail.com)
Izmir Katip Celebi University: Izmir Katip Celebi Universitesi https://orcid.org/0000-0002-7876-6589

Research Article

Keywords: Land Surface Temperature, UHI, Time series, Urbanization, Climate Change, LANDSAT

Posted Date: March 29th, 2021

DOI: https://doi.org/10.21203/rs.3.rs-313554/v1

SSD Analyze for The Assessment of Long Term Thermal Effect of Urbanization on The Izmir City's Local Climate Change.

Özşen Çorumluoğlu[*,1]

Abstract

Background: Urbanization provides several opportunities to human being to live better and comfortable life. On the other hand, it also comes with some costs and side effects like worsen climate conditions. In local concept, pre-climate conditions in rural area can be called as natural when they are compared against post-climate conditions after urbanization expands over and swallows these natural areas. So, these natural conditions are changed to worsen conditions by some civic activities in cities through urbanization. One of the urbanization side effects is thermal pollution caused by specific urban activities and patterns on land surfaces in cities. Thus, thermal pollution changes city's local climate and negatively affects the city's comfort level at least locally. There are several researches focusing on that issue in cities. Each one made its contribution to the area to build up a strong knowledge. One great contribution comes from the researches focusing on analyzing time serious thermal data with continuous distribution over cities.
Method: Here in this research is introduced and suggested a Simulated Single Data (SSD) statistical analyze method for the studies based on time serious data. Therefore the method was applied to Remote Sensing (RS) LANDSAT satellites' bands especially to time series' thermal bands of Izmir city to reveal where generally Urban Hot Spots (UHS) appear and Urban Heat Islands (UHI) develop in the city w.r.t. this SSD image from long period of time. Stereo representation of the study region is also used to visually examine the topographical effect on UHI distribution.
Conclusions: The study clearly demonstrated that industrial regions and roads with large surfaces, somehow bare lands even with spare bushes or grassy lands and more significantly the slope urban land parts within special aspects are the main contributors of UHSs and UHI developments in the city even w.r.t. long term data. Thus those contributors affect the city pre-natural climate conditions negatively and then let UHSs to appear and UHIs to develop at and around where these urban land cover structures are located or seen in the city. Those city parts are the most risky zones that city authorities take serious actions for caring their city chronical climate (thermal) conditions and to focus on for returning these zones back to their pre-natural climate environmental conditions. There are also some nature based solutions that are given and suggested in the conclusion section of the paper for compensation of the effects caused by those contributors in the city.

Keywords: Land Surface Temperature, UHI, Time series, Urbanization, Climate Change, LANDSAT

[*] Correspondence: ocorumlu@hotmail.com, ozsen.corumluoglu@ikcu.edu.tr, orcid.org/0000-0002-7876-6589
[1] University of Izmir Katip Celebi, Geomatics Department, Izmir 35620, Turkey.

Introduction

Human have been experiencing drastic urban sprawl especially since the beginning of second half of 20th century (Kii et al., 2017). Currently, almost 5% of global lands has also been converted to urban lands, more than half of the world's population moved into these urbanized areas, and this is expected to reach 66% by 2050 (Lutz et al., 2001; Schneider, 2012). Because human benefits from urbanization by getting better economic status due to economic growth and better life style. On the other hand, drastic urbanization has caused numerous environmental problems such as cropland occupation, urban heat island effects, ecological degradation, and jeopardized ecological and socioeconomic systems (He et al., 2014; Liu and Zhang, 2011). Thus, cities as urbanized areas can be assumed as living organisms invading the earth natural lands, like swallowing those natural lands surrounding urbanized areas previously while they grow and spread around. Thus, uncontrolled urbanization causes a big serious treat over these natural areas through the time sooner or later. Therefore, the development of society and the rapid urbanization together have changed the game by dominating the Earth in several ways, thus the energy balance, infiltration, storm water runoff, precipitation, temperature, air quality, storage carbon and local biodiversity regimes have been changing contrarily to their previous natural conditions especially at the places where the cities locate and grow in a period of time, and this change also contributes the environmental degradation and depreciates the quality of life even in cities (Cheng et al., 2008; Pickett et al., 2011).

Because of such migration rural to urban, urban expansion is often rapid and unplanned, which mostly lead to unwanted results as those mentioned above (Oke, 1997; Zhao and Chen, 2005; Gao, 1996). Furthermore, urbanization mostly ends up with decrease in natural lands especially in developing countries (e.g., decreases seen in green space, open spaces and water bodies). Even if green spaces as most important natural signs and key factors for an urban ecological system fulfil an indispensable mission for cleaning the air, adjusting the microclimate, eliminating noise, beautifying the surroundings and so on. They also support high-quality life style for urban settlers, since green spaces act as "lungs" for cities (Boryan et al., 2011). As mentioned above, uncontrolled urbanization generally leads to the destruction of this natural environment, mainly swallows the green spaces in or around the cities, particularly in developing countries. Urbanization makes environment vulnerable to natural hazards too and even causes channel-bank and road-surface erosion, habitat destruction, landscape degradation and fragmentation, climate change, species extinction as bad as the reduction of net primary productivity (Oke, 1997; Zhao and Chen, 2005; Gao, 1996; Guo, 2015; Kalnay & Cai, 2003).

Collectively, uncontrolled growth of many cities and towns in the world nowadays takes a great national and global attention about energy security, greenhouse gas emissions, environmental changes and major modifications to the natural landscape. Knowing the huge negative effect of uncontrolled urban growth in the world on the natural resources, understanding the extinction of natural environment and ecosystem, and spatial and temporal land cover change as well as the factors affecting these changes are important for rising up sustainable rational economic, social and environmental policies (Coseo & Larsen, 2014; Zhong et al., 2014; El Garouani, 2017).

In fact, cities generally provide some opportunities to their residents by supplying new urban lands to dwell and startup businesses. In most developing and undeveloped countries, cities mainly attract people for these reasons and some other opportunities provided by cities. This rapid move to cities especially after second half of the last century concludes with uncontrolled urban growth mostly in a wildest way. So, this new land provision offered by cities and resulting uncontrolled urban growth mostly ends with harmful effect costing to the same residents as uncomfortable life style and unfortunately in an unsustainable way. However, sustainability measures should be taken as top priorities by city authorities to meet the information society expectations in today's world especially when it comes to cities. One of priorities in terms of sustainability measures for our cities today and in the future is thermal sustainability since cities are the place of several urban activities which rapidly become sources of heat pollution in the world. The effect of heat increase caused by cities can be the source of several and serious problems for the entire world like degradation of local comfort by climate change, drought to sea level rise and etc.

Importance of UHI analyses for cities

One of prominent consequences of Global Warming is rapid increase in temperature at some particular areas in addition to the general increase in the earth. These particular areas mostly are 'Urbanized' or "built up" regions where the most of the land in these regions are covered with buildings and artificial entities. In addition to the urban structures, several reasons like emission of gases from vehicles and industries, high population density, less green patches, heavy machineries have caused to originate higher temperature sites called "Urban Heat Islands (UHI)" (Kim, 1992). According to the United State Environmental Protection Agency (US EPA), the term of "Heat Island" describes "built up areas that are hotter than nearby rural areas and the annual mean air temperature of a city with 1 million people or more can be 1.8-5.4°F (1-3°C) warmer than its surroundings" (Liu and Zhang, 2011).

The intensive civilian immigration from rural to urban areas especially during the second half of the last century due to the industrialization especially in developing countries can be shown as the most important reason for the development of UHIs in our cities today. Since this movement causes a rapid and unplanned urban growth in cities almost all around the world, this process then ends up with a cost as a reduction of vegetated areas and invasion of impervious built-up surfaces at where cities are located in the world. Thus, our natural environments at those parts of the Earth are transformed into solid concrete blocks or impervious surfaces. On the other hand, this transformation in cities causes a significant negative effect on city local weather and climate too (Landsberg, 1981). One of the most familiar effects of this transformation is the urban heat island developments in cities (Streutker, 2002), which is the direct representation of environmental degradation (Lu et al., 2009).

The concept of urban heat island was first described by Luke Howard in 1833 (Howard, 1833; Kim, 1992). Since then, UHI researchers payed more attention (Liu and Zhang, 2011; Detwiller, 1970; Gartland, 2008) and it is studied by so many researchers (Detwiller, 1970; Fukui, 1970; Camilloni and Barros, 1997). Recently, due to the uncontrolled growth of cities with the developing society and corresponding accelerated urbanization, the urban heat island has become more and more significant issue and has had severe impact on different urban parts and on the comfort conditions of some urban environments especially for city residents (Chen et al., 2009). There are also several other studies carried out to investigate the impacts of UHIs in cities (Yan et al., 2012; Choi et al., 2012).

These previous studies clearly demonstrated that rapid urban growth concludes with the decrease in the vegetated areas, the increase of the surface temperature and hence changes the urban microclimate. Actually, one of the significant impact of an urbanization process due to specific city activities which cause local temperature increase and then consequently negative changes in the local climate is the emerge of urban head spots (UHSs) and then the formation of urban heat islands (UHIs), which furtherly deteriorates life style and quality of city inhabitants and energy consumption and then impacts urban planning (Chen et al., 2016; Streutker, 2002; Chen et al., 2009). Therefore, changing and increasing recent requirements of society and accelerated urbanization processes nowadays, make the urban heat island more and more significant issue for cities and it has had a severe and contra impact on developed urban areas and city residents' living environments (Chen et al., 2009).

Urban heat spot and urban head island analyses fundamentally depend on determination of Land Surface Temperature (LST) values. Thus, urban LST data analyze has become a useful indicator of the ecological environment and climatic conditions over different spatiotemporal concern for cities (Reza et al., 2009; Kuang et al., 2013). Land surface temperature therefore takes an active role in many environmental analyses by providing important information for the surface physical properties and regional climate (Weng, 2001). A scientific analyze on urban land expansion is a must for integrative urban planning and regional sustainability and mitigating climate change effect (Kalnay & Cai, 2003; Guo, 2015; Tozer, 2018). Therefore, LST analyses become an important issue for today's cities to deal with thermal pollution and carrying our cities to sustainable and resilience levels.

As emphasized above, urban lands which are generally covered by impervious surfaces transferred from pre-natural lands cause serious problems, such as heat islands, waterlogging and photo-chemical smog in cities. Many remote-sensing researchers have been studying with LST to reveal these negative effects of built-up lands transferred from natural environment (Nie et al., 2016; Mustafa et al., 2019). Remote Sensing (RS) is one of the most promising techniques providing spatiotemporal image based earth observation data (Lu et al., 2014). Along with Geographical Information Systems (GIS), remote sensing helps widely to the studies focusing on for example urbanization by providing urban land coverage even for entire cities and quantification of urban sprawl and also urbanization side effects like emerge of UHSs and formation of UHIs (Almazroui et al., 2017; Sun et al., 2015; Son et al., 2018; Dadras et al., 2014; Zhao et al. 2020).

Urban heat island can be observed when the surface heat fluxes at the urbanized sites are monitored through mapping the land surface temperature (LST) distribution spatially (Dousset and Gourmelon, 2003; Sun et al., 2010). Mapping the spatial distribution of LST in a city is the most fundamental process for the determination of urban heat island distribution having a great negative impact on cities' local climate. Without mapping LST distribution by the help of geospatial technologies there will be no chance to perform UHI analyzes for today's cities especially where information societies nested and whose residents desperately need their cities to be governed smartly and sustainably in every possible ways since UHI data gathering and analyzes and UHI mitigation, all become a part of today's smart city concept. If city authorities decide about transferring their cities to smart one, in addition to other issues, they should also consider mapping UHI distribution even in timely manner by gathering appropriate and periodic data and setting up an analyzing environment. This must also help to construct a strong, reliable and sustainable decision support system to meet their smart cities' requirements at high levels.

Since thermal conditions in a city are time depended, timely analyses of land surface temperature distribution in cities become an important issue in terms of cities' local climate sustainability under the threat of thermal conditions. Therefore, this study focuses on spatio-temporal analyses of local climate formation driven by

thermal conditions in a city (here is Izmir) by the help of remote sensing (RS) data, so LANDSAT 5 and 8 time series images.

UHI development and its relation with urbanized lands

Evapotranspiration is the process which water is transferred to the atmosphere by evaporation process from soil and water and by transpiration from plants (Kalma et al., 2008; Zhang et al., 2016b). Therefore, it is also a natural cooling process that decreases the surface temperature naturally (Santamouris et al., 2019; Miralles et al., 2011).

As it is mentioned above, transformed land surfaces in cities mostly are impervious, which causes rain water runoff greater than natural surface in rural areas (Xiao et al., 2007; Tang and Xu, 2016). Less vegetation cover and high rated runoff on impermeable surfaces cause reduce the soil moisture, shading and the rate of evapotranspiration in urban areas since these impervious urban surfaces are not capable of capturing and trapping enough water to increase evaporation to cool down and reduce temperature of these surfaces (Sun et al., 2016). Because replacement of natural land surfaces with impermeable surfaces (built surfaces) reduces the vegetation and moisture-trapped soils which use a relatively large proportion of the absorbed radiation during the evapotranspiration process and release water vapors that contribute to cool the surrounding air (Mohammad et al., 2019). Therefore temperature of these surfaces accumulates in time and rich to high levels especially during the long hot summer daytimes. Then this process contributes UHIs to develop at certain regions in cities. In short, the cooling down process of a land surface needs evaporation (Dong et al., 2019). It even means that the water or moisture content of the land and land cover in a certain extent regardless of land cover type is the main issue for cooling down process of the land (Anderson, 2012). In other words, if a land covers having some water in its content (like plants) or holds some water as capillary process (like soil), temperature of the land is transferred to that water content. This also means that the surface transfers and releases its temperature by using its water content through evapotranspiration or transpiration and this process cools down that land part itself. Land parts with soil and vegetation covers in cities are capable of holding water in their contents in some extent but not impervious surfaces because of runoff. Therefore more heat energy enters into air in urban area with impervious surfaces and makes the temperature rise rapidly and also increases the local warming and then worsens the local climate and comfort level at that part of the city (Nie et al., 2016). All those closely located and locally warmed areas contribute each other and then accumulate local heat, finally cause to develop UHIs in cities and in general similar processes in different cities then contribute the global warming in the world like butterfly effect.

Except trees and water bodies and soil lands even with very few bushes and urban lands with grass cover which are capable of water infiltration, the other land use/land cover types in cities are generally built-up (shelters, residential, commercial, administrative and industrial building areas with single, double, triple or multi-storey) and open areas (like paved areas) and even barren lands, so those areas in cities are impervious areas as mentioned above and they occupies cumulatively a largest portion of a city especially in developing countries. This improper urban growth issue in developing countries causes loss of forest lands and trees by replacing natural vegetation sites with urbanized lands and proceeds with significant increase in impervious urban lands and consequently with an increase in the surface radiant temperature (Kumar et al., 2012). While such an urban growth happens, most of the natural areas like forest fields are transferred to urban areas with several types of city built-up materials such as concrete, stone and most importantly metal and asphalt which significantly contribute UHI developments at where these types of urbanized lands are in cities. This land cover change causes those areas absorb more heat than when they intertwined with the nature. So, the increase in the land surfaces covered by artificial material with high heat capacity, and then the increase in these permeable surfaces which they can absorb heat during daylight time much more than the previous cases and heat release during cooling processes even with high energy consumption in such urban area cause UHIs to develop at these city parts and to severely affect the surrounding areas (Takeuchi et al., 2010). Due to different land use/land cover composition, slight variation in the mean temperature distribution is normally expected which it is also experienced here in this research as well (Fig. 6, 7 and 9).

The urban heat island (UHI) phenomenon has been becoming more or less an important issue for most of the cities throughout the world especially in developing countries and then in terms of global warming and consequently even for global climate change. As it is mentioned by Shahmohamadi et al. (2011) they are the city regions under the threat of temperature accumulating in the way discussed as in the previous paragraph and therefore they are the city parts which are hotter than the rural or natural areas surrounding the city. In other words, an urban heat island is a metropolitan area which is significantly warmer than its surrounding rural areas; thus, the higher urbanization leads to more distinct urban heat islands with huge temperature differences between urban and rural areas and even between these UHI sites and the cool sites in cities. So, urban heat island appears as higher temperatures areas in cities, in comparison to temperatures of suburban and rural areas, which means the higher the urbanization level the more prominent the UHI process (Pickett et al., 2011; Santamouris, 2013). Thus, one of the negative affects appearing as UHSs and UHI developments over cities is because of significant

decrease in the ; natural areas where they turn into impervious built-up urban sites. These previous natural city areas which recently turned into built areas now start to absorb incoming radiation from the sun much more than their previous natural cases and then they re-radiate it back into the surrounding environment and consequently this process causes UHIs to build up in cities (Solecki et al., 2004; Gartland, 2008). Is short, buildings, concrete, asphalt and industrial structures are generally the most responsible urbanization materials and the transformations from natural to build up surfaces causing urban heat island developments in cities (Amir et al., 2020; Mohajerani et al., 2017). This is actually because of that these built surfaces tend to absorb a significant proportion of incident radiation, which is later released as heat and these city construction materials including concrete, brick, tar and asphalt cause higher absorption of solar radiation and low albedo (low reflection) due to difference of thermal properties (Mohajerani et al., 2017; Ji Zhou et al., 2010). These urban materials have also high heat capacity and they retain heat and slowly release at night. As well as those materials, anthropogenic heat which is released by industrial activities, vehicle traffic, power plants, air conditioners, and as heat waste in urban areas is also other key factors causing UHSs to appear and then UHIs to develop (Shahmohamadi et al., 2011; Coseo & Larsen, 2014). This additional heat causes the increase of temperature especially even in night time at that land parts in cities if there is no cooling precautions in these city parts (Ayanlade, 2016; Bala et al., 2020).

Air pollution and greenhouse gas emissions also cause to increase the temperature in urban areas (Shahmohamadi et al., 2011). Main polluters are generally industrial activities taken place in cities' industrial zones. It is obvious that air pollutants, particularly aerosols released after some industrial activities are seen as abundant amount in that over polluted urban areas (Wei et al., 2017; Lim et al., 2009). These polluted air including aerosols and greenhouse gases absorb the large proportion of re-radiated long wave (infrared) radiation and inhibit the corresponding radiative surface cooling producing a pseudo-greenhouse effect, which is also another process that is responsible for urban heat island to develop (Chen et al., 2020; Zoran M. and Zoran L., 2005).

Urban geometry is also other one of key factors for forming UHIs which represent the building structures and space among the buildings in cities (Li et al., 2020). The lack of urban spaces for city extension in developing countries increases the public demand for denser constructions; this requirement transforms them into vertical cities. The intense urbanization with dense building coverage and narrow streets and without green spaces results in high urban heat island effect in the cities (Shafaghat et al., 2016; Mohammed and Salman, 2018). The temperature variations may be linked with greater temperature absorbance by man-made materials and denser building pattern which creates a blockage to air-flow in narrow streets like steep valleys between tall buildings and trapped air with accumulated temperature in these urban valleys and then these sites appear as UHI development sites in cities (Gunawardena et al., 2017).

UHS, UHI, LST in terms of Local Climate

Takeuchi (Takeuchi et al., 2010) in their study emphasized that currently more green spaces, forest and unused lands have been converted into commercial and business centers, government offices, residential areas and public amenities. This conversion contributes UHI phenomena to develop in these urbanized lands transformed from natural or bare fields. Therefore it is useful to know UHI distribution in cities to protect these lands from heat pollution due to urbanization causing local climate change. This information will be very helpful for city administrators who like to govern their cities sustainably (Zurina and Hukil, 2012).

UHSs

There is also a special urban thermal feature which is called as urban hot spot (UHS) appearing at some city zones with certain urban activities, like industrial activities (Corumluoglu et al., 2015). So, these UHS locations are the city spots under an extreme heat stress mainly seen at where anthropogenic activities are in cities (Chen et al., 2006; Ren et al., 2016). The places where anthropogenic heat releases from vehicles, air conditioners, industrial and other urban activities and from other heat sources in cities like power plants and even from city parts experiencing removal of vegetation cover in great extent and then increase in impervious surfaces happen are the main suspicious urban parts where UHSs probably appear and contribute the UHI formation (Memon et al., 2008; Du et al., 2016a; Senanayake et al., 2013). UHI development is also a matter of time especially during long and hot summer seasons (Chen et al., 2002). Therefore, it is highly important to make timely analyses on urban heat island distribution in cities for providing an information base to city authorities to make them to produce sustainably affective solutions for their cities' futures in terms of cities heat problems. Only in this way, they would have a chance to make successful decisions for their city plans in a sustainable way, for the future of their cities and to protect their cities' natural environments where city residents live and like to live (Liu and Zhang, 2011).

UHI development

City regions developed as rapid, dense and uncontrolled vertical urbanization sites which minimize vegetated areas by transferring these fields into the built-up surfaces, urban canyons with several floor buildings appearing as street valleys between these dense and vertical buildings on both sites of these problematic city streets cause the reflected radiance to scatter between the buildings and contribute the warming (Giannopoulou et al., 2010). During a day time, solar energy is trapped due to these multiple reflections between the buildings which create mentioned urban canyons. Thus, the incoming solar radiation heats up such buildup areas in cities during daylight times of an entire day especially in summer seasons and then some amount of this absorbed energy by the buildings and impervious surface materials in the urban canyon streets are regenerated and radiated back as heat energy especially at nights by these same buildings and materials in the street (Senanayake et al., 2013; Solecki et al., 2004; Nie et al., 2016). Therefore rough, intricate and complex structure of urban valleys is another problem of urban areas, which reduces the convective heat removal and transfers it by wind (Williams and Davis, 2007). According to the studies on that issue, it became a well-known and well documented fact that urbanization progress has a significant effect on local weather and climate (Landsberg, 1981). Then urban heat island becomes one of most familiar reason causing local weather and climate change in urban areas (Streutker, 2002). Therefore, it directly depends on degradation of natural environmental (Lu et al., 2009). As it is given above, an urban heat island is a metropolitan area which is significantly warmer than natural lands surrounding these urbanized regions in a city; thus the higher urbanization leads to more distinct urban heat island development with extensive temperature differences between urban and these untouched lands (Koomen and Diogo, 2017).

LST

Surface temperature is an important issue and theme in earth sciences for studying urban climatology, global environmental change and human-environment interactions. Furthermore, land surface temperature (LST) is driven by a complicated landscape composition and configuration (Asgarian et al., 2015; Zhou et al., 2014). From UHI point of view, urban heat islands mainly appear as spatial distribution of accumulated heat at the locations having higher LST values w.r.t the LST values at surrounding land parts and it is governed by surface heat fluxes obviously affected by dense and certain urbanization structures (Dousset and Gourmelon, 2003; Sun et al., 2010). As it is emphasized earlier, the built-up areas and bare lands directly affect UHI development, whereas green spaces and water bodies reduce the UHI intensity (Amiri et al., 2009; Song et al., 2014).

LST values in urbanized areas of a city differ during day, night and seasonal periods. The larger LST changes are usually seen at night but not that large change in day time (Ayanlade, 2016). On the other hand, heat in high magnitudes caused by some urban structures seen in city lands with specific land cover types in day times may cause large UHI developments especially during summer seasons in moderate climate zones (Majkowska et al., 2017). Heat island affect is usually strongest during the summer times in the mid latitude cities as it is experienced in Izmir (Corumluoglu et al., 2015). Some researchers showed that natural and anthropogenic activities in urban areas simultaneously cause oppositely particular LST patterns (Chaudhuri and Kumar, 2020; Zhao et al., 2020; Shafaghat et al., 2016; Du et al., 2016b). With consistent urban development, the UHI zones may worsen the eco-environmental quality and fall under worst ecological level too (Li et al., 2020).

In the climate change studies, it is important to determine the changes in LST values at specific city land parts during a period of time (Zhao et al., 2021). Identification of LST changes at regional levels in time is one of the main requirements to analyze the local climate changes (Tan et al., 2020). LST is one of the most important environmental parameters and is used for determination of energy exchange between the surface of the earth and the lower layer of the atmosphere and this energy exchange is the most dominant factor controlling the local climate and its changes in time (Jia G. et al., 2020). So, timely monitoring task of LST distribution over a city and then the change analyses region by region will let to reveal the suspected local climate change in the city (Mohan, 2000).

As they are mentioned previously, here can also be summarized as those; types of buildup and impervious areas like buildings, concrete, asphalt structures and some specific urban activity areas (like those areas where industrial activities are) in cities are the main causes of urban heat islands developments which effect the wide areas in the city and then change the local climate at these city parts (Gartland, 2008). Transformation of natural lands into pavements, buildings and other urban infrastructures even decreases natural cooling in cities (Tsoka et al., 2020). Also, regional city building structure and pattern with multi-storey adjoining buildings and with narrow streets can heat the air trapped between those buildings and also reduce airflow as mentioned above (Ujang et al., 2018; Kleerekoper et al., 2012). In addition to those above, heat released from vehicles, factories and air conditioners warm up the surrounding city parts, further these additive effects especially at the UHI suspicious urban parts are responsible for the heat island effect to develop severely (Kershaw, 2017). Urban heat island can also represent an impact on local weather and climate by altering local wind patterns, spurring the development of clouds and fog, increasing the number of lightning events, and influencing the rates of precipitation (Liu and Zhang, 2011). Furthermore, the poor air quality that results from the increased energy

usage for cooling in heat-island city parts can cause discomfort for residents and affect health, aggravating asthma and promoting other respiratory illnesses (Liu and Zhang, 2011; Lin et al., 2010). Thus, one of the major problems faced especially in developing countries that is generally ignored is the UHI formation in the cities under the current conditions seen in these countries and we must straggle all together with this problem without considering whether it is in micro or macro scales (Filho et al., 2018). UHI impact on cities then became globally considerable (Chen et al., 2014; Peng et al., 2016). The impact of the heat island also appears in many ways such as increase in energy consumption, management of storm water run-off, environmental disturbance, community health, and altering climatic conditions in cities (Zhao and Chen, 2005). Conclusively, it can be suggested that UHI development in cities is a multi-criteria issue (Sangiorgio et al., 2020). Therefore, multi-criteria analyses must be accounted for every aspect representing impact on UHI (Putra et al., 2019). The digital database which is capable of UHI multi-criteria analyzes is the most promising strategy that can work sufficiently and successfully for building up a sustainable future for our cities which are currently under severe UHI pressure and in fact, this strategy allows them to have a reasonable climate while responding to the needs of the smart city and information society as well.

It is very important to conduct an urban heat island analysis and also evaluating its impact on urban environment to prevent our cities from heat pollution (Ahmad and Goparaju, 2016). Thus, this analyzes and related processes must find an important place in city planning projects to build up livable, sustainable and resilient cities supported with natural environments for our city residents and for our future generations.

There are also several studies for investigating UHI impact on urban environment, climate and weather and for mitigation strategies to minimize the UHI adverse effects (Yan et al., 2012, Choi et al., 2012; Gago et al., 2013; Shahmohamadi et al., 2009) which are going to be mentioned in the further sections.

How to control high LSTs and UHI developments in cities

Determination of LST distribution and consequently identification of UHSs and UHI developments become one of important tasks of today's city authorities who want to sustainably manage their city local climate and its change especially during hot summer times (Guha et al., 2017). Thus, they will have a chance to maintain their cities' urban ecology and local climate by ensuring their cities' thermal sustainability and also taking the precautions on high thermal conditions seriously at where they occur. Probably, those regions will be the UHI development areas in the cities.

For compensating the negative effect of high thermal conditions and maintaining the thermal stability in cities, it is quite important which the city authorities should pay attention to the fact that the vegetation and water bodies represent relatively lower LST than those at city build-up areas (Guha and Govil, 2021; Gupta et al., 2019).They affirmatively retrieve the thermal conditions of the neighboring city parts even if they are build-up areas. Since the existence of the vegetated sites in a city lowers the temperature as they enhance the evapotranspiration by maintaining the heat flux, these regions act as heat sinks for the cities (Joshi et al., 2012).

An urban heat island (UHI) accumulates in time and one of the most common negative impacts of UHI developments is experienced in the unconsciously urbanized city sections in the world (Lee, et al., 2020). The planning of urban green areas (e.g., creation of parks, urban forest lands and afforestation of streets with long, wide and dense trees) are one of the most crucial parts of today's city development plans approved by authorities and assigned to city services even it greatly helps to reduce and to compensate UHI effects where they appear in cities (Huang et al., 2018). This section of the plans must include first the determination and positioning of UHSs and then timely UHI development areas for mitigating and straggling with their effects in cities effectively by taking proper course of actions for example tree plantation (with tall and dense tree pattern and with large canopy cover) at the correct locations, so at exactly where UHSs and UHI developments happen in the city of interest and even taking into account the extent of the UHIs as well.

Even if urban forestry is widely recognized and practiced in developed countries and also it is less known in developing countries, it also offers a nature based solutions to city authorities for tussling with and mitigating UHI effect in cities under high thermal pollution risk (Buyadi et al., 2013). The temperature of urban parks is found to be 1–2 ◦C, and sometimes even 5–7 ◦C cooler than surrounding urban areas according to Vidrih and Medved work (Vidrih and Medved, 2013) (Fig. 6c and 7). Trees and vegetation in cities therefore play a vital role to mitigate the UHI effects especially by regulating high temperature in densely urbanized areas and their surroundings city parts (Gillner et al., 2015). Thus, such actions with natural solutions are integral parts of struggling with UHIs (Brown et al., 2018) that shouldn't be overlooked since they ensure a sustainable urban development and enhance the quality of citizens' life and the environment conditions where the city inhabitants live (Riffat et al., 2016). However, rapid urbanization as mentioned earlier has altered the cities' local climate by increasing heat pollution of land surface and air consequently in cities (Ren, 2015). Since the development of city infrastructures and buildings which increased the impervious surfaces in the cities have left very little space for the development of greenery too (Buyadi et al., 2014).

The current strategies to minimize the UHI effects in cities in the world are urban greening, the use of high-albedo building material, the use of suitable pavement material and proper distribution of urban buildings and

structures (O'Malley et al., 2014; Gago et al., 2013). Urban greening strategy as being a unique nature based and sustainable solution among those above solutions helps to keep the local temperature lower at the city sites where this solution applied and at the surroundings sites than the developed impervious sites with no vegetation (Choi et al., 2012; Rehan, 2016).

Another important issue that needs more attention when greening strategy is being taken into consideration is the maturity of trees (Rehan, 2016; Livesley et al., 2016). It is considered as a vital parameter to ensure lower temperature in urban areas through shadow and evapotranspiration (Georgi and Zafiriadis, 2006; Qiu et al., 2013). That should also be kept in mind that trees are more effective for cooling their surrounding areas than the parks which are mostly covered with grassy surfaces (Lin, B., and Lin, Y., 2010). The tree planted (urban forest) areas can create a cooling effect that extends few hundred meters into the surrounding areas especially during the daytimes in summer seasons even if they are impervious urban areas (Oliveira et al., 2011). Trees and vegetation do not only reduce the UHI effect but also they help to solve some other urbanization problems experienced in cities as they provide nature based solutions. So, they can even help to reduce the adverse effects of air quality and noise level in the surrounding areas (Fang and Ling, 2005). The cooling effect intensity is mainly due to the compactness of green spaces (not the solely grassy lands or park in cities) and tallness (maturity) of trees not the extend of them especially when they are discretely distributed (Gago et al., 2013). So, city parts or parks covered with solely grass or mixed with soil do not work well for reducing the surface temperature as good as tree covered areas (Rajabi et al., 2014). Depending on tree types, maturity and the density, such sites represent a proportionally more cooling effect and a reduction in surface temperature at these sites of urban areas (Barbierato et al., 2019; Yu et al., 2020).

In short, the highest temperature values are seen in residential parts of cities at where impervious surfaces are proportionally high and contrary to that, lowest land surface temperature values are then found in the city lands where water bodies are and in the areas vegetated with trees, especially in the city parts where dense and long trees are (Yu et al., 2020). It is clear that water bodies and trees or city forests or city parks with dense and long trees with large canopy coverage contribute to lowering the surface radiant temperature at where they are planted and at their surrounding area in some extent. In short, the vegetation growth areas like urban forested areas and urban parks especially with high-density mature and long trees clearly contribute the decrease in temperature within and surrounding areas (Barbierato et al., 2019; Yu et al., 2020).

Methodology

The UHIs in big cities such as Izmir city which is the third most populated metropolitan city in Turkey have risen up gradually for last few decades (Akbari et al., 2001; Stone, 2007) with the increase of urban concentration causing improper changes in regional temperature and consequently local climate (Georgescu et al., 2011; Li et al., 2004).

As it is mentioned above sections, urbanization results in higher radiation absorption for the land part transformed rural to urban and then causing UHIs to develop. Contrary to that, green vegetation and tree plantation or urban forests in cities help to reduce the UHI effects, and then they provide thermal comfort (Coutts et al., 2016). Therefore, identification of UHI developments depending on timely LST distribution in cities is now becoming an important issue for urban management and planning to transfer our cities to sustainable and even resilient city levels. Thus, the determination of local climate distribution w.r.t. thermal conditions for a city is an important task to be done by the city authorities promising to govern their cities sustainably, especially in developing countries.

The aim of this study consequently became the evaluation of spatiotemporal distribution of urban heat islands (UHISs) in the city of Izmir, Turkey. The study follows these steps: 1) to map emissivity for LST computation, it is required to map distribution of urban green areas and the green area changes for spatiotemporal data analyses by using temporarily produced NDVI images from RS MS time series' images; 2) LST spatiotemporal distribution pattern are obtain across the entire city by using the RS thermal data; 3) trend images individually for the distributions of LST and the normalized difference vegetation index (NDVI) are computed; and 4) then Simulated Single Images (SSI – to be explained in forthcoming sections).

UHSs which are controlled by the heat flux in urban surfaces depending on the surface material and then consequently UHIs appear as a spatial distribution of accumulated high land surface temperatures (LSTs) in cities, and are exacerbated by urbanization (Dousset and Gourmelon, 2003; Sun et al., 2010). Thus, obtaining LST is crucial for the analysis of UHIs (Liu and Zhang, 2011). If the land surface temperature is not available, the near-surface air temperature can be used to map LST distribution for validating the urban heat island affect (Mutiibwa et al., 2015). Up to nowadays, mapping of urban heat island distribution was depending on the LST data as in situ measurements obtained at meteorological sites and gathering data for classical UHI analyses depended on LST data obtained at those rarely distributed local meteorology stations across a city (Lu et al., 2009). However, unevenly distribution and locational isolation of these meteorological sites may result in not fully representation of LST distribution across the city under investigation (Liu and Zhang, 2011). Since these restricted amount of data from meteorological stations are not sufficient to resample an entire study area, remote

sensing offering high-resolution data with almost continuous coverage of the entire world which makes large-scale urban heat island research possible therefore became the most reliable method for LST data collection for example within 30m by 30m sampling tiles and even in different intervals such as within 16 days after 1960s when the high-resolution earth-observing satellites were launched like LANDSAT series of satellites to provide MS image data (Liu and Zhang, 2011; Lu et al., 2009). This even means that multi temporal analyses are available as LANDSAT MS image data for several decades in that high spatial resolution. Thus an archived temporal data is now available almost half a century from the LANDSAT Earth Observing Satellite Program (Wulder et al., 2019). Nowadays, remote sensing technology is also the most reliable technology providing archived and continuous data almost without any gap and overcame the problem of unevenly distributed temporal LST measurements which are the fundamental data for the urban heat island time series analysis especially for today's greatly extended cities turned into megacities (Zhou et al., 2019).

The Landsat TM data from a long life LANDSAT earth-observing satellite program is the most widely used satellite images providing continuous LST data distribution even for an entire world so, full coverage for cities and even as freely downloadable data from the website of US Geological Survey (USGS) (U.S. Geological Survey, 2020). Data from LANDSAT programs provides great advantages than the traditional meteorological data that it can never ever provide for LST studies (Urban et al., 2013). On the other hand, LANDSAT served with only one thermal infrared (TIR) band up to the provision of two bands by LANDSAT 8 launched at 2013 (Wulder et al., 2019). Therefore, Landsat 5 data with one thermal infrared band is also capable of deriving the land surface temperature, even if Landsat 5 TM multi-spectral image scenes for the dates before 2011 is mostly used for monitoring the changes on lands and to model the biophysical characteristics of the earth surfaces (Wulder et al., 2019). As it is mentioned in the study by (Mallick et al., 2008), Landsat 5 TM thermal data is used to estimate heat distribution as a control for local climate, Landsat 5 TM and Landsat 8 OLI thermal infrared data with 120^2 and 100^2 m^2 spatial resolutions both, have been utilized for UHI studies in local-scales, respectively since 1984 (Gong et al., 2013; Weng, 2001; Bendib et al., 2017; Zhang et al., 2016a). The thermal infrared band 6 and band 10 from Landsat 5 and 8 (TIRS) with a spatial resolution of 100^2 m^2 and 120^2 m^2 respectively are actually the bands resampled by using the nearest neighbor algorithm to a pixel size of 30 m by 30 m to fit their pixel resolutions to the optical bands' spatial resolutions for the sake of data compatibility (Wulder et al., 2019).

Freely available archived LANDSAT 5 and 8 data are preferred as time series data for the LST analyzes here in this research. Since LANDSAT 5 which is the only satellite offering freely available archived data since 1984 provides only one channel thermal band and optical spectral data without missing lines (as being experienced in LANDSAT 7 data), single band LST computation algorithm was preferred to extract LST values from LANDSAT data to analyze LST distribution over the city of Izmir for 32 years. Even if use of a single thermal band from old LANDSAT satellite (or sensor) makes retrieving LST more difficult, it is actually easier than those from multiple thermal bands for example from LANDSAT 8 (Kafer et al., 2020). Qin proposed a single TIR band algorithm using Landsat TM data to map LST distribution (Lu et al., 2009; Feyisa et al., 2016; Qin et al., 2001). According to Lu (Lu et al., 2009), the use of single band offers a simple and yet highly effective method for computation of LST values, thus it facilitates the study and the analysis of UHI effects.

In the case of LANDSAT 8, it is decided to use only band 10 as a single thermal band for LST extraction for the compatibility with LANDSAT 5's thermal band 6 and then the single band algorithm without attempting the use of algorithm depending on two thermal channels due to the calibration uncertainties in band 11, although LANDSAT 8 provides 10th and 11th bands as thermal two channel data (Sekertekin et al., 2020). The only thermal band of LANDSAT 5 which is the band 6 was used to delineate the LST distribution for the dates between 1984 and 2013. Thus, both thermal data from LANDSAT 8 and 5 were processed for the delineation of LST distribution across the entire city of Izmir for the all dates studied in the project spanning from 1985 up to 2018. The optical bands from both satellites' TM and OLI sensors have also been processed to extract the NDVI distributions across the whole city of Izmir for different dates for computing the emissivity. High-resolution Google Earth data corresponding with the processing dates has been used for the confirmation of different types of urban land cover distribution in the city and for different type of anthropogenic city activities which may be correlated with low or high LST values (Du et al., 2016a; Du at al, 2016b). ERDAS Imagine 2015 and ArcGIS 10 were utilized for remote sensing and GIS data analysis and to obtain the final outputs for the entire study area.

Here in this study, the spatial distribution of emissivity to reveal and to correct its effect on the LST values distributed all over the entire city was obtained by help of NDVI distribution for the city of Izmir having Eigen climate conditions which are similar to Mediterranean humid climate conditions, since the city of Izmir is located on the Eigen sea coast of the western Turkey (Fiqure 1).

First phase of this project was on demonstrating of LST distribution across the city of Izmir using only one day data (LANDSAT multispectral image data) and representing which land use types contribute to UHI development in the city. Even if one date data was used, our previous research's results emphasized that some industrial areas especially with specific activities appeared as Urban Hot Stops (UHSs) affecting neighboring areas up to several kilometers and causing UHIs to develop at those parts of the city (Corumluoglu et al., 2015). Here, in the current stage of this ongoing project, it is investigated if the same founding is able to be confirmed

by data of a long period of time. Therefore, temporal remote sensing data is obtained and analyzed to reveal whether the results show up with a similar output contributing our previous study outcomes thorough a certain period of time. Thus we will have a robust argument to make strong and locationally precise suggestions to our city authorities who will then take further actions by improving our city future plans taking into account such effective and reliable arguments to be confirmed by our research outcomes to be being here in the example of Izmir city. Then we would have chance to prevent our city from heat pollution and make the city much more sustainable, comfortable and livable one and even to cut our cooling bills further down in the future. By the decrease in energy consumption for such cooling purposes, it means low greenhouse and carbon foot print effects and the saved nature or increased environmental conditions of our city by given chance to nature based solutions. Thus, here in the current state of the research it is not specifically focused on only UHSs, but also investigating the city regions under heavy UHI developments in a long period of time to find out which specific city activities and urban land cover types cause strong and significant UHI effects. Afterward, we will have a chance to take effective and correctly positioned actions to prevent our city nature in a sustainable way from harmful side effects of anthropogenic activities like UHIs.

At the prevention stage, there are several suggestions given and applied by researchers in the literature to struggle with UHI developments in cities such as the use of lighter-color, reflective surfaces on new developments, as well as the replacement of existing dark-color surfaces with lighter ones. On the other hand, the most effective one for tackling with UHI offers a natural solution like strategic planting of vegetation and the use of green technology in urban areas (Dousset and Gourmelon, 2003; Saffuan et al., 2018).

To carry our cities to a smart and sustainable future by supporting the decision makers of our city authorities with most effective and natural solutions, here in this stage of the project, some statistical analyses were carried out for the extraction of UHI developments in the city of Izmir by the help of long term historical land surface temperature (LST) distribution (32 years of data) using LANDSAT multispectral images (thermal for UHI and optical bands for emissivity by NDVI computations) to reveal the varying effects of changing anthropogenic activities on UHI developments in the city of Izmir over that period of time. The outcome of this process is not a pack of timely images for LST distributions spanning through 32 years, but a statistically projected single image representing a long period of temporal LST distribution over the city of Izmir. Therefore, it is an image from a mapping process of statistically optimized and projected long time distributions of LST. This single output image also represents a unique UHI distribution over the city for that period of time. Thus, this project plan will also help us to understand UHI distribution and its relation with the distribution of urbanized land cover types in a certain long period of time. Thus, it helps us to reveal the main suspicious urban factors which strongly effect the UHI developments in an urban environment even by the support of a long period of temporal data. So this will encourage city authorities to take most effective precautions beforehand they happen in the future.

Study Area and Data Used

Study Area

Izmir is the third of the first three metropolitan cities in Turkey with almost 4.37 million citizens living in the12 studied central districts which they hold the densest urban population in Izmir. The City is located on Menderes and Gediz deltas and on some hilly terrain inlands almost all around the Izmir Gulf of Aegean Sea. Geographic coordinates of Izmir are between 37° 49' and 39° 23' North latitudes and 26° 13' and 28° 29' East longitudes.

The studied city land in the province of Izmir covers almost 400 km2 urbanized area (the area covered by red curved boundary in Fig. 1) around the Gulf of Izmir and the wide of the urbanized city part generally extend 3 to 5 km towards inlands all around the gulf. But at somewhere it reaches up to 10 - 12 km, especially at the Sought where the surrounding parts around the ancient city center (now called Konak) are. On the other hand, it shrinks down to few kilometers at the North section of the city (where Karsiyaka district is and city newly developing areas towards to the North are). This is probably because of local mountains running towards the Gulf. At those parts of the city, in generally speaking, city stops extending at the forested lands where they begin to cover the field and toward the tops of these mountainy areas because of the topography which rises rapidly, but not at low altitude hilly lands. So, several hills next to the coast of Izmir Gulf are covered by city urban structures and buildings. City also extents towards the valleys between these mountains at least at two locations more than 10 km inlands of these valleys, the one is seen as city sprawl at the East part and the second is similar to the first but with a wider sprawl at the South. The sprawl extending towards the north is not a sprawl extending into valley, this city extension only follows the Gediz delta parts just right, next to the mountain slopes running into that plain delta which are not smooth hilly terrains. Another, but very narrow urban sprawl with more vegetation cover can be seen at the South. This is because of rough and high mountain slopes with forest covers running along very closely, right next to the gulf coast. Other very narrow sprawl is also seen in the east valley formed by high mountain slopes running towards Aegean Sea and ends up at the city center on the large plain coast formed by Gediz delta. All those descriptions for the urban area of Izmir city can be followed by the stereo illustration represented in Fig. 6a.

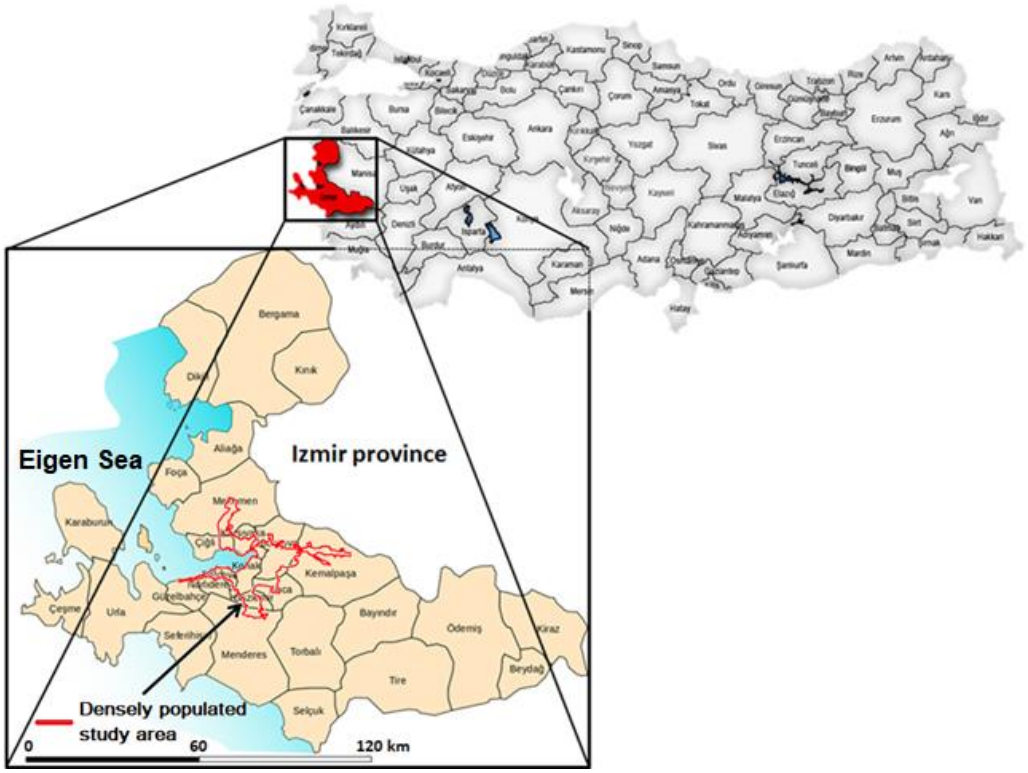

Fig. 1 Izmir province and densely populated central metropolitan city part (study area is in red boundary).

Izmir is also the mostly developed cultural, economic and industrial center in the Aegean region which is the western part of Turkey (Fig. 1) (Yucekaya, 2018). It represents high temperature values (mostly over moderate climate temperature values) especially in summer times and temperature in the some city regions sometimes reaches extreme levels (Unal et al., 2013). It is also the most attractive economic, cultural and tourism center offering several types of activities in the region (Gunlu et al., 2009). It therefore attracts so many people to move in to the city every year. Because of increasing population, as it is seen from the stereo 3D illustration of the City in Fig. 6a, city expands towards Kemalpasa district in the East and towards Menderes district in the South by occupying the valley plains left between the mountains running towards the Izmir Gulf of the Aegean Sea and also towards Menemen district in the North and Urla district in the West directions. In other words, Izmir metropolitan extends along the coasts of Izmir Gulf at the Aegean Sea and Gediz River's delta in the North, along the alluvial plain created by several small streams in the East and to slightly rugged terrains in the South (Fig. 5 and 6).

In recent years, the rapid population increase and corresponding urban expansions towards available terrains following the topographical structures around the existing parts of the city caused several problems such as air pollution and greenhouse gas emission problems which seriously impact the human health and also increases in LST and then UHIs to develop in some parts of the city following the UHSs appearing at where certain anthropogenic activities are in the city like industrial activities which are emphasized by Corumluoglu (Corumluoglu et al., 2015) in their previous research.

Data Used

To understand the temporal effect of urbanization on the temporal diversity of LST and UHI formation, a long period of remote sensing data is required. For this reason, 32 years of freely available LANDSAT 5 (TM) and 8 (OLI and TIRS) data with WRS path number of 181 and WRS row number of 33 acquired at almost 11:15 in Izmir local time during the summer season (August) (Table 1) were downloaded from USGS Earth Explorer web site (U.S. Geological Survey, 2020) and processed sequentially almost for every year between 1985 and 2018 (except 2002 and 2012). The August data is chosen for the sake of doing LST time serious analyses at the time when the city of Izmir is having hottest annual temperate to catch the possible hot spots and heat islands when they are most significant and at their peak levels (Fig. 2) and also having MS LANDSAT scenes with minimum cloud cover in the region.

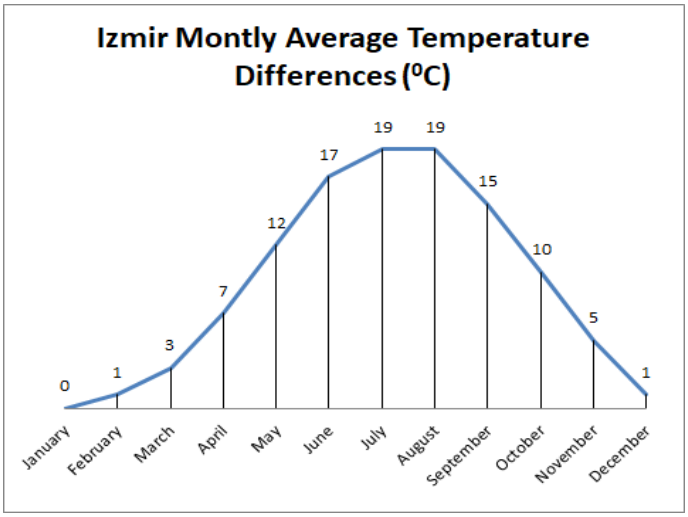

Fig. 2 Long term monthly average temperature differences for the city of Izmir w.r.t the annually minimum average temperature.

The Landsat Thematic Mapper (TM) sensor was carried by Landsat 4 and Landsat 5 satellites, and creates an image scene consisting of images for six spectral reflectance bands 1 to 5 and 7 with a spatial resolution of 30 by 30 meters, and one thermal band (Band 6) with a spatial resolution of 120 by 120 meters (Wulder et al., 2019). The approximate sizes of one LANDSAT scene along and across track are 170 km north-south and 183 km east-west directions (106 mi by 114 mi). The Landsat Operational Land Imager (OLI) and Thermal Infrared Sensor (TIRS) sensors are carried on Landsat 8 satellite. One scene of image consists of nine spectral reflectance band images 1 to 7 and 9 with a spatial resolution of 30 by 30 meters. New band 1 (ultra-blue) is useful for coastal and aerosol studies. Other new band 9 is useful for cirrus cloud detection. The resolution of band 8 which is produced as panchromatic band is 15 by 15 meters. Produced two channel thermal bands by TIRS, 10 and 11 are useful in providing more accurate surface temperatures and are collected for every 0.01 km2 (100m x 100m) for the land part corresponding with a whole scene, are finally provided as thermal bands resampled to 30 meter in the delivered data product (Wulder et al., 2019). Approximate scene size is 170 km (in north-south direction) by 183 km (in east-west direction).

Table 1 32 years of LANDSAT data used in the study

Number	SPACECRAFT	Data type	WRS path and row	Acquisition date	File date	Number	SPACECRAFT	Data type	WRS path and row	Acquisition date	File date
1	lt05_l1tp_181033_19850825_20171212					17	lt05_l1tp_181033_20010821_20180501				
2	lt05_l1tp_181033_19860828_20170216					18	lt05_l1tp_181033_20030726_20161205				
3	lt05_l1tp_181033_19870831_20170211					19	lt05_l1tp_181033_20040813_20161130				
4	lt05_l1tp_181033_19880801_20171208					20	lt05_l1tp_181033_20050816_20161124				
5	lt05_l1tp_181033_19890820_20170808					21	lt05_l1tp_181033_20060819_20161119				
6	lt05_l1tp_181033_19900823_20171208					22	lt05_l1tp_181033_20070822_20161111				
7	lt05_l1tp_181033_19910826_20171214					23	lt05_l1tp_181033_20080824_20161029				
8	lt05_l1tp_181033_19920828_20180210					24	lt05_l1tp_181033_20090827_20161021				
9	lt05_l1tp_181033_19930815_20180210					25	lt05_l1tp_181033_20100830_20161013				
10	lt05_l1tp_181033_19940818_20180302					26	lt05_l1tp_181033_20110817_20161008				
11	lt05_l1tp_181033_19950805_20180210					27	lc08_l1tp_181033_20130822_20170502				
12	lt05_l1tp_181033_19960823_20180210					28	lc08_l1tp_181033_20140825_20170420				
13	lt05_l1tp_181033_19970826_20180210					29	lc08_l1tp_181033_20150828_20170405				
14	lt05_l1tp_181033_19980829_20170908					30	lc08_l1tp_181033_20160830_20170321				
15	lt05_l1tp_181033_19990816_20180210					31	lc08_l1tp_181033_20170801_20170811				
16	lt05_l1tp_181033_20000818_20161214					32	lc08_l1tp_181033_20180820_20180829				

According to the literature, temperature in summer time is commonly high and UHIs are spatially more significant during the summer daytime (Nichol et al., 2009). In the study area, as it is seen from the Fig. 2, highest temperature values are experienced in July and August. The August daytime cloud-free image scenes were therefore selected and downloaded from the USGS web site for this study. Since a LANDSAT scene frame covers much larger area than the urbanized lands in the city of Izmir, all temporal LANDSAT image scenes used in the project were subset to study only the densely urbanized land parts of the city as shown with red boundary lines in Fig. 1. Appropriate atmospheric correction was also applied independently to each band of MS images in every used scene in the study (Table 1) w.r.t. the Dark Object Subtraction atmospheric correction algorithm (DOS1). Thus the atmospheric effect is removed from every pixel of those individual MS band images in the preprocessing step.

Preprocessing of LANDSAT MS images

DN to spectral radiance conversion

Especially when time is concerned, all MS images in all scenes must go through some preprocessing steps before moving to RS data analyze. The first thing to do in that image preprocessing step is "DN to spectral radiance conversion" (Chander and Markham, 2003; Chander and Markham, 2007). It is applied to brightness value of every pixel in each MS band image packed in every MS scene (like those given in the Table 1) using equation 1 below. The computed radiance in a certain spectral wavelength range (band's spectral resolution) is actually total or top of atmosphere radiance reaching to satellite sensor's individual detector corresponding with one certain pixel in a relevant band image that mimics the observed value at detector in graphical form, so as gray tones in a purposed radiometric resolution (for example 8 bit radiometric resolution) and also corresponding with certain land part in the size of Sampled Tiniest Area on Ground (called as Ground Sampling Distance – GSD - in the literature, but it is actually the area of instantly scanned or sampled tiniest land part by detector, so, it is STAG- Sampled Tiniest Area on the Ground). Therefore, the top of atmosphere radiance does not include only the radiance from an object on land surface, but also the radiance from the atmosphere along the path between this instantly scanned tiniest land part which it corresponds with a certain pixel in band images in a MS image scene and the sensor. Therefore, the atmospheric radiance must be removed from the total radiance reached any detector in sensor to obtain only the radiance off the object on the earth surface. Here in this study; DOS1 procedure which is one of the Dark Object Subtraction (DOS) models (Nazeer et al., 2014) was followed to remove the radiance caused by atmosphere and accumulated into the radiance at sensor or at TOA (therefore, below it is called as total radiance). The dark object atmospheric correction should not be applied directly to the brightness values (DNs) of pixels in each individual MS band image in interest as a subtraction process between pixels' brightness values (DNs) in that single band image and brightness value (DN) of dark object determined through visual analyses of graphical representation of the same single band image's statistics (Zhang et al., 2010). "DN to spectral radiance conversion" first must be applied to all pixels' DNs in every band individually in a scene by using the first formulas in the equation groups below (Equations 1 and 2 which are for LANDSAT 5 and for LANDSAT 8 respectively) (Chander and Markham, 2003; Chander and Markham, 2007) and then secondly, the unique dark object radiance value for each band must be obtained by using the second formulas in the same equation groups given below. Dark object radiance value of each band in a scene is then computed from the dark object brightness value (DN) determined individually for relevant single MS band image in the scene by visual interpretation of that relevant image band statistics. Finally, the computed dark object radiance value is then subtracted from the total radiances at the sensor's detectors to get the radiances for the objects at the corresponding sampled ground areas represented as pixels in that individual band images by using the third formulas in the same equation groups (refer to the follow chart in Fig. 3). Thus, this procedure must be followed individually for each band in each MS image scene used for different dates as well.

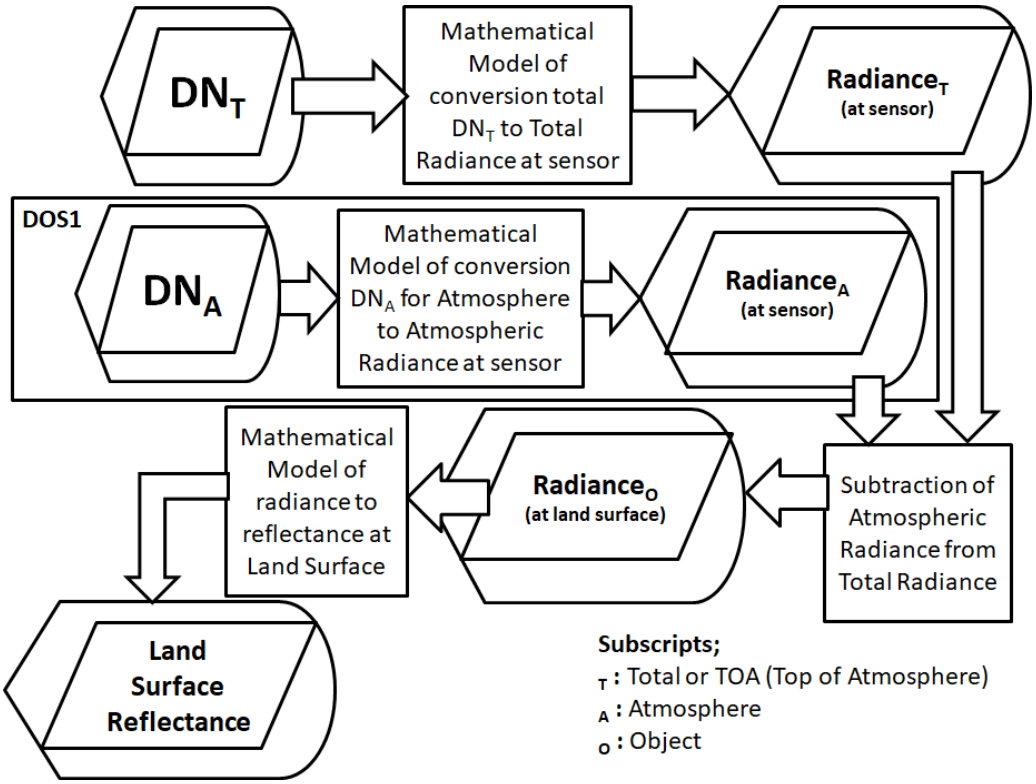

Fig. 3 Conversion algorithm DN to Radiance and Radiance to Land Surface Reflectance.

$$
\begin{aligned}
L_{\lambda(T)} &= M_{L\lambda}\, Q_{cal\lambda(T)} + A_{L\lambda} \\
L_{\lambda(DO)} &= M_{L\lambda}\, Q_{cal\lambda(DO)} + A_{L\lambda} \\
L_{\lambda(O)} &= L_{\lambda(T)} - L_{\lambda(DO)}
\end{aligned}
\qquad (1)
$$

$$
\begin{aligned}
\rho'_{\lambda(T)} &= M_{\rho} Q_{cal\lambda(T)} + A_{\rho} \\
\rho'_{\lambda(DO)} &= M_{\rho} Q_{cal\lambda(DO)} + A_{\rho} \\
\rho'_{\lambda(O)} &= \rho'_{\lambda(T)} - \rho'_{\lambda(DO)}
\end{aligned}
\qquad (2)
$$

where:

L_{λ} : band-specific spectral radiance [Watts/ (m^2 * srad *µm)].

ρ'_{λ} : reflectance without solar angle correction.

$M_{L\lambda}$: band-specific multiplicative rescaling factor for conversion from DN to radiance (that can be obtained from the metadata - RADIANCE_MULT_BAND_x, where x is the band number for LANDSAT 5's reflectance bands).

$A_{L\lambda}$: band-specific additive rescaling factor for conversion from DN to radiance (that can be obtained from the metadata - RADIANCE_ADD_BAND_x, where x is the band number for LANDSAT 5's reflectance bands).

M_{ρ} : multiplicative rescaling factor for conversion from DN to reflectance (that can be obtained from the metadata - REFLECTANCE_MULT_BAND and 2 x 10-5 for LANDSAT 8's reflectance bands).

A_{ρ} : additive rescaling factor for conversion from DN to reflectance (that can be obtained from the metadata - REFLECTANCE_ADD_BAND and -0.1 for LANDSAT 8's reflectance bands).

$Q_{cal\lambda}$: Band-specific quantized and calibrated standard product pixel values (DN) – derived from raw input band image.

λ : Multi-spectral image band number.

Subscrits $_{(T)}$, $_{(DO)}$, $_{(O)}$: are for Total or Top of Atmosphere, Dark Object and Object respectively.

Since this conversion procedure is band-specific it is individually applied to every pixel's brightness values (DNs) in each specific band image of a MS scene including bands of reflected wavelengths and thermal bands as well.

Spectral radiance to reflectance conversion for the bands of reflected wavelengths

This conversion is for the bands of reflected wavelengths in a MS image scene. Reflectance is required for description, determination and discrimination of objects and their details and even properties of those objects and also for analyses of indices to extract information from remote sensing image bands except thermal bands (Bowker, 2010). Reflectance conversion in RS makes band images comparable even if they are obtained at different time and by different sensors to eliminate the case dependent biases. So, the radiance to reflectance conversion process removes the cosine effect caused by changing solar zenith angles due to the time difference between sequential image acquisitions by satellites (Robinove, 1982). Reflectance is referred to a single band because of different amount of irradiance reaching to the earth in every different wavelength range (so, called as band) from sun. Changing solar irradiance should also be accounted for the variation in the earth-sun distance between different image acquisition dates (Young, 2017; Chander et al., 2009). Therefore, it is crucial to use reflectance values in such projects requiring temporal analyses of band images in a RS MS scene obtained at different times as it is being in this study since not only thermal bands but also reflectance bands are used (for example, emissivity computations from NDVIs) and even from different sensors as if LANDSAT family satellites are exploited (images scenes from LANDSAT 5 and LANDSAT 8 satellites are utilized).

The conversion is applied to pixel radiances of reflectance bands in RS MS image scenes using the first and second formulas given in the equation group 3 below (in our case, LANDSAT 5's and LANDSAT 8's reflectance bands were used).

$$\rho_{\lambda(O)} = \frac{\pi L_{\lambda(O)} d^2}{E_{SUN_\lambda} \cos\theta_s} \qquad (3)$$

$$\rho_{\lambda(O)} = \frac{\rho'_{\lambda(O)}}{\cos\theta_s}$$

where:

$\rho_{\lambda(O)}$: band-specific spectral reflectance of an object (land surface reflectance) [unitless]

π : mathematical constant [unitless] (3.14159).

d : earth-sun distance [astronomical unit] (that can be obtained from the metadata - EARTH_SUN_DISTANCE, for LANDSAT 5 and 8's reflectance bands).

$E_{SUN\lambda}$: spectral mean solar irradiance [Watts/(m^2 *μm)]

θ_s : solar zenith angle [degree] (90 - θ_E).

θ_E : solar elevation angle [degree], (that can be obtained from the metadata - SUN_ELEVATION, for LANDSAT 5 and 8's reflectance bands).

$\rho'_{\lambda(O)}$: band-specific spectral reflectance of an object without solar angle correction [unitless]

At-sensor spectral radiance to at-sensor brightness temperature conversion for the thermal bands

Considering black body assumption for the heat transfer from the Earth, emissivity can then be assumed as uniform for the Earth surface and equation 4 below is used for the at-sensor spectral radiance to brightness temperature conversion (Sekertekin et al. 2020; Chander and Markham 2009).

$$T_{B(O)} = \frac{K_2}{\ln\left(\frac{K_1}{L_{\lambda(O)}}+1\right)} \qquad (4)$$

where:

$T_{B(O)}$: at sensor brightness temperature of land surface cover in the size of STAG [K]

K_1 : calibration constant 1 for thermal band [Watts/(m2 *sr * μm)] (that can be obtained from the metadata - K1_CONSTANT_BAND_x, where x is the band 6 and band 10, so 607.76 and 774.89 for LANDSAT 5 and LANDSAT 8 respectively).

K_2 : calibration constant 2 for thermal band [K] (that can be obtained from the metadata - K2_CONSTANT_BAND_x, where x is the band 6 and band 10, so 1260.56 and 1321.08 for LANDSAT 5 and LANDSAT 8 respectively).

Brightness Temperature to Land Surface Temperature conversion

Since temperatures of objects on the earth surface are the main concern of UHI analyses, brightness temperature values are then converted to Land Surface Temperatures (LST – TS) by using the equation 5 below (Salih et al., 2018). In this respect, the land surface emissivity must be accounted to reach LST values at the land surface as it is required for this conversion.

$$T_{S(O)} = \frac{T_{B(O)}}{1+\left(\lambda_T T_{B(O)}/\rho\right)\ln \varepsilon} - 273.15 \quad (5)$$

where:

$T_{S(O)}$: Land Surface Temperature of an object (LST) [ºC]

λ_T : the central wavelength of the thermal infrared band [m] (λ_T(mid) =11.45μm and λ_T(mid) =10.90μm for LANDSAT 5 and LANDSAT 8 respectively)

ρ : thermal constant [m K] ($\rho = h*c/\sigma$, $\rho = 1.438*10^{-2}$ mK)

c : the speed of light [m / s] ($c=2.998*10^8$ m/s)

h : the Planck constant [J s] ($h=6.626*10^{-34}$ Js)

σ : the Boltzmann constant [J / K] ($\sigma = 1.38*10^{-23}$ J/K)

ε : the land surface emissivity [unitless].

Equation 5 (Memon et al., 2008; Solecki et al., 2004) above represents the conversion formula using Brightness Temperature (TB) values to compute the Land Surface Temperature (TS) values in Celsius degree (with that additional term for the absolute zero, −273.15 ºC) (Choi et al., 2012; Mejbel et al., 2018). Except brightness temperature, the other unknown term in this equation is the emissivity. So that, the emissivity values for each pixel must be computed before LST computation as it is mentioned above.

Computing NDVI values from LANDSAT reflectance bands

Even if emissivity is an indirect requirement for local climate studies based on temperatures of objects on land, the use of MS satellite images provide the most appropriate materials like MS images to compute the emissivity from Normalized Difference Vegetation Index (NDVI) algorithm extracted from these MS band images (Sun et al., 2010; Corumluoglu et al., 2015; Ng et al., 2012; Mushore et al., 2017). Therefore, in such UHI and temperature related climate studies from RS satellite images; the first requirement is the computation of NDVI from satellites' reflectance bands for computation of emissivity correction. Therefore, the next step here became the computation of temporal NDVI values for the Izmir's urbanized lands using the time serious LANDSAT MS image scenes.

On the other hand, there are several vegetation indexes computed from RS MS band images. Output index images represent the healthy vegetation distribution in the land part corresponding with RS MS image scene's whole frame or with a delineated boundary for a sub-set area. Mostly preferred vegetation index especially for the determination of emissivity is the Normalized Difference Vegetation Index (NDVI) in the literature (Chen et al., 2009). Therefore, in the case of LANDSAT, the bands to be used for the computation of such vegetation index values for each pixel corresponding with STAG are the 3th and 4th bands of LANDSAT 5 MS image scenes and 4th band and 5th band of LANDSAT 8 MS image scenes (Sekertekin et al., 2020). Normalized Difference Vegetation Index values at the time when each MS image scene was acquired (NDVIt) (Fig. 4) are then computed from the formulas given in Equations group 6 using the certain bands in MS image scenes acquired by LANDSAT 5 and LANDSAT 8 respectively.

$$NDVI_t = \frac{\rho_{BAND4\_L5(t)} - \rho_{BAND3\_L5(t)}}{\rho_{BAND4\_L5(t)} + \rho_{BAND3\_L5(t)}}$$

$$NDVI_t = \frac{\rho_{BAND5\_L8(t)} - \rho_{BAND4\_L8(t)}}{\rho_{BAND5\_L8(t)} + \rho_{BAND4\_L8(t)}} \quad (6)$$

where:

NDVIt : Normalized Difference Vegetation Index at the time of MS image acquisition.

$\rho_{BAND3\_L5(t)}$: Computed Land Surface Reflectance Value of each STAG for the wavelength corresponding with the 3th band of LANDSAT 5 MS image scene at the time of acquisition.

$\rho_{BAND4\_L5(t)}$: Computed Land Surface Reflectance Value of each STAG for the wavelength corresponding with the 4th band of LANDSAT 5 MS image scene at the time of acquisition.

$\rho_{BAND4\_L8(t)}$: Computed Land Surface Reflectance Value of each STAG for the wavelength corresponding with the 4th band of LANDSAT 8 MS image scene at the time of acquisition.

$\rho_{BAND5\_L8(t)}$: Computed Land Surface Reflectance Value of each STAG for the wavelength corresponding with the 5th band of LANDSAT 8 MS image scene at the time of acquisition.

t : stands for the time (date) when an individual MS image scene is acquired.

Emissivity

Land Surface Emissivity (ε) depends on the surface capability of transforming heat energy into radiant energy (Kumar et al., 2012). As it is mentioned previously, it is the most efficient way to use remote sensing satellite MS band images to compute the emissivity from Normalized Difference Vegetation Index (NDVI) to reach most reliable LST values in the case of remote sensing projects. Therefore, here in this research NDVI Threshold Based Emissivity Method was adapted for the estimation of ε from Landsat data (Kumar et al., 2012; Jenerette et al., 2007; Zhang, 2006). The following equation 7 is used in this research to estimate emissivity from NDVI using LANDSAT 5 and 8's appropriate reflectance image bands for the land surfaces representing mixed land cover with soil and vegetation (Willett and Sherwood, 2012).

$$\varepsilon_t = \varepsilon_V + \varepsilon_S (1 - P_{vt}) + d\varepsilon \text{ and } d\varepsilon = (1 - \varepsilon_S)(1 - P_{vt}) F \varepsilon_V \quad (7)$$

where:

ε_t : is emissivity at the time of image acquisition.

P_{vt} : is the proportion of vegetation on the land at time of acquisition (Lu et al., 2014).

ε_V and ε_S: are the soil and vegetation emissivity, respectively.

$d\varepsilon$: is the cavity effect due to surface roughness.

F : is a geometrical shape factor with the mean value of 0.55 (Lopez et al., 2017).

$$P_{vt} = [(NDVI_t - NDVI_s) / (NDVI_v - NDVI_s)]^2 \quad (8)$$

where:

$NDVI_t$: Normalized Difference Vegetation Index at the time of image acquisition.

NDVIv = 0.5 and NDVIs = 0.2 represent the general NDVI threshold values in NDVI graph in Fig. 4 for vegetation coverage on land at where mixed land cover starts to turn into vegetation and for soil at where mixed land cover starts to turn into soil in the opposite direction towards 0 and negative values respectively (Lopez et al., 2017).

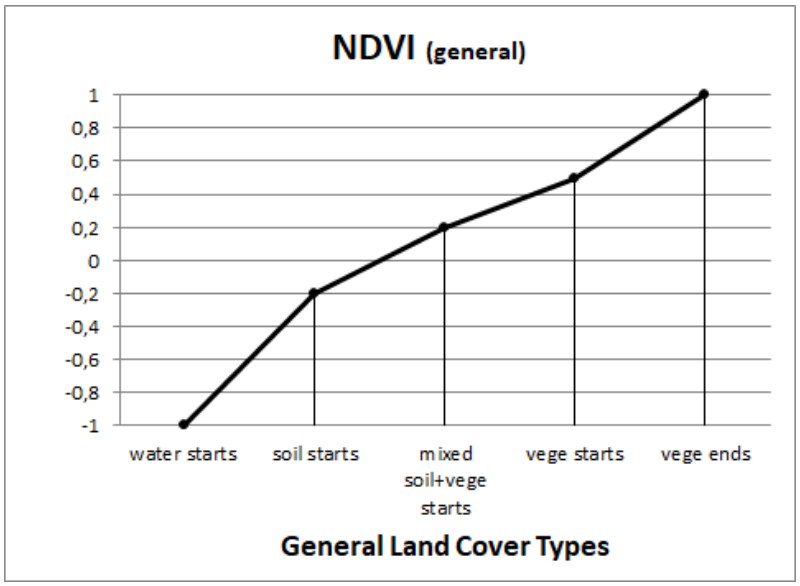

Fig. 4 General NDVI values for general land cover types.

Table 2 Emissivity from NDVI.

NDVI	Emissivity (ε) for LANDSAT 5	Emissivity (ε) for LANDSAT 8
If $0.2 > NDVI_t$	$\varepsilon = 0.979 - 0.035\ \rho_R$	$\varepsilon = 0.979 - 0.046\ \rho_R$
If $0.2 \leq NDVI_t \leq 0.5$	$\varepsilon = 0.986 - 0.004\ P_v$	ε = Equation 7
If $0.5 < NDVI_t$	ε = 0.99	ε = 0.987 + dε

Emissivity values are suggested as 0.985 and 0.960 for vegetation and soil respectively in Equation 7 (Bendib et al., 2017). Thus, the formulas in table 2 take care of the land covers like soil, vegetation and mixed land cover types individually for estimating emissivity from NDVI. ρR in the table 2 is for the red band reflectance values.

After producing time series emissivity images by following the instructions given in Table 2 (Shahmohamadi et al., 2011; Solecki et al., 2004), Land Surface Temperature (LST) values, TS at the each image acquisition time were then computed by using Equation 5 in Celsius as time series LST images as well (Corumluoglu et al., 2015).

Deviation and Mean Value of Computation of Trend, Standard Time Serous Data

A significant correlation between land cover and land surface temperature indicated that land cover dominates land surface temperature changes in most areas on the earth especially in urbanized regions (Firoozi et al. 2020). In this study, LST images for the period of 32 years between 1985 and 2018 were analyzed to reveal temperature distribution and to find out UHI development regions that effect and change the city natural climate condition over time. Therefore, spatiotemporal trends of land surface temperature were then computed and analyzed for every STAG in the land boundary corresponding with subset image boundary by using the pixels of each subset LST image in time series data set. Here in this research, analyzed subset LST image data set is a time series data set of 32 years covering almost entire urbanized land parts in Izmir city.

Trend analysis in RS is a linear regression analysis of a variable against time that variable represents one of the land characteristics of a tiniest land part (STAG) represented as a pixel in RS images in a time series data set (Firoozi et al., 2020; Forkel et al., 2013). Therefore, each pixel value in the output image represents change trend of the variable for that tiniest land part of the ground (STAG) over the time. They are computed from the series of values for each pixel in variable images obtained in annual temporal resolution and covering the entire study area and at the same time, they also simulate inter-annually average Variable Change Rate (VCR) here in this study (Song et al., 2015). VCR can also be defined as timely slope of a variable computed from the values of the same pixel in the time series variable images by using the linear regression equation (Equation 8) given below (Song et al., 2018; Tan et al., 2017). In this paper, every individual LST pixel values in time serious images obtained in month August that set up one pixel cube through 32 years of data are used to simulate the change trends, the standard deviation of the change and the mean chance of LST variable for each STAG in the urbanized region. The regression slope is calculated by the least square method. The trend (or slope) formula is then given as followings:

$$Slope_k = \frac{n\sum_{i=1}^{n} i*V_{ki} - \left(\sum_{i=1}^{n} i\right)*\left(\sum_{i=1}^{n} V_{ki}\right)}{n*\sum_{i=1}^{n} i^2 - \left(\sum_{i=1}^{n} i\right)^2}, k\ (1,\dots,l),\ i\ (1,2,3,\dots,n) \quad (8)$$

where k is for variables, l is the total number of the variables and here we have only one variable, LST, therefore k is 1 and $Slope_k$ is for slope of k^{th} variable, V_{ki} stands for kth variable's pixel value in the i^{th} time serious image and i stands for the number of sequential year and n is for the total number of years in the time series, here is 32.

After the computation of LST slope (or trend) image including every corresponding STAG in the urban area of Izmir from LST time serious image data for the years between 1985 and 2018, similarly to the computation of that trend image, standard division (SD) and mean (M) value images were then also computed using the equations 9 and 10 below.

$$SD_k = \sqrt{\frac{\sum_{i=1}^{n}(V_{ki} - m_k)^2}{n-1}} \quad (9)$$

$$m_k = \left(\sum_{i=1}^{n} V_{ki}\right)/_n \quad (10)$$

where, mk is LST mean values computed by using the LST pixel values through the entire time series LST image data set for each corresponding STAG in the study area.

Computation of Simulated Single Data (or Image) (SSD or SSI) for a time series data set

Trend, standard division and mean images of the variable (here LST) are all single images computed after a statistical processes of time series data. The next step in the study is the computation of an individually simulated single image for a certain variable using Equation 11 below. The output image from the equation 11 mimics the entire related time serious data as a Simulated Single Image (SSI) for the variable in interest, here is LST. So, the SSI represents and encompasses statistically the trend, the change range and the mean value of entire time serious data for the related variable at study region. In other words, a SSI pixel value for a variable stands as a single value estimated statistically from slope, standard division and mean values of the same pixel through entire time serious data corresponding with an individual STAG and therefore simulates the properties' change of that tiny land part statistically in terms of related variable during a certain period of time (here, it is the yearly august LST variable for 32 years). This let us to do represent time serious distribution of variable as a single image. If there would be several variables, then SSI process let us to carry out multi-criteria analyses using single images instead of dealing with several time serious data or images.

$$SSI_k = Slope_k * SD_k + M_k \quad (11)$$

If SSI equation (Equation 11) is reviewed, it can be realized that there is no need to put SD value (multiplied by slope) into the equation with a plus-minus sign because the slope value comes together with the direction sign as plus sign for an increasing trend or as minus sign for a decreasing trend through every individual pixel's values in the entire time series data. Thus, the standard deviation of the variable obtained from an individual pixel's values through the time series data represents the change in the variable through this entire data range w.r.t. mean value and similarly to that, slope also represents the change trend of the LST through again this time series data. When these two statistical values are multiplied, than simulated single image is obtained for an entire time series data set, but at that step, in fact it is referred to zero. For a realistic simulation, it must be shifted to mean value. Therefore, final simulated single value of the variable for the pixel in process must be computed just by adding that statistical product term to the mean value from the values of the same pixel through the whole time series image data to obtain simulated realistic LST value for a pixel in SSI image.

Results and Discussions

After analyses of the results as SSI output of LST distributions to reveal the hot spots and heat island developments in the urbanized areas of Izmir city over the years which these urbanized regions can be followed with the delineated red boundary polygon in Fig. 6a presented as a 3D illustration, it is recognized that some specific parts of the city are the most candidate and prone sites for the appearance of such hot spots and UHI developments. For the sake of easy following the relationship between land structures and/or covers and LST distribution and for the determination of hot spots and heat island developments in the Izmir urban areas, some

parts of the city are grouped and lebaled w.r.t. apparent structures driven by specific anthropogenic activities at those regions. Thus, they are tagged as CC, I, R and A in Fig. 5 (and in Fig. 6a as 3D illustration by a stereo image pair) which they represent city center, industrial, residential and airport areas respectively.

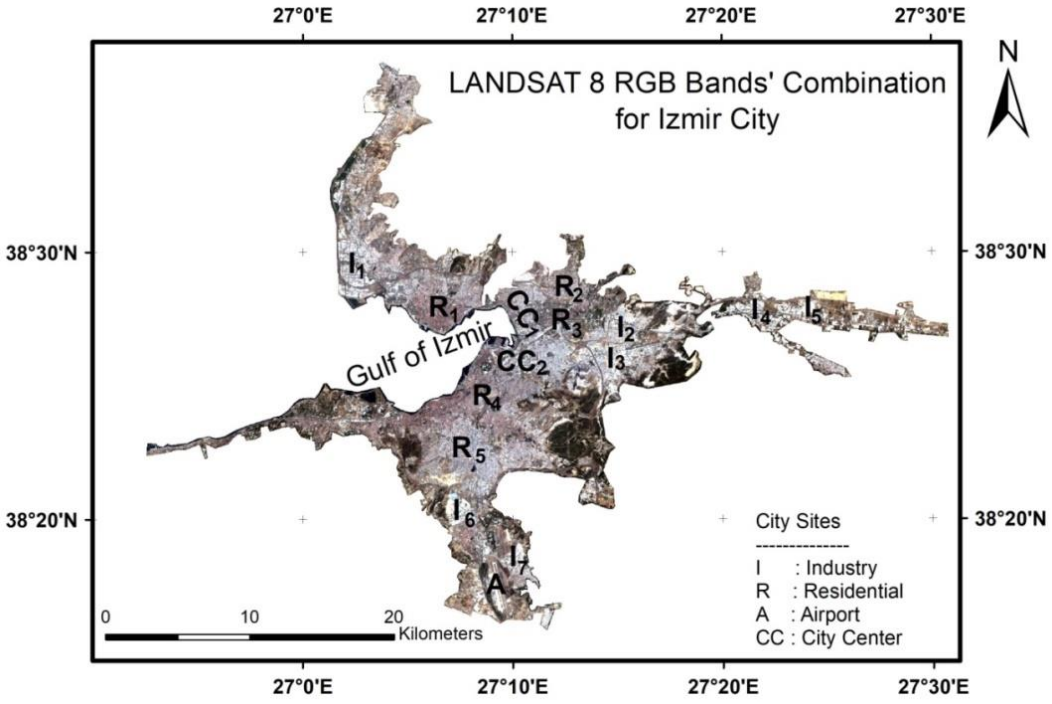

Fig. 5 City of Izmir, urban areas distribution by RGB true color LANDSAT images

Now, here can be discussed the land structures and types of urban areas in the city of Izmir. As it can be seen from the Fig. 5 and 6a, city sprawl in the East includes no other types of urban structures but almost entirely two industrial zones (I4 and I5) at where they are spread on the bottom of the narrow valley trapped between two mountains running towards the gulf of Izmir. There are also two other industrial sites (I2 and I3) located at where this valley ends and reaches to the city part occupying plain area just next to the mouth of this valley with a width of almost 7 km in north-south direction even if the mountains still run along the both sites of the plain towards the gulf (follow the local terrain and the topography of the region by checking the stereo pair perspective images provided in the Fig. 6a). It is also seen from Fig. 5 and Fig. 6b (in 3D illustration by a stereo image pair) that heat islands and so the hot sites of the city appear at the slightly high slopes at the bottom of these mountains up to where the urban land parts reach to the high slopes until they are interrupted by green areas like forested regions on high sloppy terrains of these mountains, even if the valley forms a natural channel for local wind blow and breeze. So, these forested or green areas are the coolest sites around the city. Other cool sites in the city are seen at the city regions developed on the lowlands with some slightly rugged terrains, so at the mouth of the previously mentioned valley. It is where it reaches to the coast of Izmir gulf east to west in the middle of the city. Those cool sites almost completely met with urban sites at where residential and some commercially active areas are, but none is seen at the industrial regions. So, the research pointed out that even the city has 7 industrial sites (Fig. 5 and 6a) none of them appears in these cool sites. This is a significant result even if it represents only a SSI of LST distribution it is actually an output from 32 years of time series LANDSAT thermal data analyses (Fig. 6b and 6c and Fig. 7). Thus, urban parts where industrial activities are in the city almost entirely contribute to and coincide with heat island developments in the city. So, generally these sites cause hot spots to appear first and then accumulation heat problem which ends up with heat pollution as heat island and finally distribution of this heat pollution towards neighboring urban areas next to these industrial sites in the city and effect these neighboring zones in great extents (in some cases up to 5-10 km) (Fig. 6a and 6b and Fig. 7). This outcome also confirms our previous research outcome, even if it reviled the heat island distribution over the city of Izmir for only one specific date (Corumluoglu et al., 2015).

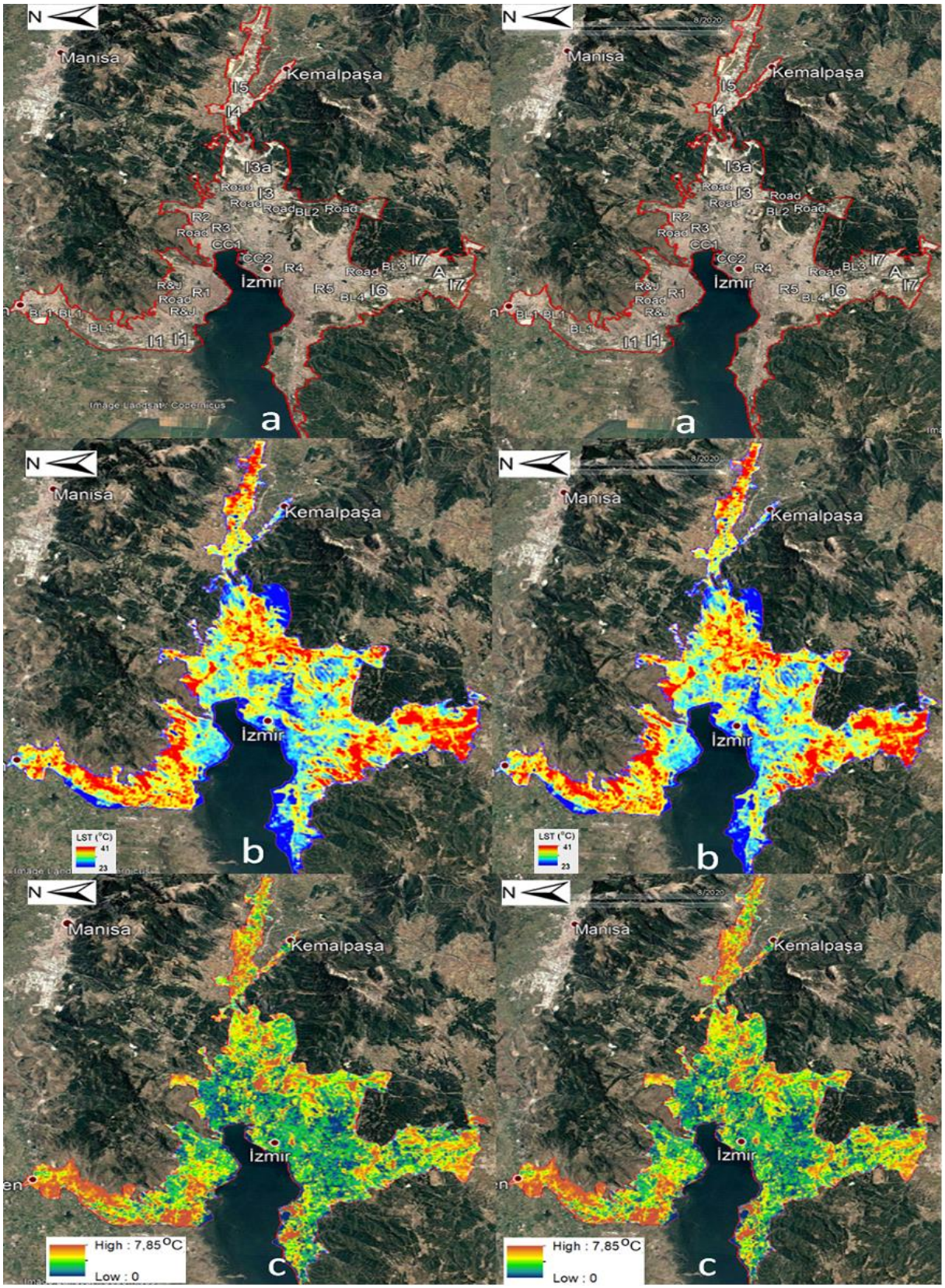

Fig. 6 3D representation of study area (red curved line) (a) with some urban details, and (b) for the Simulated Single Image (SSI) LST distribution and (c) for the distribution of SSI Local LST differences in the city of Izmir for the month August as a summary of 32 years' time span between 1985 and 2018 by using stereo display techniques with embedded illustrations on Google Earth captured images (use converging eye lines' method to see the 3D illustrations above).

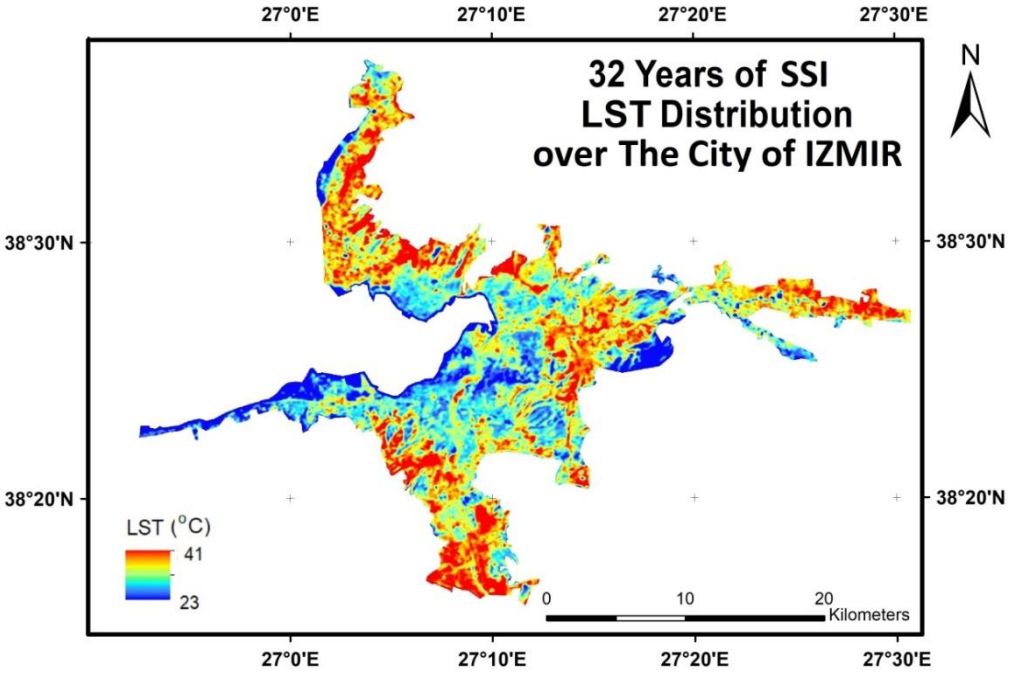

Fig. 7 32 years of Simulated Single Image (SSI) LST distribution for the month August over the city of Izmir between 1985 and 2018

There are also several other outcomes from this research. These results will be explained w.r.t. the thermal conditions in some sub-urban sections of the city showing a similar LST distribution behavior. Thus, the city is divided into several subsections with certain types of LST distributions for the sake of easily understood and noticed the corresponding urban structures behind that specific types of LST distribution over such urban areas (these sub-sections are represented as black and white rectangles in Fig. 8).

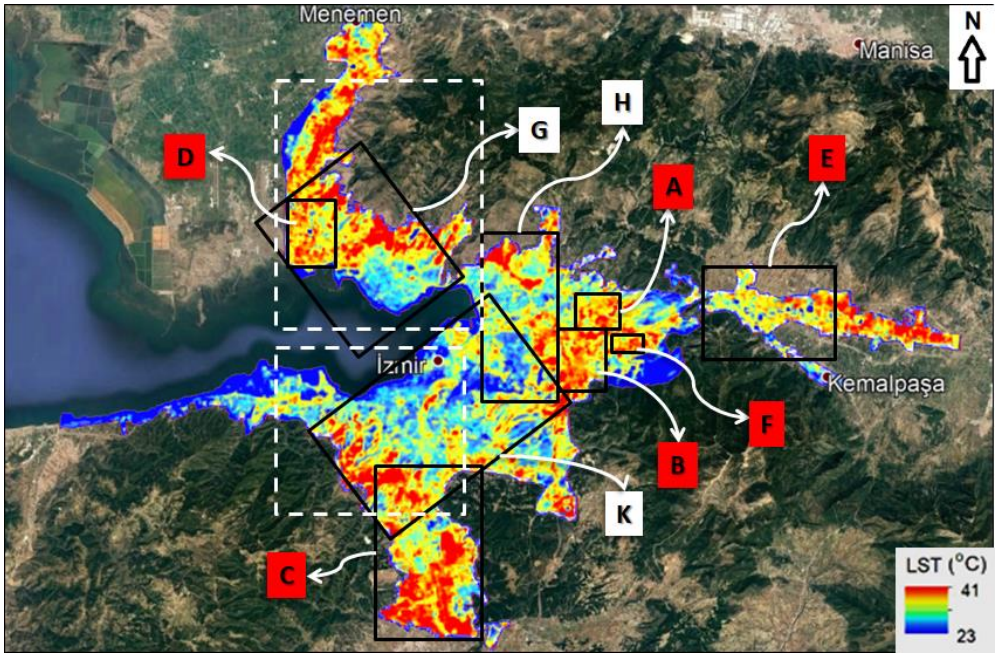

Fig. 8 Subsections of the project covering the different urban zones in the city w.r.t. the LST distribution.

Fig. 9 also represents these subsections in detail with related letter tags A to K as shown in Fig. 8. Every tagged part seen in the Fig. 9 shows details of the urban structures at that specific urbanized city parts in RGB color image form along with thematic representation of detailed SSI LST distribution related to that specific city part. Fig. 9 shows the details of every city urban subsection with corresponding tag given in Fig. 8 as mentioned above and also highlights some areas with specific urban structures in these subsections by marking them with black and white geometrical shapes on the Fig. 8 since they represent distinct LST distributions. These

corresponding SSI LST distributions are also shown in the Fig. 9 next to that tagged RGB illustrations of these urban subsections.

As it can be seen from SSI illustration of LST distribution corresponding with A tagged RGB image part in Fig. 9, there are several hot areas which they also contribute the heat island development covering almost entirely this A tagged subsection in the city. In fact, this A tagged area is almost entirely covered by one of the industrial areas among several others in the city. The buildings in this region are generally single-storey industrial buildings with high ceiling and large metal roof tops. Because of that, when they are generally exposed to solar energy during daylight times in summer seasons, they absorb the solar energy in great extent and are heated up extremely, then start to reradiate this absorbed great amount of energy as thermal energy back into the surrounding environment. Therefore, they appear as hot spots contributing the heat island developments in the whole subsections of the city which are tagged with A to E as shown in Fig. 9. Almost all of the industrial regions in the city are the regions labeled with "I" as shown in the tagged RGB images in Fig. 9 w.r.t. the tags in Fig. 8. They are such as those regions marked with dashed black rectangle and black solid line rectangle and ellipse in the RGB image with tag A and even the large industrial area appearing in the top middle section of the image and are also marked by rectangles with black dashed line and dotted circle in the B tagged RGB image and represented by black dashed rectangle and the area labelled as "I6 and I7" in the RGB image with tag C and delineated by black solid, dotted and dashed ellipses in the RGB image with tag D and also delineated by black dashed circle in the RGB image with tag F and all white details in the regions labelled as "I5 and I6" in the RGB image with tag E and two city urban sections labelled with "I1" as seen in G tagged RGB image and also the region with wide white details on the top right corner of the K tagged image. They all contribute hot spots to appear and then heat island to develop as seen in the colorful thematic images just next to the tagged RGB images. All those colored thematic images are the subset images from SSI LST distribution in the entire urban land. The sections appearing in dense red color representing the hot spots and heat islands correspond with those marked regions in the tagged RGB images. Probably the industrial activities and processes in industrial regions and the industrial building structures cause heat increase in these regions and create heat pollution and then changes the local climate and natural condition of the environment in these regions and in the surrounding city parts (so these regions are seen as brownish and yellowish colors in the subset SSI LST distribution images next to the RGB images). This harmful effect in these city parts deteriorates and disturbs the comfort of the local people who lives and works in these regions and also increases the cooling cost for bringing back the comfort artificially in vehicles and buildings.

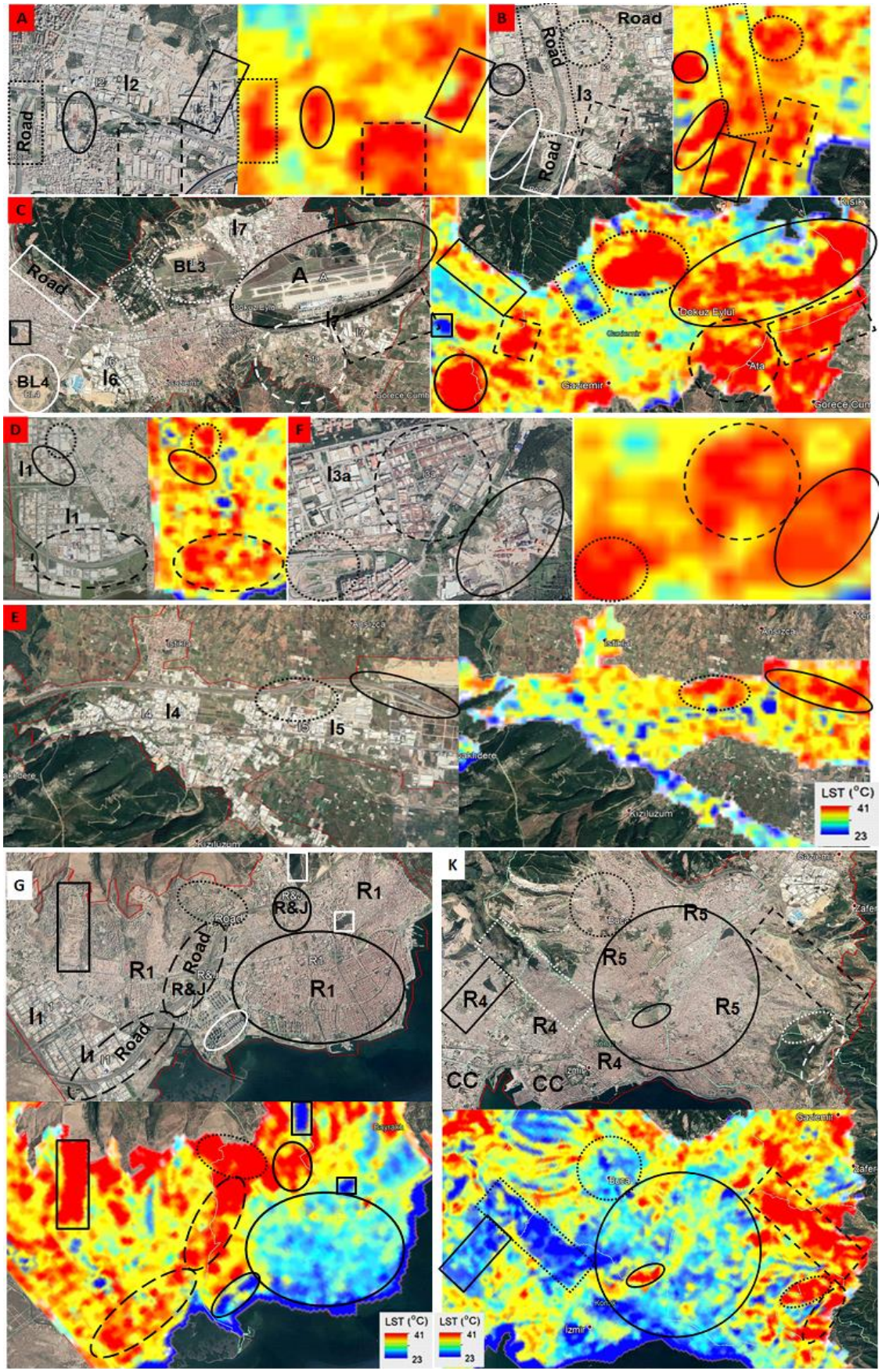

Fig. 9 Representation of detailed subsections covering areas with specific urban features shown in different geometrical shapes for the comparison with specific LST distributions in the city.

The research also emphasized that another suspicious urban detail in the city contributing the heat island developments are the roads. When the wide of an asphalt roads becomes larger as it is being experienced with highways and since the city of Izmir has a long one of them as a ring highway which some cases it occupies surrounding terrains around and at the city boundaries and even with large highway junctions at several locations, then they become other group of most suspicious candidate urban structures causing hot spots to emerge and contributing heat islands to develop as it can be seen through the same tagged RGB images and those corresponding color images of SSI LST distributions given next to the every RGB image in Fig. 9 such as those highway road sections and junctions marked by dotted black rectangle in A tagged RGB image and again dotted black rectangle and white rectangle with solid line in RGB image with B tag and white rectangle and dashed white square in the RGB image with C tag and black dashed ellipse in the RGB image with tag D (with some industrial buildings) and both ellipse shapes in the RGB image with tag E and both dashed ellipse (for highway) and small solid line ellipse (for large highway junction) in the RGB image with tag G.

Other urban land features which are important to highlight here in this research as other suspicious urban structures that cause heat islands to develop and consequently heat pollution in cities can be grouped as bare lands with no urban structures, so the lands within these forms; bare soil lands, barren lands, excavated bare lands and even grassy green lands and green lands covered with grass, brush and scrub. These areas can be followed from the tagged RGB images in Fig. 9. So, these are the areas marked with white ellipse in the B tagged RGB image and the excavated bare soil area labeled BL4 and marked with white soled line ellipse and grassy land labelled as BL3 and delineated with dotted white ellipse and the area with mostly grassy, brushy and barren land mixed with few small dwelling houses and marked with dashed white circle in the C tagged RGB image and also the areas including grassy lands, excavated barren soils and barren lands mixed very few small buildings marked with dotted black circle and black solid line ellipse in the F tagged RGB image and even hilly slope barren land with dwelling structures facing towards south delineated with black solid line rectangle in the G tagged RGB image and finally the almost entirely barren slope land facing towards south marked with black dashed line rectangle and also excavated barren and some grassy and brushy hills' slope land parts facing towards south-east and south marked with white dotted and dashed ellipses in the K tagged RGB image. All these land features, structures and patterns cause to emerge hot spots and to develop heat islands in the urban regions with specific urban features as mentioned above and even by effecting the neighboring urban lands in great extents as seen in the labelled images in Fig. 9 above and they can also be followed as red areas for hot spot sites and all red-reddish and yellow-yellowish areas for heat island development sites from the colored SSI-LST images given along with tagged RGB images in Fig. 9.

In addition to these bare, bare soil, excavated and barren lands and even with grass, brush and scrub urban land features, if an urban land having any types of these land covers is on a hill slope facing towards either south-east or directly east or south (Fig. 10), then the topographical aspect of the land w.r.t. its slope direction facing directly toward either east, south or south-east becomes the dominant factor contributing greatly the emergence of hot spots and development of heat islands over those urban lands having such sort of certain specifications (Estoque et al., 2017). This is probably because of the increase of heat retention capability of such lands having above mentioned land cover types when they face directly or almost perpendicularly towards the sun. Thus, thermal energy coming from the sun is absorbed in high amount with minimum scattering by such land surfaces when they face towards the sun. In the case of Izmir, realizing examples of that process on such urban land slopes having together with one of the aspects of either east, south or south-east and land covers mentioned above which cause hot spots to emerge and heat islands to develop can be followed from Fig. 7 and even from the 3D illustration of Izmir city and also 3D illustration of SSI-LST distribution over the city in Fig. 9 and Fig. 10. This is probably the most important outcome of this research concluded after the topographical structure of the entire city is analyzed through these stereo 3D illustrations. As it is seen from the same figures that urban hill slopes not facing to the mentioned directions (so, if they are facing towards North, West or North-West) are having cool climates relatively w.r.t. the hot slopes discussed previously and they are shown with black solid line arrows in 3D illustrations in the Fig. 10 and marked with black solid line and white dotted line rectangles in K tagged RGB image in the Fig. 9.

Other relatively cool sites in the city are seen at residential and commercial areas delineated with large black solid line ellipse in G tagged RGB image and large black solid line circle in K tagged RGB image in the Fig. 9 and they are also located on (in general) almost flat or slightly rough terrains as shown in 3D illustrations with dotted line and solid line ellipses in both stereo images of Fig. 10. It is probably because of city building structures and building materials being different than industrial sites since they are generally dwelling houses or apartments or mostly commercial buildings in city centers in these regions. So, all those work together and behave like scattering surfaces w.r.t. the sunlight coming form an angle. Therefore, these regions within described structural form do not absorb much energy but scatter it around contrary to the sites causing UHI developments. There are also some dotted line arrows which they point some sites appearing in darker blue color in both stereo illustrations of SSI LST embedded images in Fig. 10. So, these areas are the parks with mature and tall trees with large canopy surrounded by urban structures as it can be followed in the Fig. 11 as well which

represents SSI-NDVI distribution over the city of Izmir. Other cool sites marked by black arrows again in Fig. 10 are slope lands facing towards North, West or North-West directions. They are the coolest areas in the region.

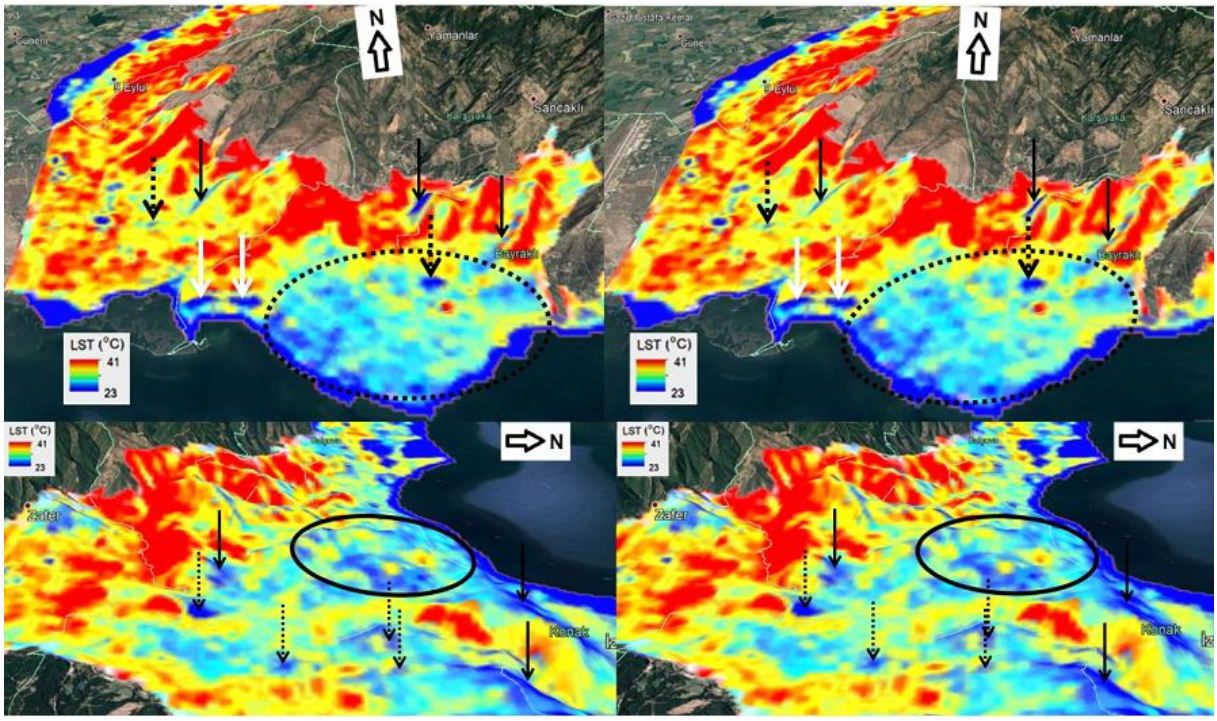

Fig. 10 3D illustrations of SSI-LST distribution over the city of Izmir with cool sites marked with arrows and ellipses.

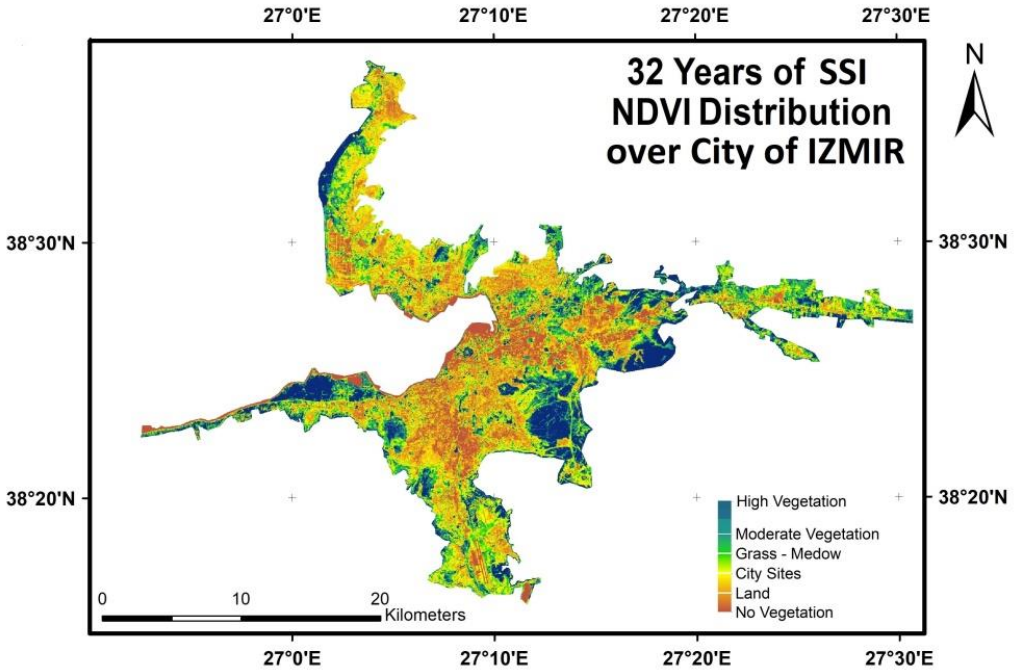

Fig. 11 32 years of Simulated Single Image (SSI) NDVI distribution for the month August over the city of Izmir between 1985 and 2018

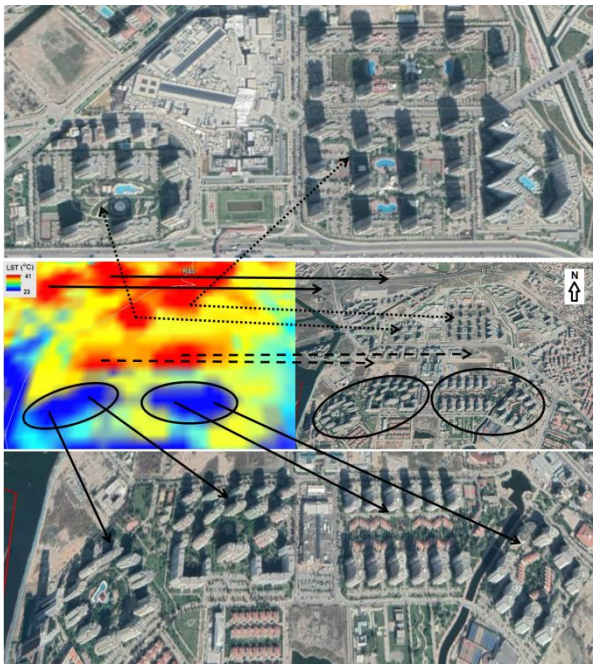

Fig. 12 Unique formation of high rise dwelling apartments with specific natural recreation areas for cool site creation in cities.

One of the most interesting founding in this research is related with a residential area including tall and high rise apartments in discrete formation and recreation sections between these apartments decorated with green vegetation and trees as shown in large scale image at the bottom of Fig. 12 and with black solid line ellipses in the left middle part of the figure which includes the thematic form of SSI LST distribution. What should be kept in mind here related with this research is that the SSI-LST distribution means in one sense, single image output of 32 years of statistical analyses of thermal data. So, the middle left part of the Fig. 12 illustrates that SSI-LST appearance over that region as dark blue color which is referred to coolest temperature and over other sites surrounding this specific apartment site. Here, it must be strongly emphasized that it means the mentioned apartment site is one of the coolest city region in the entire city even if it is still urbanized residential area just next to the heat island or in the heat island developed area like an isolated city section in this heat island appearing in this part of the city. This is probably because of the above described specific formation of the site. This outcome becomes meaningful when it is compared with the similar apartment sites with tall buildings in again discrete pattern but with recreation areas between the apartment blocks decorated as car parks with asphalt or paved lands or grassy lands with some bushes and even if they are located just next to the mentioned coolest site, they appear as two of the hot spot areas in the city and they are shown with two black dotted arrows in the Fig. 12. The figure also represents other two hot spot sections. They are highway road and junction shown with two black solid line arrows and the others are empty bare lands with very rare vegetation shown with two black dashed line arrows in the middle image.

Conclusions

Local climate studies for urban areas under thermal stress reviled a strong correlation between different urban land cover types and urban LST distribution (Chen et al., 2006; Weng and Yang, 2004; Deilami and Kamruzzaman, 2017; Tran et al., 2017). This relationship introduces the driving forces on UHI developments w.r.t. urban land cover types in cities. On the other hand, it became a well-known fact that UHI determined by LST analyzes is a temperature dependent climatic phenomenon exposing which urban areas have higher air temperature than their surroundings (Shahmohamadi et al. 2011). Thus, LST dependent thermal analyses became a phenomenon representing heat related local climate condition and distribution over an entire city and city parts under severe thermal risks caused by the heat pollution when LANDSAT MS and fundamentally thermal images are used for the related analyses in high resolutions like 30 m by 30 m land tiles resolution without any gab. This study demonstrates timely changes and decreases in natural areas w.r.t. their normal thermal conditions because of transformation of these natural areas into different types of urban lands and activity areas caused by urban growth in time, then increases in surface temperature and the modified urban microclimate due to these increased LST values and also UHI developments during a certain course of time following UHSs at where they emerge in cities and at where specific urban activities are. Here in this research it is strongly confirmed that industrial sites in urban areas are the major contributors and one of the most candidate sites in urban areas with suspicious industrial activities and certain building structures causing urban hot spots to appear and then heat islands to

develop in time. As it can be seen from the Fig. 13, relative temperature differences for the entire city computed w.r.t. standard deviation of LST distributions through 32 years for each land part in 30 meter by 30 meter tile size can reach up to 7.85 oC. The results also mean that the highest LST standard deviation value in UHI development areas is 7.85 °C higher than those in the coolest sites where they are generally seen at the lands covered by trees in residential areas on flat or smooth terrains without any industrial activities (they are the areas appearing in dark blue color and are marked whit dotted arrows in Fig. 10) and on slopes facing towards north, west or northwest directions (Fig. 6c and 13).

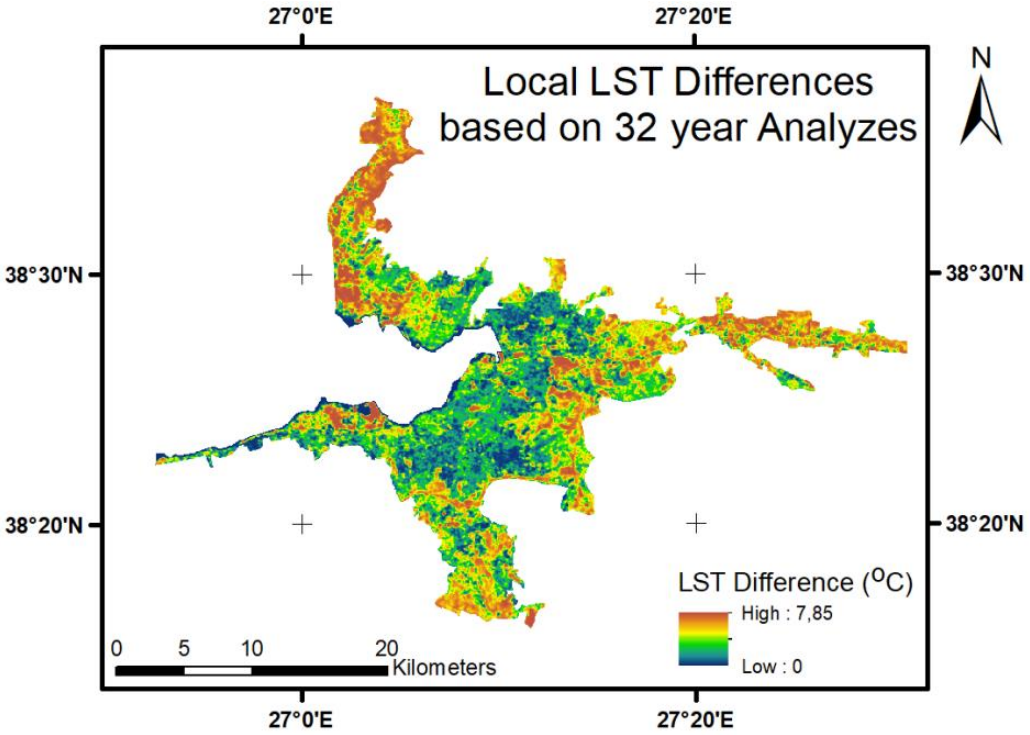

Fig. 13 Distribution of Local LST Differences for the entire city of Izmir.

The sites with industrial facilities using heat for their specific industrial processes and building structures with large and flat metal roofs generally appearing as roof installation style of industrial factories are the most suspicious anthropogenic urban and activity patterns for UHSs to appear and then in time UHIs to form in cities. Therefore, industrial zones cause severe UHI developments over the urban lands where industrial zones are located at and clustered in the city and their affects also extent to the neighboring city parts in great extent. This was also the outcome of our previous research depending on only one day data (Rizwan et al., 2008). Similar results are also reached here in this research, but this time from the analyses of time serious data. Therefore this outcome of the research is now a strongly confirmed with the results from SSI analyses based on time series data. Such type of UHI patterns appearing over industrial zones is seen especially at the three industrial sites in the city of Izmir, the first one is in the Cigli district at the far North city part, the second one is in the Bornova district at the far East city part and the final one is the industrial zone in the Gaziemir district at the far South part of the city. All represent worst temperature conditions causing heat pollution over locally large areas that change and effect natural form of the local climate, living conditions and comfort level in and surrounding areas in these city districts.

LST–NDVI builds a strong negative correlation between thermal condition and vegetation cover in urban lands and even in rural landscapes. The urban sections with trees are remained as preserved natural islands in an impervious, rough and rugged urban sea. Meanwhile LST-NDVI also represents a weak relation in small areas like those vegetated and green lands with rare and short trees appearing mostly in dense urban built-up regions (Fig. 5, Fig. 6a and Fig. 11). High values in a NDVI image is first highly dependent on existence of vegetation and then the types and the state of vegetation based on some factors such as the canopy coverage, maturity, density and height of trees where trees are involved. Normally, high NDVI values are for trees and green vegetation and low NDVI values for built-up areas and bare lands. Moreover, high LST values can basically be related with the increase in built-up areas and bare lands whereas low values are for the increases in forest, wetland and water bodies. The existence of vegetation and water bodies reduces the LST value at that land parts of the city. UHSs generally appear within the UHI zones as high concentrated LST locations. Therefore UHSs affect the neighboring areas and then cause UHIs to develop over those areas. Only the regions in UHI zones where the UHSs or eyes of UHIs appear are under a severe heat stress. With inconsistent urban development, the

UHI zones may worsen the eco-environmental quality and fall under worst ecological condition (Guha et al. 2018).

Moreover, the relationship between LST and non-vegetation urban covers (not including build up areas) represented in this study by SSI-LST and SSI-NDVI distributions based on a 32 years of time series data analyses indicates a strong positive effect of non-vegetated urban lands (like bare, excavated or soil lands and even low vegetated areas such as grassy or bushy urban land parts) on hot spot emergence and heat island developments since these lands have almost a very little or negligible amount of vegetation and water bodies or none of them (Fig. 11). Contrary to that, vegetated areas with mature and/or long trees and with trees having large canopy cover appear as one of the coolest sites in the city and as reducing factor of UHI affect and heat pollution in and around such urban lands.

There is also another contributing factor that carries UHI developments to further severe levels. It is the influence of land aspects depending on the topographical structure of urban lands. If urban land located on a hill slope facing towards either East, South or South-East, these land parts heat up by sun during day time but not losing their temperature during the night times especially in summer seasons and then daily heat accumulates on top of the previous times' temperature which could not reduce much during night times (Fig. 10). This process goes on and on in daily manner and ends up as hot spots on that sites and affects to develop UHIs in time. Thus aspect conditions of urban lands cause these UHI developments influence large areas and widely extent over neighboring city lands especially when it works together with other factors such as industrial zones appearing in special building patterns with very large metal roofs as seen in all three industrial regions in the city mentioned previously and even with bare, excavated or rarely vegetated grassy bushy urban lands on hill slopes facing towards those directions given previously.

Other suspicious city urban features which cause UHSs to appear and then contribute the development of UHIs are wide asphalt roads such as highways passing through cities or occupying surrounding city terrains and large highway intersections (Fig. 9). Asphalt absorbs the incoming energy from the sun and then this process heats up the urban land parts where these roads are. Afterward, asphalt starts to reradiate that absorbed energy in longer wavelengths such as those in thermal wavelength region of electromagnetic spectrum. Thus, wide asphalt roads become another contributing factor causing increase in temperature and heat pollution in that suspicious city parts and they even affect the surrounding urban parts in cities as being experienced in the Izmir case, here in this research.

There is another outcome of this study which is about building structure and building site design pattern. Depending on the SSI-LST analyses here, a dwelling site in Izmir represents quite a cool region. A certain layout pattern of this site consists of several apartment blocks in a discrete order with large common areas between the buildings. These common areas include not paved surfaces (usually which are not encountered in most cases) but green spaces with mature trees which are tall and having large canopy. Other sites with similar layout pattern (even next to this site in Izmir) but with paved surfaces between building blocks as car parking areas appear as one of the contributors of UHI development in the region (Fig. 12). In addition to that, the residential areas supported with commercial activities and buildings and also dwelling units (as apartment blocks, houses and etc.) generally show relatively cool local climates being contrary to the situations encountered in the regions under severe UHI pressures and with suspicious urban structures mentioned earlier since these cool sites include discrete or even row housing buildings and apartment blocks with low-rise storey and generally with tile roofs and most importantly they are recreationally supported by mature and large canopy trees which are closely planted around and just next to the buildings and also at the sides of the streets between these dwelling apartments and houses in the region. This mature and large canopy tree supported recreational area and housing urbanization layout style works together with the heights of low-rise and high-rise storey buildings (no matter they are for dwelling or commercial purposes) and closely planted mature trees for creating significant amount of shadowy regions in these urban sites which are generally located on almost slightly rough terrains in the city (areas with blueish colors and marked by ellipses seen in Fig. 10).

Suggestions for the mitigating the UHI impact on city local climate

As an essence from this study, one can come up with a conclusion such as that, if there would be no industrial sites next to regions where city residents dwell, shop and live and in short, spend most of their out work time or if the industrial zones would be in distant locations to such city zones, the city would be more comfortable than the cases under the pressure of industrial zones and even people's cooling bills would be cut down in residential and commercial buildings and in their cars as well. So this means considerable amount of cost saving in total for cooling issue in cities when city population is taken into consideration especially in metropolitans and then maybe, this would create extra financial resources coming from individuals for supporting more recreational areas and activities at where city residents mostly spent their time in cities with a more comfortable and calm city local climate (temperature) conditions which would need only few centigrade degrees to be cooled down, not as much as that seen in the cases of UHIs.

The above urban areas with above mentioned specific features are all urban regions contributing UHSs to appear and UHIs to develop which make people to live in harsh and uncomfortable environmental conditions and even costly in term of several aspects. Consequently, these outputs of the study suggest us to create a guidance to prevent our cities from such sort of environmental pollution, so thermal pollution caused by aforementioned urban structures. With the light of another outcome of this study it can be suggested a nature based solution. This solution focuses on a future urban forest plantation plan (to grow urban forest) to be taken into consideration at those industrial sites as a priority to mitigate the negative effect of heat islands at and around and even at where they accumulate in cities in an effective, an efficient and a sustainable way. It then promises providing thermal comfort for the residents living close to these sites, reducing sera effect, contributing prevention of climate change, increasing energy save, reducing fossil fuel usage and many more. This will also increase the current city rank to a city rank which is more resilient, sustainable, livable and etc. by only using nature based solutions; tree plantation in a compatible pattern so tall and mature trees with large canopy coverage. This sort of nature based solutions can also be suggested for the highway sides and surrounding terrains as well. In addition to that especially in the industrial zone with large and wide roof and even not tiled but roofing with metal materials it can be suggested some more solutions as those followings to reduce heat causing UHS appearance and UHI development and then to prevent our cities from heat pollution and to restore local climate as comfortable as at the times when people enjoy the natural. The first, the large and wide roofs of existing industrial buildings can be divided in to several sections almost in the extent of normal dwelling building roofs with tiles and then a serious of gable, hip or shed types of roofs with tiles can be installed on one meter high scaffolds and in the case of new industrial buildings, the roof construction plans can be rearranged appropriately or modified with the suggested roof styles. Another solution could be the installation of green roofs on top of existing industrial buildings' roofs even if it is labor intensive and a costly solution, even after the construction it will need continuous care, survival and maintenance attentions. On the other hand, mostly cost effective one could be the setting up a water sprinkle system on top of industrial roofs that sprinkle water in an appropriate time order which is similar to the water sprinkle systems used by municipalities to water grassy urban lands like ring road intersections and also in parks (Tsoka et al., 2020). In the industrial buildings' roof case, a different process than the watering in parks takes place. So, in this case, the water is used for absorbing the heat from industrial building roofs and then for removing it through existing rainwater drainage systems on the roofs. Same approach can be applied to the wide asphalt roads such as highways to remove heat from the road surface (Dong et al., 2019) and then drainage it through the existing road side drainage system. As a side benefit, the heated water can be used for different purposes in the cities as well.

Long term urban LST distribution was studied to determine the thermal and ecological comfort level of Izmir city. In accordance with the statement of that the urban heat island (UHI) effect indicates the higher air and land surface temperature (LST) generated by high amount of near-surface energy emission, solar radiation absorption of ground objects and low rates of evapotranspiration in impervious urbanized areas in comparison with the surrounding non-urbanized regions (Oke, 1997; Rizwan et al., 2008; Buyantuyev and Wu, 2010; Oke, 1982), even w.r.t the results from long term analyzes, several locational urban heat islands (UHIs) were extracted as the most heated zones within the city boundaries in Izmir due to increasing anthropogenic activities, especially like those experienced in the city industrial zones, at where wide roads are and at the slopes facing towards south, east and south-east directions (Fig. 7).

As it is discussed earlier, LST shows a negative strong correlation with NDVI (Fig. 11). Moreover, most of the UHIs even from SSI analyzes are found within none vegetated areas in the Izmir city urban lands appearing as ecologically stressed zones when low vegetated areas seen as low NDVI values in Fig. 11 were compared with the areas in high LST values in Fig. 7. The natural vegetated areas such as forest and agricultural areas found at and around the boundary of urbanized lands of Izmir city as seen in the SSI NDVI image (Fig. 11) appear with low radiant temperatures in the SSI LST image (Fig. 7), so even these long period of data used in this study (compare the areas in Fig. 7 and Fig. 11). Dense vegetation can prevent lands to store high amount of heat in the case bare soil or land and also surfaces with dense vegetation let lose high amount of heat through evapotranspiration w.r.t. the results of the study concluded with that the textures of land cover and land use types and also changes in land use and land cover can have profound effects on the surface radiant temperature (Buyadi et al., 2013), here in this study this is also strongly approved by SSI analyses depending on long period of data. In the same study it is also mentioned that vegetation regulates the radiant temperature in the zones surrounding them up to 100 meters towards built-up areas depending on type and density of vegetation and also water body helps lowering the surface radiant temperature as well. According to the study here using the long period of data, it is shown that UHI effects can reach up to several kilometers from the UHSs by contributing one another into the neighboring regions. So, the LST differences between UHI regions like built-up areas and barren lands and cool sites like vegetated areas reach up to 7.85°C w.r.t. analyses of the standard deviation differences (Fig. 13). The vegetation mitigates high temperature in urban areas by its regulating effect (Fig. 7 and 11). An initiative to replace of loss of natural green spaces is a must in sustainable urbanization approach which offers nature based solutions for such kind of city problems. Thus, such studies could provide an insight and create perception on the effects of vegetation for mitigating UHI phenomenon in built-up areas and could assist

decision makers or planners to plan our cities for a sustainable future with those smart technologies supported by Geospatial Technologies (GeoTech).

Future researches

The results are shown here are the early outcomes of the current stage of the project on local climate change in Izmir over several decades. There are still some sequential research steps to be completed as further stages of the project. First, it will be analyzed the change trend of specific urban lands turned into impervious urban areas (such as those suspicious urban lands mentioned above sections of the paper and appearing as UHSs and causing UHI developments) which were previously natural lands by using NDVI and build-up index with time serious data. For this reason, these sections of the city will be extracted by a classification process using SSI NDVI, Build-up and LST time serious data. Then the correlation will be computed between LSTs from time serious data and these previous natural lands which are urbanized in time by using time serious data of combined NDVI-build-up index algorithm to analyze the impact of above mentioned suspicious urban land cover types on UHI developments. So that, this will let us to find out how effective of each suspicious land type is on UHI development. So, the outcome of this research will help us to develop a heat pollution warning system for smart and sustainable future and calm local climate conditions for our cities.

Acknowledgements I thank the Google Earth Incorporation for providing high resolution data to extract the urban land formations and structures effecting LST distributions especially in cities at where UHSs and UHI appear and develops respectively and also USGS for providing LANDSAT MS time series image data made available for all those analyses done in this research.

Declarations

Authors' contributions
Conceptualization, methodology, formal analysis, writing and original draft preparation, writing, review, and editing, visualization, data acquisition: Corumluoglu Ozsen. Author read and approved the final manuscript.

Funding Not applicable.

Availability of data and materials The datasets used and/or analyzed during the current study are available from the corresponding author on reasonable request.

Ethics approval and consent to participate Not applicable.

Consent for publication Not applicable.

Competing interests The author declares that he has no competing interests.

Author details
University of Izmir Katip Celebi, Faculty of Engineering and Architecture, Geomatics Department, Izmir 35620, Turkey

References

Ahmad, F. and Goparaju, L. (2016). Geospatial Technology in Urban Forest suitability: Analysis for Ranchi, Jharkhand, India. *Ecological Questions,* 24/2016: 45 – 57. http://dx.doi.org/10.12775/EQ.2016.011.

Akbari, H., Pomerantz, M., & Taha, H. (2001). Cool surfaces and shade trees to reduce energy use and improve air quality in urban areas. *Solar Energy*, 70(3), 295–310.

Almazroui, M., Mashat, A., Assiri, M.E. et al. (2017). Application of Landsat Data for Urban Growth Monitoring in Jeddah. *Earth Syst Environ,* 1, 25. https://doi.org/10.1007/s41748-017-0028-4

Amir, S. M., Dongyun, L., Li, P., Rasool, U., Ullah, K. T., Javaid, A. F. T., Wang, L., Fan, B., Rasool, M.A. (2020). Assessment and simulation of land use and land cover change impacts on the land surface temperature of Chaoyang District in Beijing, China. *PeerJ,* 8:e9115 http://doi.org/10.7717/peerj.9115

Amiri, R., Weng, Q., Alimohammadi, A., & Alavipanah, S. K. (2009). Spatial-temporal dynamics of land surface temperature in relation to fractional vegetation cover and land use/cover in the Tabriz urban area, Iran. *Remote Sensing of Environment*, 113, 2606–2617. (https://www.sciencedirect.com/science/article/pii/S0034425712000326)

Anderson, M. C., Allen, R. G., Morse, A., Kustas, W. P. (2012). Use of Landsat thermal imagery in monitoring evapotranspiration and managing water resources. *Remote Sensing of Environment*, Volume 122, Pages 50-65, ISSN 0034-4257, https://doi.org/10.1016/j.rse.2011.08.025.

Asgarian, A., Amiri, B.J., & Sakieh, Y. (2015). Assessing the effect of green cover spatial patterns on urban land surface temperature using landscape metrics approach. *Urban Ecosystems*, 18, 209–222.

Ayanlade, A. (2016). Seasonality in the daytime and night-time intensity of land surface temperature in a tropical city are. *Science of The Total Environment*, Volumes 557–558, Pages 415-424, ISSN 0048-9697,https://doi.org/10.1016/j.scitotenv.2016.03.027.

Bala, R., Prasad, R., Yadav, V. P. (2020). A comparative analysis of day and night land surface temperature in two semi-arid cities using satellite images sampled in different seasons. *Advances in Space Research*, Volume 66, Issue 2, Pages 412-425, ISSN 0273-1177, https://doi.org/10.1016/j.asr.2020.04.009.

Barbierato, E., Bernetti, I., Capecchi, I. & Saragosa, C. (2019). Quantifying the impact of trees on land surface temperature: a downscaling algorithm at city-scale. *European Journal of Remote Sensing*, 52:sup4, 74-83, DOI: 10.1080/22797254.2019.1646104

Bendib, A., Dridi, H., & Kalla, M.I. (2017). Contribution of Landsat 8 data for the estimation of land surface temperature in Batna city, Eastern Algeria. *Geocarto International*, 32(5), 503–513.

Boryan, C., Yang, Z., Mueller, R., Craig, M. (2011). Monitoring US agriculture: The US Department of Agriculture, National Agricultural Statistics Service, Cropland Data Layer Program. *Geocarto Int*. 26, 341–358.

Bowker, David E. (2010). Spectral Reflectances of Natural Targets for Use in Remote Sensing Studies 1139. cilt/*NASA reference publication* (NASA)/USA, 5 Eki 2010, 185 p.

Brown, H., Proust, K., Newell, B., Spickett, J., Capon, T., Bartholomew, L. (2018). Cool Communities—Urban Density, Trees, and Health. *International Journal of Environmental Research and Public Health*. 15(7):1547.

Buyadi, S. N. A., Wan Mohd, W. M. N., & Misni, A. (2013). The Impact of Land Use Changes on the Surface Temperature Distribution of Area Surrounding the National Botanic Garden, Shah Alam. *AMER International Conference on Quality of Life* (p. 10). Pulau Langkawi.

Buyadi, S. N. A., Wan Mohd, W. M. N., & Misni, A. (2014). Quantifying Green Space Cooling Effects on the Urban Microclimate using Remote Sensing and GIS Techniques. *FIG Congress 2014*, Engaging the Challenges – Enhancing the Relevance Kuala Lumpur, Malaysia 16-21 June 2014.

Buyantuyev, A., & Wu, J. (2010). Urban heat islands and landscape heterogeneity: Linking spatiotemporal variations in surface temperatures to land-cover and socioeconomic patterns. *Landscape Ecology*, 25, 17–33.

Camilloni, I., Barros, V. (1997). On the urban heat island effect dependence on temperature trends. *Clim. Change*. 37, 665-681.

Chander, G., and Markham, B. (2003). Revised Landsat-5 TM radiometric calibration procedures and postcalibration dynamic ranges. *IEEE Transactions on Geoscience and Remote Sensing*, vol. 41, no. 11, pp. 2674-2677, Nov. 2003. doi: 10.1109/TGRS.2003.818464.

Chander, G., Markham, B. L., Barsi, J.A. (2007). Revised Landsat-5 Thematic Mapper Radiometric Calibration. *IEEE Geoscience and Remote Sensing Letters*, vol. 4, no. 3, pp. 490-494, July 2007. doi: 10.1109/LGRS.2007.898285.

Chander, G., Markham, B. L., Helder, D. L. (2009). Summary of current radiometric calibration coefficients for Landsat MSS, TM, ETM+, and EO-1 ALI sensors. *Remote Sensing of Environment*, Volume 113, Issue 5, Pages 893-903. ISSN 0034-4257, https://doi.org/10.1016/j.rse.2009.01.007.

Chaudhuri, S., Kumar, A. (2021). Evaluating the contribution of urban ecosystem services in regulating thermal comfort. *Spat. Inf. Res.* 29, 71–82. https://doi.org/10.1007/s41324-020-00336-8

Chen, A., Yao, X.A., Sun, R., & Chen, L. (2014). Effect of urban green patterns on surface urban cool islands and its seasonal variations. *Urban Forestry & Urban Greening*, 13, 646–654.

Chen, Q., Ren, J., Li, Z., Ni, C. (2009). Urban Heat Island Effect Research in Chengdu City Based on MODIS Data. *In Proceedings of 3rd International Conference on Bioinformatics and Biomedical Engineering, ICBBE 2009*, Beijing, China, 11–13 June 2009. pp. 1-5.

Chen, X., Ding, J., Wang, J., Ge, X., Raxidin, M., Liang, J., Chen, X., Zhang, Z., Cao, X., Ding, Y. (2020). Retrieval of Fine-Resolution Aerosol Optical Depth (AOD) in Semiarid Urban Areas Using Landsat Data: A Case Study in Urumqi, NW China. *Remote Sens.,* 12, 467.

Chen, X.C., Zhao, H.M., Li, P.X., & Yin, Z.Y. (2006). Remote sensing image-based analysis of the relationship between urban heat island and land use/cover changes. *Remote Sensing of Environment*, 104(2), 133–146.

Chen, Y., Wang, J., & Li, X. (2002). A study on urban thermal field in summer based on satellite remote sensing. *Remote Sensing for Land Management and Planning*, 4, 55–59.

Chen, Y.C., Chiu, H.W., Su, Y.F., Wu, Y.C., Cheng, K.S. (2016). Does urbanization increase diurnal land surface temperature variation? Evidence and implications. *Landsc. Urban Plan.*, 157, 247–258. http://dx.doi.org/10.1016/j.landurbplan.2016.06.014.

Cheng, K.S., Su, Y.F., Kuo, F.T., Hung, W.C., Chiang, J.L. (2008). Assessing the effect of landcover on air temperature using remote sensing images: a pilot study in northern Taiwan. *Landsc. Urban Plan*., 85(2) 85–96. http://dx.doi.org/10.1016/j.landurbplan.2007.09.014.

Choi, H., Lee, W., & Byun, W. (2012). Determining the Effect of Green Spaces on Urban Heat Distribution Using Satellite Imagery. *Asian Journal of Atmospheric Environment*, 6(June), 127-135. doi:http://dx.doi.org/10.5572/ajae.2012.6.2.127.

Corumluoglu, O., Asri, I. (2015). The effect of urban heat island on Izmir's city ecosystem and climate. *Environ Sci. Pollut. Res.,* 22, 3202–3211. https://doi.org/10.1007/s11356-014-2874-z

Coseo, P., & Larsen, L. (2014). How factors of land use/land cover, building configuration, and adjacent heat sources and sinks explain urban heat islands in Chicago. *Landscape and Urban Planning*, 125, 117–129.

Coutts, A.M., White, E.C., Tapper, N.J., Beringer, J., & Livesley, S.J. (2016). Temperature and human thermal comfort effects of street trees across three contrasting street canyon environments. *Theoretical and Applied Climatology*, 124(55), 55–68.

Dadras, M., Shafri, H. Z. M., Ahmad, N., Pradhan, Bi., Safarpour, S. (2014). Land Use/Cover Change Detection and Urban Sprawl Analysis in Bandar Abbas City, Iran. *The Scientific World Journal*. vol. 2014, Article ID 690872, 12 pages. https://doi.org/10.1155/2014/690872.

Deilami, K., & Kamruzzaman, M. (2017). Modelling the urban heat island effect of smart growth policy scenarios in Brisbane. *Land Use Policy*, 64, 38–55.

Detwiller, J. (1970). Deep soil temperature trends and urban effects at Paris. *J. Appl. Meteorol*., 9, 178-180.

Dong, Q., Wang, C., Xiong, C., Li, X., Wang, H., & Ling, T. (2019). Investigation on the Cooling and Evaporation Behavior of Semi-Flexible Water Retaining Pavement based on Laboratory Test and Thermal-Mass Coupling Analysis. *Materials* (Basel, Switzerland), 12(16), 2546. https://doi.org/10.3390/ma12162546

Dousset, B., Gourmelon, F., (2003). Satellite multi-sensor data analysis of urban surface temperatures and landcover. *ISPRS J. Photogramm. Remote Sens.,* 58:43–54. http://dx.doi. org/10.1016/S0924-2716(03)00016-9.

Du, H.,Wang, D.,Wang, Y., Zhao, X., Qin, F., Jiang, H.,&Cai, Y. (2016a). Influences of land cover types, meteorological conditions, anthropogenic heat and urban area on surface urban heat island in the Yangtze River Delta urban agglomeration. *Science of the Total Environment*, 571, 461–470.

Du, S., Xiong, Z., Wang, Y., & Guo, L. (2016b). Quantifying the multilevel effects of landscape composition and configuration on land surface temperature. *Remote Sensing of Environment*, 178, 84–92.

El Garouani, A., Mulla, D.J., El Garouani, S., Knight, J. (2017). Analysis of urban growth and sprawl from remote sensing data: Case of Fez, Morocco. *International Journal of Sustainable Built Environment*. Volume 6, Issue 1, Pages 160-169, ISSN 2212-6090. https://doi.org/10.1016/j.ijsbe.2017.02.003.

Estoque, R.C., Murayama, Y., & Myint, S.W. (2017). Effects of landscape composition and pattern on land surface temperature: An urban heat island study in the megacities of southeast Asia. *Science of the Total Environment*, 577, 349–359.

Fang, Chih-Fang and Ling, Der-Lin (2005). Guidance for noise reduction provided by tree belts. *Landscape and Urban Planning*, Volume 71, Issue 1, 28 February 2005, Pages 29-34.

Feyisa, G.L., Meilby, H., Jenerette, G.D., & Pauliet, S. (2016). Locally optimized separability enhancement indices for urban land cover mapping: Exploring thermal environmental consequences of rapid urbanization in Addis Ababa, Ethiopia. *Remote Sensing of Environment*, 175, 14–31.

Filho, W. L., Icaza, L. E., Neht, A., Klavins, M., Morgan, E. A. (2018). Coping with the impacts of urban heat islands. A literature based study on understanding urban heat vulnerability and the need for resilience in cities in a global climate change context. *Journal of Cleaner Production*, Volume 171, 2018, Pages 1140-1149. ISSN 0959-6526, https://doi.org/10.1016/j.jclepro.2017.10.086.

Firoozi, F., Mahmoudi, P., Jahanshahi, S.M.A. et al. (2020). Modeling changes trend of time series of land surface temperature (LST) using satellite remote sensing productions (case study: Sistan plain in east of Iran). *Arab J Geosci,* 13, 367 (2020). https://doi.org/10.1007/s12517-020-05314-w

Forkel, M., Carvalhais, N., Verbesselt, J., Mahecha, M.D., Neigh, C.S.R., Reichstein, M. (2013). Trend Change Detection in NDVI Time Series: Effects of Inter-Annual Variability and Methodology. *Remote Sensing*. 5(5):2113-2144. https://doi.org/10.3390/rs5052113

Fukui, E. (1970). The recent rise of temperature in Japan. In Japanese Progress in Climatology; Tokyo University of Education: Tokyo, Japan, pp. 46-65.

Gago, E. J., Roldan, J., Pacheco-Torres, R., & Ordóñez, J. (2013). The City and Urban Heat Islands: A Review of Strategies to Mitigate Adverse Effects. *Renewable and Sustainable Energy Reviews*, 25, 749–758. doi:10.1016/j.rser.2013.05.057.

Gao, B.C. (1996). NDWI—A normalized difference water index for remote sensing of vegetation liquid water from space. *Remote Sens. Environ*. 58, 257–266.

Gartland, L. (2008). Heat Islands: Understanding and Mitigating Heat in Urban Areas (1st ed.). London, United Kingdom. *Earthscan*. https://doi.org/10.4324/9781849771559

Georgescu, M., Moustaoui, M., Mahalov, A., & Dudhia, J. (2011). An alternative explanation of the semiarid urban area "oasis effect". *Journal of Geophysical Research*, 116, D24113.

Georgi, N. J., & Zafiriadis, K. (2006). The Impact of Park Trees on Microclimate in Urban Areas. *Urban Ecosystems*, 9(3), 195–209. doi:10.1007/s11252-006-8590-9

Giannopoulou, K., Santamouris, M., Livada, I. et al. (2010). The Impact of Canyon Geometry on Intra Urban and Urban: Suburban Night Temperature Differences Under Warm Weather Conditions. *Pure Appl. Geophys*. 167, 1433–1449. https://doi.org/10.1007/s00024-010-0099-8

Gillner, S., Vogt, J., Tharang A., Dettmann, S., Roloff, A. (2015). Role of street trees in mitigating effects of heat and drought at highly sealed urban sites. *Landscape and Urban Planning*, Volume 143, Pages 33-42.ISSN 0169-2046, https://doi.org/10.1016/j.landurbplan.2015.06.005.

Gong, P., Wang, J., Yu, L., Zhao, Y., Liang, L., Niu, Z., Huang, X., Fu, H., Liu, S., Li, C., et al. (2013). Finer resolution observation and monitoring of global land cover: First mapping results with Landsat TM and ETM+ data. *Int. J. Remote Sens*. 34, 2607–2654.

Guha, S., Govil, H. (2021). An assessment on the relationship between land surface temperature and normalized difference vegetation index. *Environ Dev Sustain*. 23, 1944–1963. https://doi.org/10.1007/s10668-020-00657-6

Guha, S., Govil, H., Dey, A., Gill, N. (2018). Analytical study of land surface temperature with NDVI and NDBI using Landsat 8 OLI and TIRS data in Florence and Naples city, Italy. *European Journal Of Remote Sensing*, Vol. 51, No. 1, 667–678. https://doi.org/10.1080/22797254.2018.1474494

Guha, S., Govil, H., Sandip, M. (2017). Dynamic analysis and ecological evaluation of urban heat islands in Raipur city, India. *Journal of Applied Remote Sensing*, 11(3), 036020. https://doi.org/10.1117/1.JRS.11.036020

Gunlu, E., Pirnar, İ., Yagci, K. (2009). Preserving Cultural Heritage and Possible Impacts on Regional Development: Case of İzmir. *International Journal of Emerging and Transition Economies*, Vol.2, Issue 2, 213-229.

Guo-Yu Ren (2015). Urbanization as a major driver of urban climate change. *Advances in Climate Change Research*, Volume 6, Issue 1, Pages 1-6. ISSN 1674-9278. https://doi.org/10.1016/j.accre.2015.08.003.

He, C.Y., Liu, Z.F., Tian, J., Ma, Q. (2014). Urban expansion dynamics and natural habitat loss in China: A multiscale landscape perspective. *Glob. Chang. Biol*. 20, 2886–2902.

Howard, L. (1833). The Climate of London; London Harvey and Dorton: London, UK. Volume 2.

Huang, M., Cui, P., He, X. (2018). Study of the Cooling Effects of Urban Green Space in Harbin in Terms of Reducing the Heat Island Effect. *Sustainability*. 10(4), 1101. https://doi.org/10.3390/su10041101

Jenerette, G.D., Harlan, S.L., Brazel, A., Jones, N., Larsen, L., & Stefanov, W.L. (2007). Regional relationships between surface temperature, vegetation, and human settlement in a rapidly urbanizing ecosystem. *Landscape Ecology*, 22, 353–365.

Jia, G., Zhang, L., Zhu, L., Xu, R., Liang, D., Xu, X., Ba, T. (2020). Digital Earth for Climate Change Research. In: Guo H., Goodchild M.F., Annoni A. (eds). *Manual of Digital Earth*. Springer, Singapore. https://doi.org/10.1007/978-981-32-9915-3_14

Joshi, J. P. and Bhatt, B., (2012). Estimating temporal land surface temperature using remote sensing: a study of vadodara urban, Gujarat. *International Journal of Geology, Earth and Environmental Sciences*, vol. 2, pp. 123–130.

Gunawardena, K.R., Wells, M.J., Kershaw, T. (2017). Utilising green and bluespace to mitigate urban heat island intensity. *Science of The Total Environment*, Volumes 584–585, Pages 1040-1055. ISSN 0048-9697, https://doi.org/10.1016/j.scitotenv.2017.01.158.

Gupta, N., Mathew, A., Khandelwal, S. (2019). Analysis of cooling effect of water bodies on land surface temperature in nearby region: A case study of Ahmedabad and Chandigarh cities in India. *The Egyptian Journal of Remote Sensing and Space Science*, Volume 22, Issue 1, Pages 81-93. ISSN 1110-9823, https://doi.org/10.1016/j.ejrs.2018.03.007.

Kafer, P. S., Rolim, S. B. A., Diaz, L. R., Rocha, N. S., Iglesias, M. L., Rex, F. E. (2020). Comparative Analysis Of Split-Window And Single-Channel Algorithms For Land Surface Temperature Retrieval of A Pseudo-Invariant Target. *Boletim de Ciências Geodésicas*, 26(2), e2020008. Epub June 12, 2020. https://doi.org/10.1590/s1982-21702020000200008

Kalma, J.D., McVicar, T.R., McCabe, M.F. (2008). Estimating land surface evaporation: A review of methods using remotely sensed surface temperature data. *Surv. Geophys*, 29, 421–469.

Kalnay, E., & Cai, M. (2003). Impact of urbanization and land-use change on climate. *Nature*, 423, 528–553.

Kershaw, T. (2017). The urban heat island (UHI), Climate Change Resilience in the Urban Environment. IOP Publishing, 2053-2563, Book Chapter, 4-44, 2017. doi = 10.1088/978-0-7503-1197-7ch4, isbn 978-0-7503-1197-7.

Kii, M., Nakamura, K. (2017). Development of a suitability model for estimation of global urban land cover. *Transp. Res. Procedia*., 25, 3165–3177.

Kim, H.H. (1992). Urban Heat Island. *Int. J. Remote Sens*., 13, 2319-2336.

Kleerekoper, L., van Esch, M., & Salcedo, T.B. (2012). How to make a city climate-proof, addressing the urban heat island effect. *Resource Conservation Recycling*, 64, 30–38. ISSN 0921-3449, https://doi.org/10.1016/j.resconrec.2011.06.004.

Koomen, E., Diogo, V. (2017). Assessing potential future urban heat island patterns following climate scenarios, socio-economic developments and spatial planning strategies. *Mitig Adapt Strateg Glob Change*, 22, 287–306. https://doi.org/10.1007/s11027-015-9646-z

Kuang, W.H., Liu, J.Y.; Zhang, Z.X.; Liu, D.S.; Xiang, B. (2013). Spatiotemporal dynamics of impervious surface areas across China during the early 21st century. *Chin. Sci. Bull*., 58, 1691–1701.

Kumar, K. S., Bhaskar, P. U., & Padmakumari, K. (2012). Estimation of Land Surface Temperature to Study Urban Heat Island Effect Using Landsat ETM + IMAGE. *International Journal of Engineering Science and Technology (IJEST)*, 4(02), 771–778.

Landsberg, H.E. (1981). The Urban Climate; Academic Press: New York, NY, USA. pp. 84-89.

Lee, K., Kim, Y., Sung, H.C., Ryu, J., Jeon, S.W. (2020). Trend Analysis of Urban Heat Island Intensity According to Urban Area Change in Asian Mega Cities. *Sustainability*, 12(1):112.

Li, J.,Wang, Y., Shen, X.,&Song, Y. (2004). Landscape pattern analysis along an urban–rural gradient in the Shanghai metropolitan region. *Acta Ecologica Sinica*, 24, 1973–1980.

Li, Y., Schubert, S., Kropp, J.P., Kropp, J. P., Rybskio, D. (2020). On the influence of density and morphology on the Urban Heat Island intensity. *Nat Commun.*, 11, 2647. https://doi.org/10.1038/s41467-020-16461-9

Lim, H. S., MatJafri, M. Z., Abdullah, K. and Wong, C. J. (2009). Air Pollution Determination Using Remote Sensing Technique. *Advances in Geoscience and Remote Sensing*, Gary Jedlovec, IntechOpen, DOI: 10.5772/8319. Available from: https://www.intechopen.com/books/advances-in-geoscience-and-remote-sensing/air-pollution-determination-using-remote-sensing-technique

Lin, B., & Lin, Y. (2010). Cooling Effect of Shade Trees with Different Characteristics in a Subtropical Urban Park. *Science horts*, 45(1), 83-86, Jan 23, 2021. https://journals.ashs.org/hortsci/view/journals/hortsci/45/1/article-p83.xml

Liu, L., Zhang, Y. (2011). Urban Heat Island analysis using the Landsat TM data and ASTER data: a case study in Hong Kong. *Remote Sens.* 3:1535–1552. http://dx.doi.org/10.3390/rs3071535.

Livesley, S. J., McPherson, E. G., Calfapietra, C. (2016). The Urban Forest and Ecosystem Services: Impacts on Urban Water, Heat, and Pollution Cycles at the Tree, Street, and City Scale. *Journal of Environmental Quality*, 45, 1, pp 119-124. 10.2134/jeq2015.11.0567.

Lopez, J.M.R., Heider, K., & Scheffran, J. (2017). Frontiers of urbanization: Identifying and explaining urbanization hot spots in the south of Mexico City using human and remote sensing. Applied Geography, 79, 1–10.

Lu, D.S., Li, G.Y., Kuang, W.H., Moran, E. (2014). Methods to extract impervious surface areas from satellite images. *Int. J. Digit. Earth.* 7, 93–112.

Lu, Y., Feng, P., Shen, C., Sun, J. (2009). Urban Heat Island in Summer of Nanjing Based on TM Data. *Proceedings of 2009 Joint Urban Remote Sensing Event*, Shanghai, China, 20–22 May 2009, pp. 1-5.

Lutz, W., Sanderson, W., Scherbov, S. (2001). The end of world population growth. *Nature*. 412, 543–545. Plos ONE. 6, e23777.

Majkowska, A., Kolendowicz, L., Półrolniczak, M., Hauke, J., Czernecki, B. (2017). The urban heat island in the city of Poznań as derived from Landsat 5 TM. *Theor Appl Climatol*, 128, 769–783. https://doi.org/10.1007/s00704-016-1737-6

Mallick, J., Kant, Y., Bharath, B. D. (2008). Estimation of Land Surface Temperature Over Delhi using Landsat-7 ETM +. *J. Ind. Geophys.* Union, 12(3), 131–140.

Mejbel, S. M., Zakariya, J. O., Hassoon, I. K., & Jameel, A. A. (2018). Land Surface Temperature Retrieval from LANDSAT-8 Thermal Infrared Sensor Data and Validation with Infrared Thermometer Camera. *International Journal of Engineering & Technology*, 7(4.20), 608-612. doi:http://dx.doi.org/10.14419/ijet.v7i4.20.27402

Memon, R. A., Leung, D. Y. C., & Chunho, L. (2008). A Review on the Generation, Determination and Mitigation of Urban Heat Island. *Journal of Environmental Sciences (China)*, 20(1), 120–8. Retrieved from http://www.ncbi.nlm.nih.gov/pubmed/18572534

Miralles, D.G., Holmes, T.R.H., de Jeu, R.A.M., Gash, J.H., Meesters, A.G.C.A., Dolman, A.J. (2011). Global land-surface evaporation estimated from satellite-based observations. *Hydrol. Earth Syst. Sci.*, 15, 453–469.

Mohajerani, A., Bakaric, J., Jeffrey-Bailey, T. (2017). The urban heat island effect, its causes, and mitigation, with reference to the thermal properties of asphalt concrete, *Journal of Environmental Management*, Volume 197, Pages 522-538, ISSN 0301-4797. https://doi.org/10.1016/j.jenvman.2017.03.095.

Mohammad, P., Goswami, A., & Bonafoni, S. (2019). The Impact of the Land Cover Dynamics on Surface Urban Heat Island Variations in Semi-Arid Cities: A Case Study in Ahmedabad City, India, Using Multi-Sensor/Source Data. *Sensors* (Basel, Switzerland), 19(17), 3701. https://doi.org/10.3390/s19173701

Mohammed, Y., Salman, A. (2018). Effect of urban geometry and green area on the formation of the urban heat island in Baghdad city. *MATEC Web Conf.*, 162 05025. DOI: https://doi.org/10.1051/matecconf/201816205025

Mohan, M., (2000). Climate change: evaluation of ecological restoration of Delhi ridge using remote sensing and GIS technologies. *International Archives of Photogrammetry and Remote Sensing*, vol. 33, pp. 886–894.

Mushore, T. D., Mutanga, O., Odindi, J., Dube, T. (2017). Assessing the potential of integrated Landsat 8 thermal bands, with the traditional reflective bands and derived vegetation indices in classifying urban landscapes. *Geocarto International*, 32:8, 886-899, DOI: 10.1080/10106049.2016.1188168

Mustafa, E.K., Liu, G., Abd El-Hamid, H.T., Kaloop, M. R. (2019). Simulation of land use dynamics and impact on land surface temperature using satellite data. *GeoJournal*. https://doi.org/10.1007/s10708-019-10115-0.

Mutiibwa, D., Strachan, S. and Albright, T. (2015). Land Surface Temperature and Surface Air Temperature in Complex Terrain. *IEEE Journal of Selected Topics in Applied Earth Observations and Remote Sensing*, vol. 8, no. 10, pp. 4762-4774, Oct. 2015, doi: 10.1109/JSTARS.2015.2468594.

Nazeer, M., Nichol, J. E., Yung, Y.-K. (2014). Evaluation of atmospheric correction models and Landsat surface reflectance product in an urban coastal environment. *International Journal of Remote Sensing*, 35:16, 6271-6291, DOI: 10.1080/01431161.2014.951742

Ng, E., Chen, L., Wang, Y., & Yuan, C. (2012). A study on the cooling effects of greening in a high from-density city : an experience Hong Kong. *Building and Environment*, 47, 256 271. doi:10.1016/j.buildenv.2011.07.014 ,

Nichol, J. E., Fung, W. Y., Lam, Ka-se, Wong, M. S. (2009). Urban heat island diagnosis using ASTER satellite images and 'in situ' air temperature. *Atmospheric Research*, Volume 94, Issue 2, Pages 276-284. ISSN 0169-8095 https://doi.org/10.1016/j.atmosres.2009.06.011.

Nie, Q., Man, W., Li, Z., & Huang, Y. (2016). Spatiotemporal impact of urban impervious surface on land surface temperature in Shanghai, China. *Canadian Journal of Remote Sensing*, 42(6), 680–689.

Oke, T.R. (1982). The energetic basis of the urban heat island. *Quarterly Journal of the Royal Meteorological Society*, 108, 1–24.

Oke, T.R. (1997). Urban climates and global change. In A. Perry & R. Thompson (Eds.). *Applied climatology: Principles and practices*, pp. 273–287. London: Routledge.

Oliveira, S., Andrade, H., & Vaz, T. (2011). The Cooling Effect of Green Spaces as a Contribution to the Mitigation of Urban Heat: A Case Study in Lisbon. *Building and Environment*, 46(11), 2186–2194. doi:10.1016/j.buildenv.2011.04.034

O'Malley, C., Piroozfarb, P.A.E., Farr, E.R.P., Gates, J. (2014). An Investigation into Minimizing Urban Heat Island (UHI) Effects: A UK Perspective. *Energy Procedia*, Volume 62, Pages 72-8. ISSN 1876-6102, https://doi.org/10.1016/j.egypro.2014.12.368. (http://www.sciencedirect.com/science/article/pii/S1876610214033992)

Peng, J., Xie, P., Liu, Y., & Ma, J. (2016). Urban thermal environment dynamics and associated landscape pattern factors: A case study in the Beijing metropolitan region. *Remote Sensing of Environment*, 173, 145–155.

Pickett, S.T.A., Cadenasso, M.L., Grove, J.M., Boone, C.G., Groffman, P.M., Irwin, E., Kaushal, S.S., Marshall, V., McGrath, B.P., Nilon, C.H., Pouyat, R.V., Szlavecz, K., Troy, A., Warren, P. (2011). Urban ecological systems: scientific foundations and decade of progress. *J. Environ. Manag.* 92 (3), 331–362. http://dx.doi.org/10.1016/j.jenvman.2010.08.022.

Putra, M. I. J., Affandani, A. Y., Widodo, T., & Wibowo, A. (2019). Spatial Multi-Criteria Analysis for Urban Sustainable Built Up Area Based on Urban Heat Island in Serang City. *IOP Conference Series: Earth and Environmental Science*, 338(1), [012025]. https://doi.org/10.1088/1755-1315/338/1/012025

Qin, Z., Zhang, M., Amon, K., Pedro, B. (2001). Mono-window Algorithm for retrieving land surface temperature from Landsat TM 6 data. *Acta Geogr.* Sinica 2001, 56, 456-466).

Qiu, G., Li, H., Zhang, Q., Chen, W., Liang, X., & Li, X. (2013). Effects of Evapotranspiration on Mitigation of Urban Temperature by Vegetation and Urban Agriculture. *Journal of Integrative Agriculture*, 12(8), 1307–1315. doi:10.1016/S2095- 3119(13)60543-2.

Rajabi, T., Abu-Hijleh, B. (2014). The Study of Vegetation Effects on Reduction of Urban Heat Island in Dubai. *World Sustainable Building Barcelona Conference*, 28 Oct 2014 - 30 Oct 2014, Volume 7, 7 p.http://www.irbnet.de/daten/iconda/CIB_DC28619.pdf

Rehan, R. M. (2016). Cool city as a sustainable example of heat island management case study of the coolest city in the world. *HBRC Journal*, Volume 12, Issue 2, Pages 191-204. ISSN 1687-4048, https://doi.org/10.1016/j.hbrcj.2014.10.002.

Ren, Y., Deng, L.Y., Zuo, S.D., Song, X.D., Liao, Y.L., Xu, X.D., Li, Z.W. (2016). Quantifying the influences of various ecological factors on land surface temperature of urban forests. *Environmental Pollution*, 216, 519–529.

Reza, A., Weng, Q.H., Abbas, A., Seyed, K.A. (2009). Spatial-temporal dynamics of land surface temperature in relation to fractional vegetation cover and land use/cover in the Tabriz urban area. *Remote Sens. Environ*. 113, 2606–2617.

Riffat, S., Powell, R. & Aydin, D. (2016). Future cities and environmental sustainability. *Fut Cit & Env*. 2, 1. https://doi.org/10.1186/s40984-016-0014-2

Rizwan, A.M., Dennis, L.Y.C., & Liu, C. (2008). A review on the generation, determination and mitigation of urban heat island. *Journal of Environmental Sciences*, 20, 120–128.

Robinove, C.J. (1982). Computation with physical values from Landsat digital data. *Photogrammetric Engineering and Remote Sensing*, USGS Publications Warehouse, 48, 5, pp 781-784. http://pubs.er.usgs.gov/publication/70011466

Saffuan, R., Ariffin, J., & Amin, Z. (2018). Green Technology Design Approach for Liveable Park of Tasik Biru Kundang, Malaysia. *Asian Journal of Environmental-Behaviour Studies*, 3(7), p.91-98.

Sangiorgio, V., Fiorito, F. & Santamouris, M. (2020). Development of a holistic urban heat island evaluation methodology. *Scientific Reports*, 10, 17913 (2020). https://doi.org/10.1038/s41598-020-75018-4

Santamouris, M. (2013). Using cool pavements as a mitigation strategy to fight urban heat island: a review of the actual developments. *Renew. Sust. Energ. Rev*. 26:224–240. http://dx.doi.org/10.1016/j.rser.2013.05.047.

Santamouris, M. (2019). Chapter 8 - Mitigating the Local Climatic Change and Fighting Urban Vulnerability, Editor(s): Matthaios Santamouris, Minimizing Energy Consumption, Energy Poverty and Global and Local Climate Change in the Built Environment: Innovating to Zero, Elsevier, Pages 223-307, ISBN 9780128114179, https://doi.org/10.1016/B978-0-12-811417-9.00008-8.

Schneider, A. (2012). Monitoring land cover change in urban and pen-urban areas using dense time stacks of Landsat satellite data and a data mining approach. *Remote Sens. Environ*. 124, 689–704.

Sekertekin, A., Bonafoni, S. (2020). Land Surface Temperature Retrieval from Landsat 5, 7, and 8 over Rural Areas: Assessment of Different Retrieval Algorithms and Emissivity Models and Toolbox Implementation. *Remote Sens*., 12, 294. https://doi.org/10.3390/rs12020294

Senanayake, I. P., Welivitiya, W. D. D. P., & Nadeeka, P. M. (2013). Remote Sensing Based Analysis of Urban Heat Islands with Vegetation Cover in Colombo city, Sri Lanka using Landsat-7 ETM+ data. *Urban Climate*, doi:10.1016/j.uclim.2013.07.004.

Shafaghat, A., Manteghi, G., Keyvanfar, A., Bin Lamit, H., Saito, K., Ossen, D. R. (2016). Street Geometry Factors Influence Urban Microclimate in Tropical Coastal Cities: A Review. *Environmental and Climate Technologies*, 17(1), 61-75. doi: https://doi.org/10.1515/rtuect-2016-0006

Shahmohamadi, P., Che-Ani, A. I., Maulud, K. N. A., Tawil, N. M., Abdullah, N. A. G. (2011). The Impact of Anthropogenic Heat on Formation of Urban Heat Island and Energy Consumption Balance. *Urban Studies Research*, vol. 2011, Article ID 497524, 9 pages. https://doi.org/10.1155/2011/497524

Shahmohamadi, P., Sairi, A., & Surat, M. (2009). Mitigating the Urban Heat Island Effect : Some Points without Altering Existing City Planning. *European Journal of Scientific Research*, 35(2), 204–216.

Solecki, W. D., Rosenzweig, C., Pope, G., Chopping, M., & Goldberg, R. (2004). Urban Heat Island and Climate Change : An Assessment of Interacting and Possible Adaptations in the Camden, New Jersey Region. New Jersey. p 5. www.nj.gov/dep/dsr/research/Urban Heat Island and Climate Change-RPS.pdf

Son, Nguyen-Thanh, Thanh, Bui-Xuan (2018). Decadal assessment of urban sprawl and its effects on local temperature using Landsat data in Cantho city, Vietnam. *Sustainable Cities and Society*. Volume 36, Pages 81-91, ISSN 2210-6707, https://doi.org/10.1016/j.scs.2017.10.010.

Song, Dan-Xia, Huang, C., Sexton, J.O., Channan, S., Feng, M., Townshend, J.R., (2015). Use of Landsat and Corona data for mapping forest cover change from the mid-1960s to 2000s: Case studies from the Eastern United States and Central Brazil. *ISPRS Journal of Photogrammetry and Remote Sensing*, Volume 103, Pages 81-92. ISSN0924-2716, https://doi.org/10.1016/j.isprsjprs.2014.09.005.(http://www.sciencedirect.com/science/article/pii/S0924271614002305)

Song, J., Du, S., Feng, X., & Guo, L. (2014). The relationships between landscape compositions and land surface temperature: Quantifying their resolution sensitivity with spatial regression models. *Landscape and Urban Planning*, 123, 145–157.

Song, Z., Li, R., Qiu, R., Liu, S., Tan, C., Li, Q., Ge, W., Han, X., Tang, X., Shi, W., Song, L., Yu, W., Yang, H., Ma, M. (2018). Global Land Surface Temperature Influenced by Vegetation Cover and PM2.5 from 2001 to 2016. *Remote Sensing*, 10(12):2034. https://doi.org/10.3390/rs10122034

Stone, B., Jr. (2007). Urban sprawl and air quality in large US cities. *Journal of Environmental Management*, 86, 688–698.

Streutker, D.R. (2002). A remote sensing study of the urban heat island of Houston, Texas. *Int. J. Remote Sens*. 23, 2595-2608.

Sun, Q., Tan, J., Xu, Y. (2010). An ERDAS image processing method for retrieving LST and describing urban heat evolution: a case study in the Pearl River Delta Region in South China. *Environ. Earth Sci.* 59 (5), 1047–1055.

Sun, Y., Zhao, S.Q., Qu,W.Y. (2015). Quantifying spatiotemporal patterns of urban expansion in three capital cities in Northeast China over the past three decades using satellite data sets. *Environ. Earth Sci*. 73, 7221–7235.

Sun Z., Wang, Q., Batkhishig, O., Ouyang, Z. (2016). Relationship between Evapotranspiration and Land Surface Temperature under Energy- and Water-Limited Conditions in Dry and Cold Climates. *Advances in Meteorology*, vol. 2016, Article ID 1835487, 9 pages. https://doi.org/10.1155/2016/1835487

Takeuchi, W., Hashim, N., & Thet, K. M. (2010). Application of RS and GIS for Monitoring UHI in KL Metropolitan Area. *MAp Asia 2010 & ISG 2010*. Kuala Lumpur.

Tan, C., Ma, M., Kuang, H. (2017). Spatial-Temporal Characteristics and Climatic Responses of Water Level Fluctuations of Global Major Lakes from 2002 to 2010. *Remote Sensing*. 9(2):150. https://doi.org/10.3390/rs9020150

Tan, J., Yu, D., Li, Q., Tan, X., Zhou, W. (2020). Spatial relationship between land-use/land-cover change and land surface temperature in the Dongting Lake area, China. *Sci Rep*, 10, 9245. https://doi.org/10.1038/s41598-020-66168-6

Tang, F. and Xu, H. (2016). A Study on the quantitative relationship between impervious surface and land surface temperature based on remote sensing technology. *4th International Workshop on Earth Observation and Remote Sensing Applications (EORSA)*, Guangzhou, 2016, pp. 368-372, doi: 10.1109/EORSA.2016.7552831.

Tozer L. (2018). Urban climate change and sustainability planning: an analysis of sustainability and climate change discourses in local government plans in Canada. *Journal of Environmental Planning and Management*, 61:1, 176-194, DOI: 10.1080/09640568.2017.1297699.

Tran, D.X., Pla, F., Carmona, P.L., Myint, S.W., Caetano, M., & Kieua, P.V. (2017). Characterizing the relationship between land use land cover change and land surface temperature. *ISPRS Journal of Photogrammetry and Remote Sensing*, 124, 119–132.

Tsoka, S., Tsikaloudaki, K., Theodosiou, T., Bikas, D. (2020). Urban Warming and Cities' Microclimates: Investigation Methods and Mitigation Strategies—A Review. *Energies*, 13, 1414.

Ujang, U., Azri, S., Zahir, M., Abdul Rahman, A., Choon, T. L. (2018). Urban Heat Island Micro-Mapping via 3D City Model. *Int. Arch. Photogramm. Remote Sens. Spatial Inf. Sci.*, XLII-4/W10, 201–207, https://doi.org/10.5194/isprs-archives-XLII-4-W10-201-2018.

Unal, Y.S., Tan, E. & Mentes, S.S. (2013). Summer heat waves over western Turkey between 1965 and 2006. *Theor Appl Climatol,* 112, 339–350. https://doi.org/10.1007/s00704-012-0704-0

Urban, M, Eberle, J, Hüttich, C, Schmullius, C, Herold, M. (2013). Comparison of Satellite-Derived Land Surface Temperature and Air Temperature from Meteorological Stations on the Pan-Arctic Scale. *Remote Sensing*, 5(5):2348-2367. https://doi.org/10.3390/rs5052348

U.S. Geological Survey (2020). Data Management and Information Distribution (DMID). Last accessed September 11, 2020 at URL https://earthexplorer.usgs.gov.

Vidrih, B., Medved, S. (2013). Urban Forestry & Urban Greening Multiparametric Model of Urban Park Cooling Island. *Urban Forestry & Urban Greening*, 12, 220–229.

Wei, J., Huang, B., Sun, L., Zhang, Z., Wang, L., & Bilal, M. (2017). A simple and universal aerosol retrieval algorithm for Landsat series images over complex surfaces. *Journal of Geophysical Research: Atmospheres*, 122, 13,338–13,355. https://doi.org/10.1002/ 2017JD026922

Weng, Q. (2001). A remote sensing – GIS Evaluation of Urban Expansion and Its Impact on Surface Temperature in the Zhujiang Delta , China. *International Journal of Remote Sensing*, 22(10), 1999–2014.

Weng, Q., Yang, S. (2004). Managing the adverse thermal effects of urban development in a densely populated Chinese city. *Journal of Environmental Management*, 70(2), 145–156.

Willett, K.M., Sherwood, S. (2012). Exceedance of heat index thresholds for 15 regions under a warming climate using the wet-bulb globe temperature. *International Journal of Climatology*, 32(2), 161–177.

Williams, V. J., Davis, C. (2007). A case study of urban heat islands in the Carolinas. *Environmental Hazards*, 7(4):353-359, DOI:10.1016/j.envhaz.2007.09.005.

Wulder, M. A., Thomas, Loveland, R. D., Roy, P., Crawford C. J., Masek, J. G., Woodcock, C. E., Allen, R. G., Martha C. Anderson, Alan S. Belward, Warren B. Cohen, John Dwyer, Angela Erb, Feng Gao, Patrick Griffiths, Dennis Helder, Txomin Hermosilla, James D. Hipple, Patrick Hostert, M. Joseph Hughes, Justin Huntington, David M. Johnson, Robert Kennedy, Ayse Kilic, Zhan Li, Leo Lymburner, Joel McCorkel, Nima Pahlevan, Theodore A. Scambos, Crystal Schaaf, John R. Schott, Yongwei Sheng, James Storey, Eric Vermote, James Vogelmann, Joanne C. White, Randolph H. Wynne, Zhu, Z. (2019). Current status of Landsat program, science, and applications. *Remote Sensing of Environment*, Volume 225, Pages 127-147. ISSN 0034-4257. https://doi.org/10.1016/j.rse.2019.02.015.

Xiao, Rong-bo, Ouyang, Zhi-yun, Zheng, H., Li, Wei-feng, Schienke, E. W, Wang, Xiao-ke (2007). Spatial pattern of impervious surfaces and their impacts on land surface temperature in Beijing, China. *Journal of Environmental Sciences*, Volume 19, Issue 2, Pages 250-256, ISSN 1001-0742, https://doi.org/10.1016/S1001-0742(07)60041-2.

Yan, H., Wang, X., Hao, P., & Dong, L. (2012). Study on the Microclimatic Characteristics and Human Comfort of Park Plant Communities in Summer. *Procedia Environmental Sciences*. 13(2011), 755 765.doi:10.1016/j.proenv.2012.01.069

Yu, Q., Ji, W., Pu, R., Landry, S., Acheampong, M., O' Neil-Dunne, J., Ren, Z., Tanim, S. H. (2020). A preliminary exploration of the cooling effect of tree shade in urban landscapes. *International Journal of Applied Earth Observation and Geoinformation*, Volume 92. ISSN 0303-2434, https://doi.org/10.1016/j.jag.2020.102161.

Yucekaya, A. (2018). An Analysis For Industrial Development In Turkey. I: Distribution of The Largest Companies. *Journal of Engineering Technology and Applied Sciences*. 3 (1), 83-105.

Young, N. E., Anderson, R. S., Chignell, S. M., Vorster, A. G., Lawrence, R., Evangelista, P. H. (2017). A survival guide to Landsat preprocessing. *Ecology,* 98 4: 920-932.

Zhang, Y. (2006). Land surface temperature retrieval from CBERS-02 IRMSS thermal infrared data and its applications in quantitative analysis of urban heat island effect. *Journal of Remote Sensing*, 10, 789–797.

Zhang, Y., Pena-Arancibia, J.L., McVicar, T.R., Chiew, F.H.S., Vaze, J., Liu, C., Lu, X., Zheng, H., Wang, Y., Liu, Y.Y., et al. (2016b). Multi-decadal trends in global terrestrial evapotranspiration and its components. *Sci. Rep*. 6, 19124.

Zhang, Z., He, G., Wang, M., Long, T., Wang, G., Zhang, X., & Jiao, W. (2016a). Towards an operational method for land surface temperature retrieval from Landsat 8 data. *Remote Sensing Letters*, 7(3), 279–288.

Zhang, Z., He, G., Wang, X. (2010). A practical DOS model-based atmospheric correction algorithm. *International Journal of Remote Sensing*, 31:11, 2837-2852, DOI: 10.1080/01431160903124682

Zhao, H.M., Chen, X.L. (2005). Use of Normalized Difference Bareness Index in Quickly Mapping Bare Areas from TM/ETM+. *Proceedings of the 2005 IEEE International Geoscience and Remote Sensing Symposium*. Seoul, Korea, 29–29 July 2005; Volume 3, pp. 1666–1668.

Zhao H., Tan J., Ren Z., Wang Z. (2020). Spatiotemporal Characteristics of Urban Surface Temperature and Its Relationship with Landscape Metrics and Vegetation Cover in Rapid Urbanization Region. *Complexity*, vol. 2020, Article ID 7892362, 12 pages. https://doi.org/10.1155/2020/7892362

1806 Zhao, L., Oleson, K., Bou-Zeid, E., Krayenhoff, E. S., Bray, A., Zhu, Q., Zheng, Z., Chen, C., Oppenheimer, M. (2021).
1807 Global multi-model projections of local urban climates. *Nat. Clim. Chang*. 11, 152–157. https://doi.org/10.1038/s41558-
1808 020-00958-8
1809 Zhong, L., Gong, P., Biging, G.S. (2014). Efficient corn and soybean mapping with temporal extendibility: A multi-year
1810 experiment using Landsat imagery. *Remote Sens. Environ*. 140, 1–13.
1811 Zhou, D., Xiao, J., Bonafoni, S., Berger, C., Deilami, K., Zhou, Y., Frolking, S., Yao, R., Qiao, Z., Sobrino, J.A. (2019).
1812 Satellite Remote Sensing of Surface Urban Heat Islands: Progress, Challenges, and Perspectives. *Remote Sensing*.
1813 11(1):48. https://doi.org/10.3390/rs11010048
1814 Zhou, J., Hu, D., Weng, Q. (2010). Analysis of surface radiation budget during the summer and winter in the metropolitan
1815 area of Beijing, China. *J. Appl. Rem. Sens*. 4(1) 04351. https://doi.org/10.1117/1.3374329
1816 Zhou, W., Qian, Y., Li, X., Li, W., & Han, L. (2014). Relationships between land cover and the surface urban heat island:
1817 Seasonal variability and effects of spatial and thematic resolution of land cover data on predicting land surface
1818 temperatures. *Landscape Ecology*, 29, 153–167.
1819 Zoran, M. A., Zoran, L. F. V. (2005). Mapping of dispersion of urban air pollution using remote sensing and in-situ
1820 monitoring data. Proc. SPIE 5979, *Remote Sensing of Clouds and the Atmosphere X*, 597914 (1 November
1821 2005). https://doi.org/10.1117/12.627775
1822 Zurina, M., Hukil, S. (2012). Appraising Good Governance in Malaysia Based on Sustainable Development Values. *Journal*
1823 *of ASIAN Behavioral Studies: Sustainability Science and Management*, 7(2), 247–253. doi: ISSN: 1823-8556.

Figures

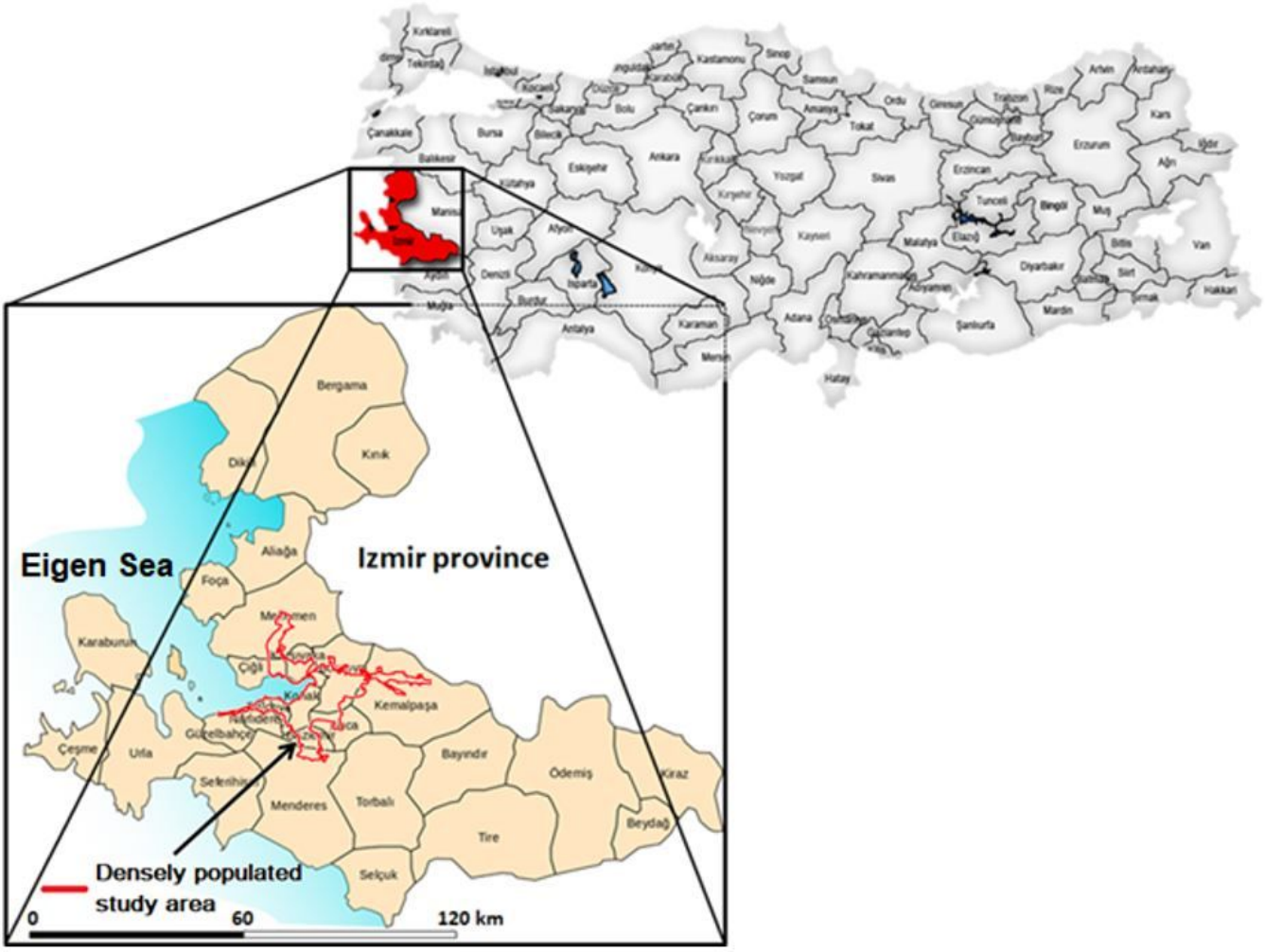

Figure 1

Izmir province and densely populated central metropolitan city part (study area is in red boundary). Note: The designations employed and the presentation of the material on this map do not imply the expression of any opinion whatsoever on the part of Research Square concerning the legal status of any country, territory, city or area or of its authorities, or concerning the delimitation of its frontiers or boundaries. This map has been provided by the authors.

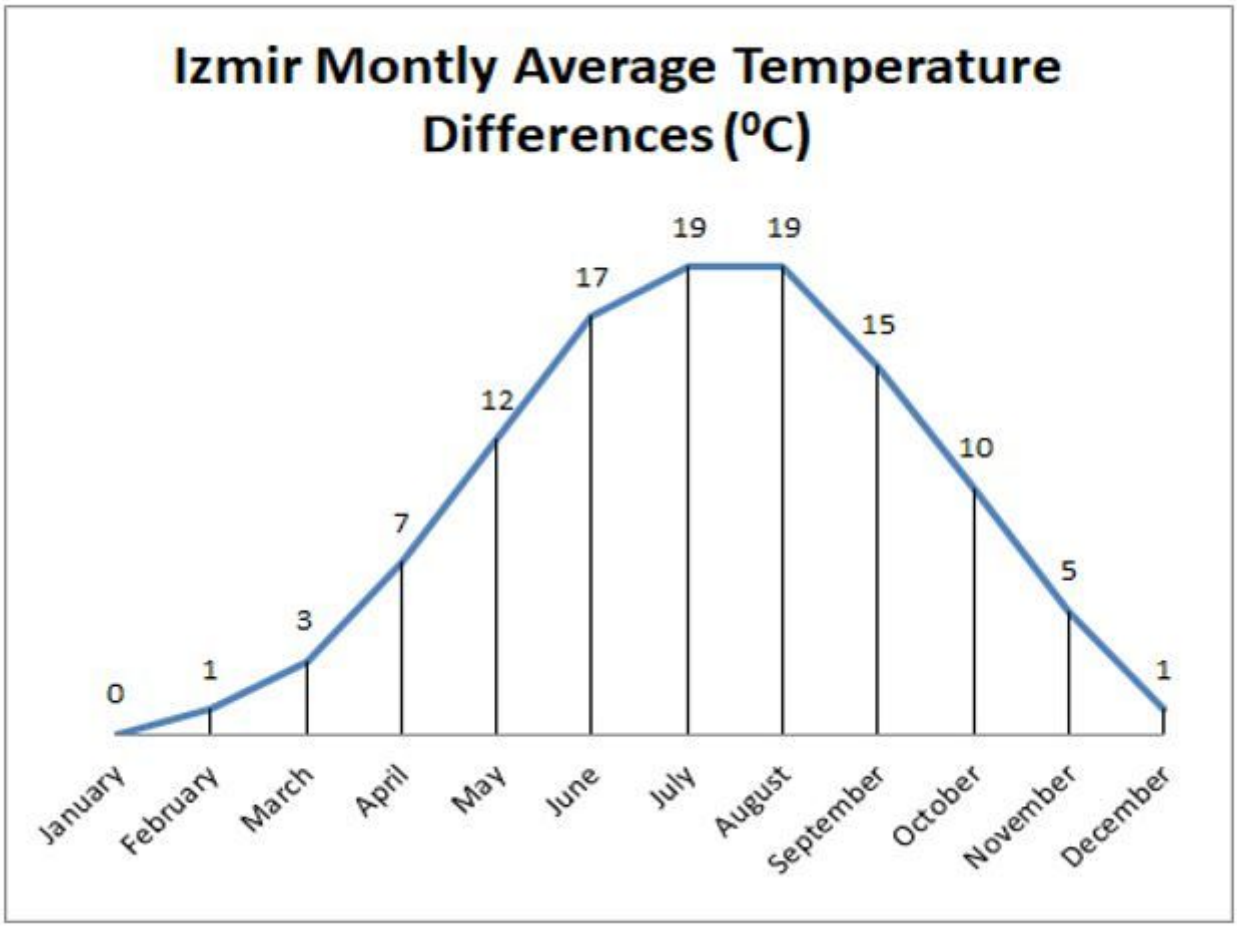

Figure 2

Long term monthly average temperature differences for the city of Izmir w.r.t the annually minimum average temperature.

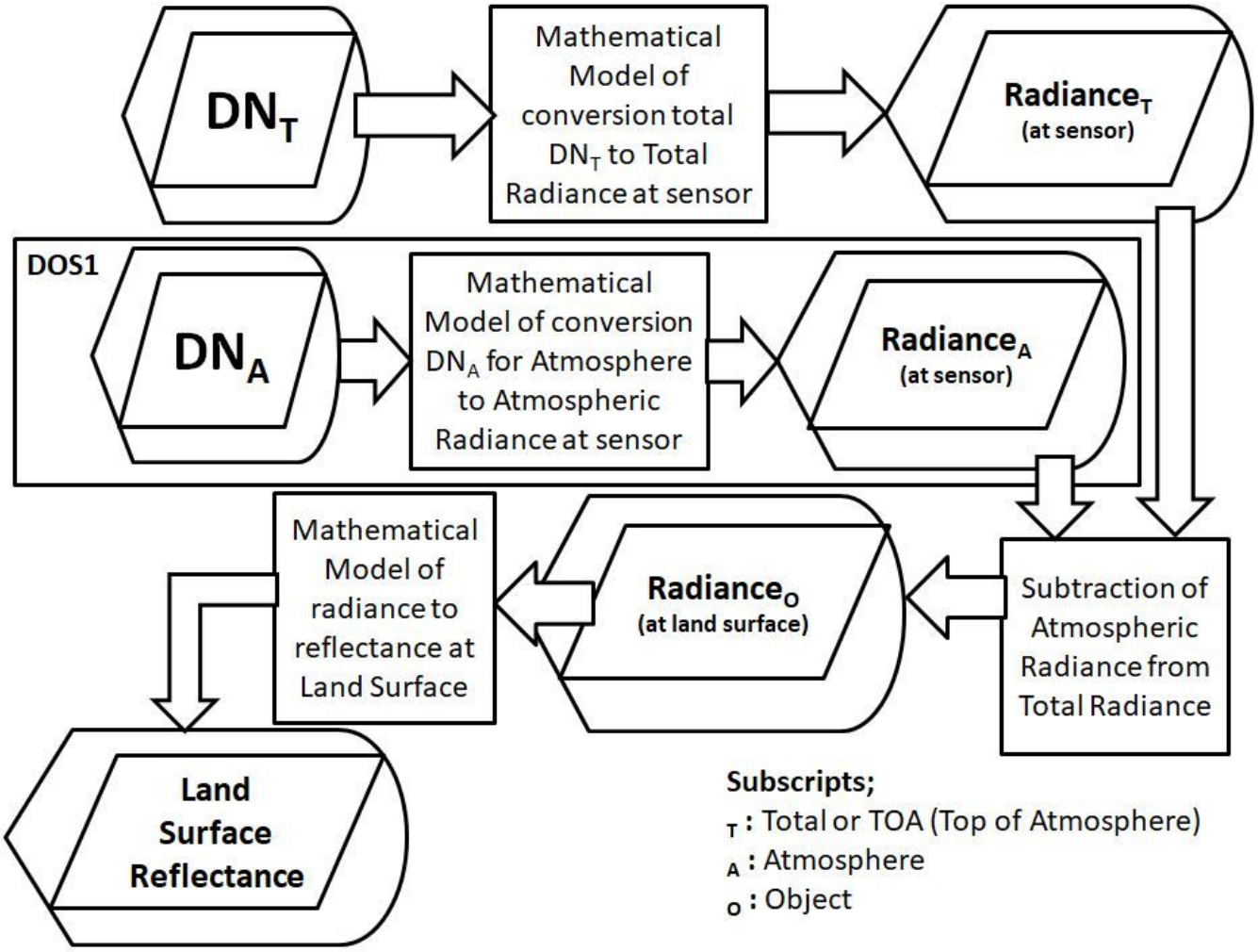

Figure 3

Conversion algorithm DN to Radiance and Radiance to Land Surface Reflectance.

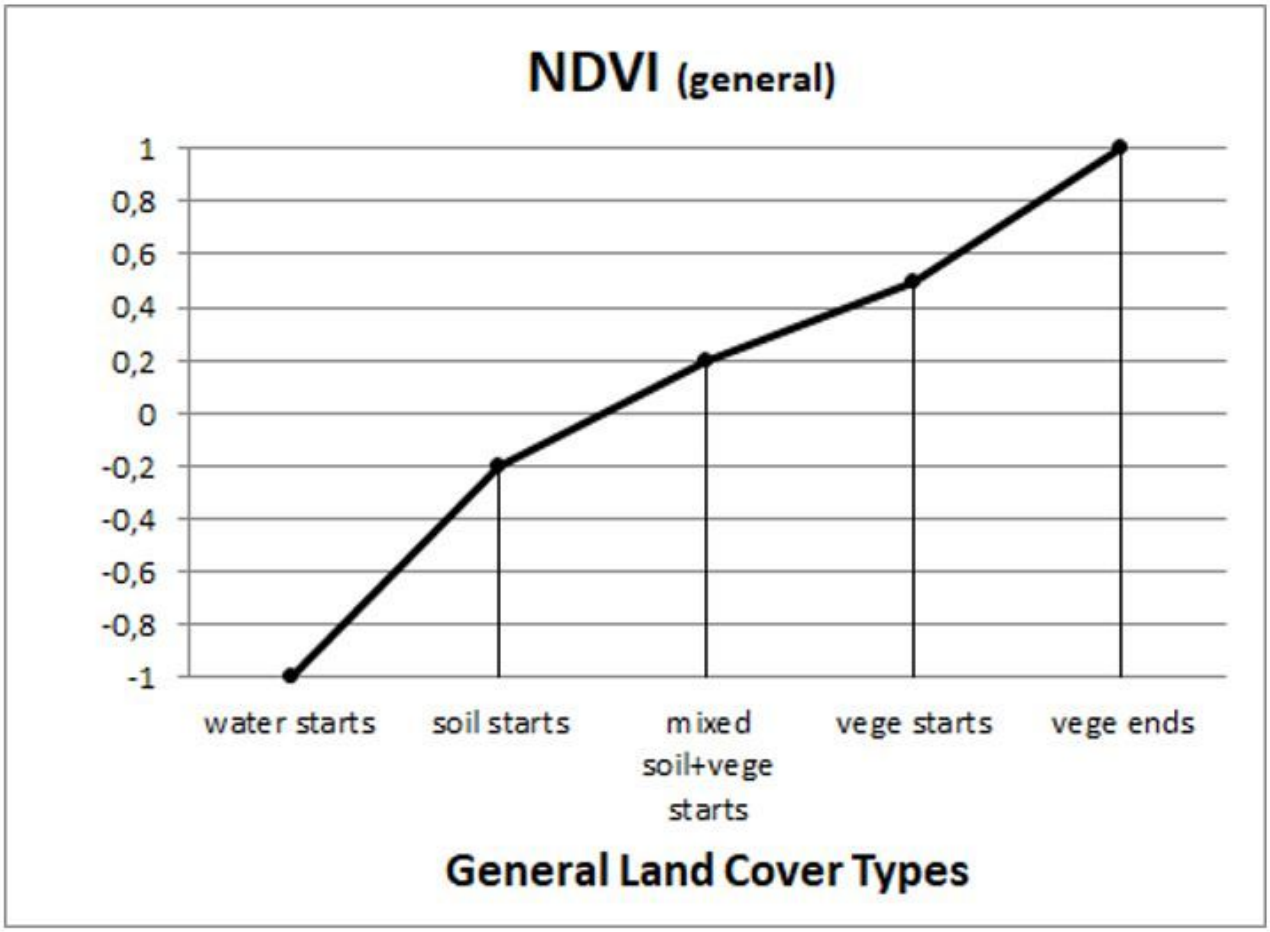

Figure 4

General NDVI values for general land cover types.

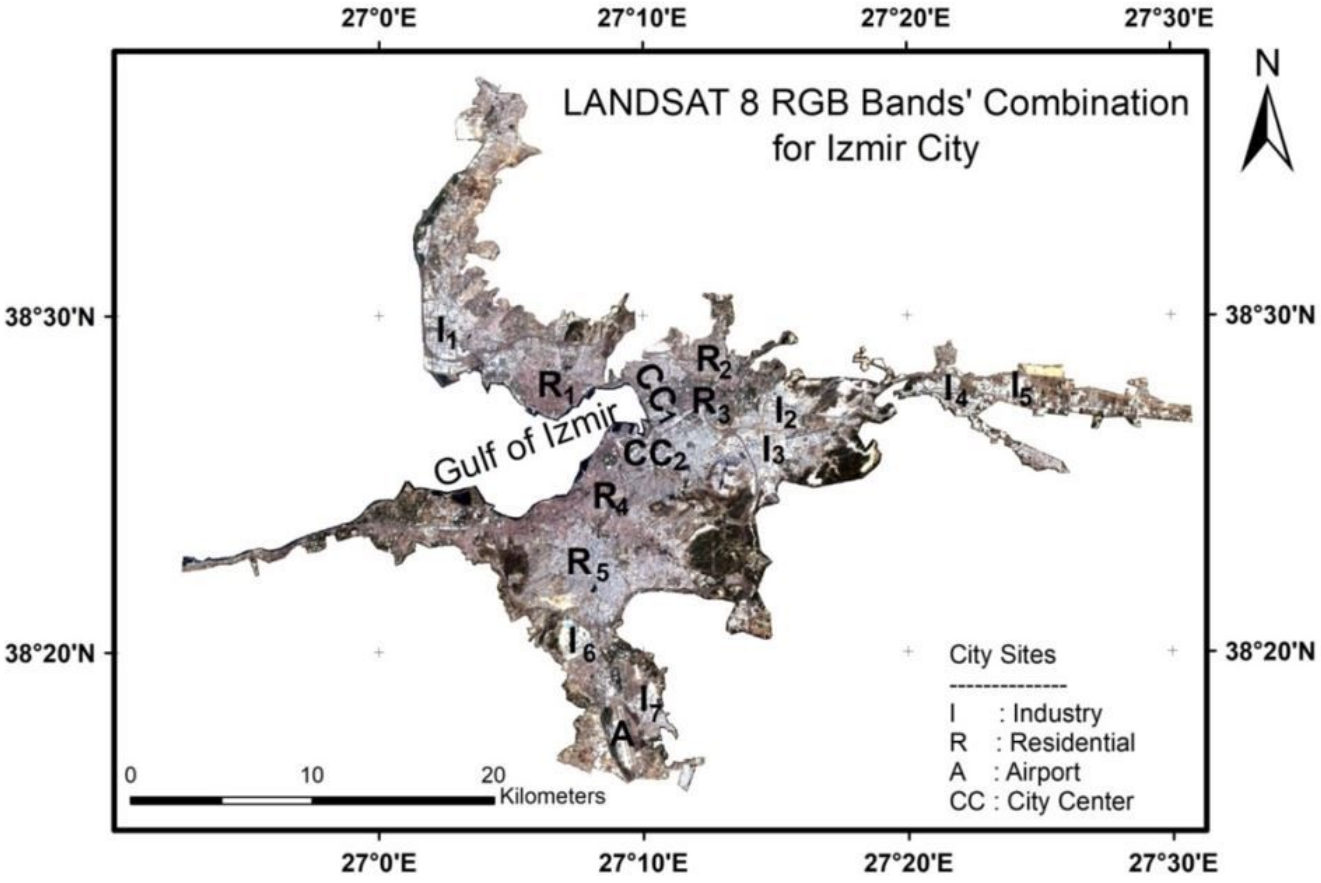

Figure 5

City of Izmir, urban areas distribution by RGB true color LANDSAT images Note: The designations employed and the presentation of the material on this map do not imply the expression of any opinion whatsoever on the part of Research Square concerning the legal status of any country, territory, city or area or of its authorities, or concerning the delimitation of its frontiers or boundaries. This map has been provided by the authors.

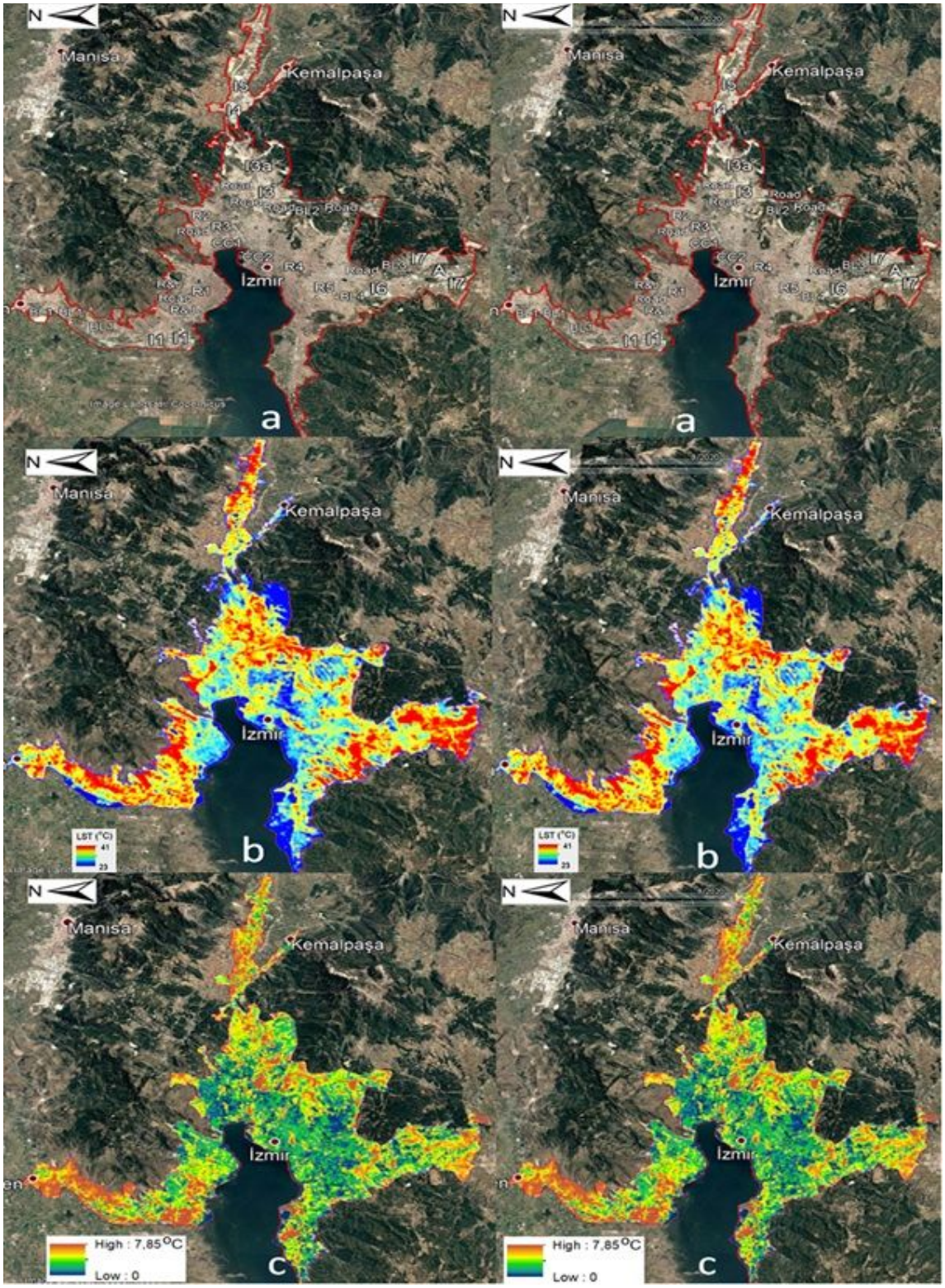

Figure 6

3D representation of study area (red curved line) (a) with some urban details, and (b) for the Simulated Single Image (SSI) LST distribution and (c) for the distribution of SSI Local LST differences in the city of Izmir for the month August as a summary of 32 years' time span between 1985 and 2018 by using stereo display techniques with embedded illustrations on Google Earth captured images (use converging eye lines' method to see the 3D illustrations above). Note: The designations employed and the presentation of

the material on this map do not imply the expression of any opinion whatsoever on the part of Research Square concerning the legal status of any country, territory, city or area or of its authorities, or concerning the delimitation of its frontiers or boundaries. This map has been provided by the authors.

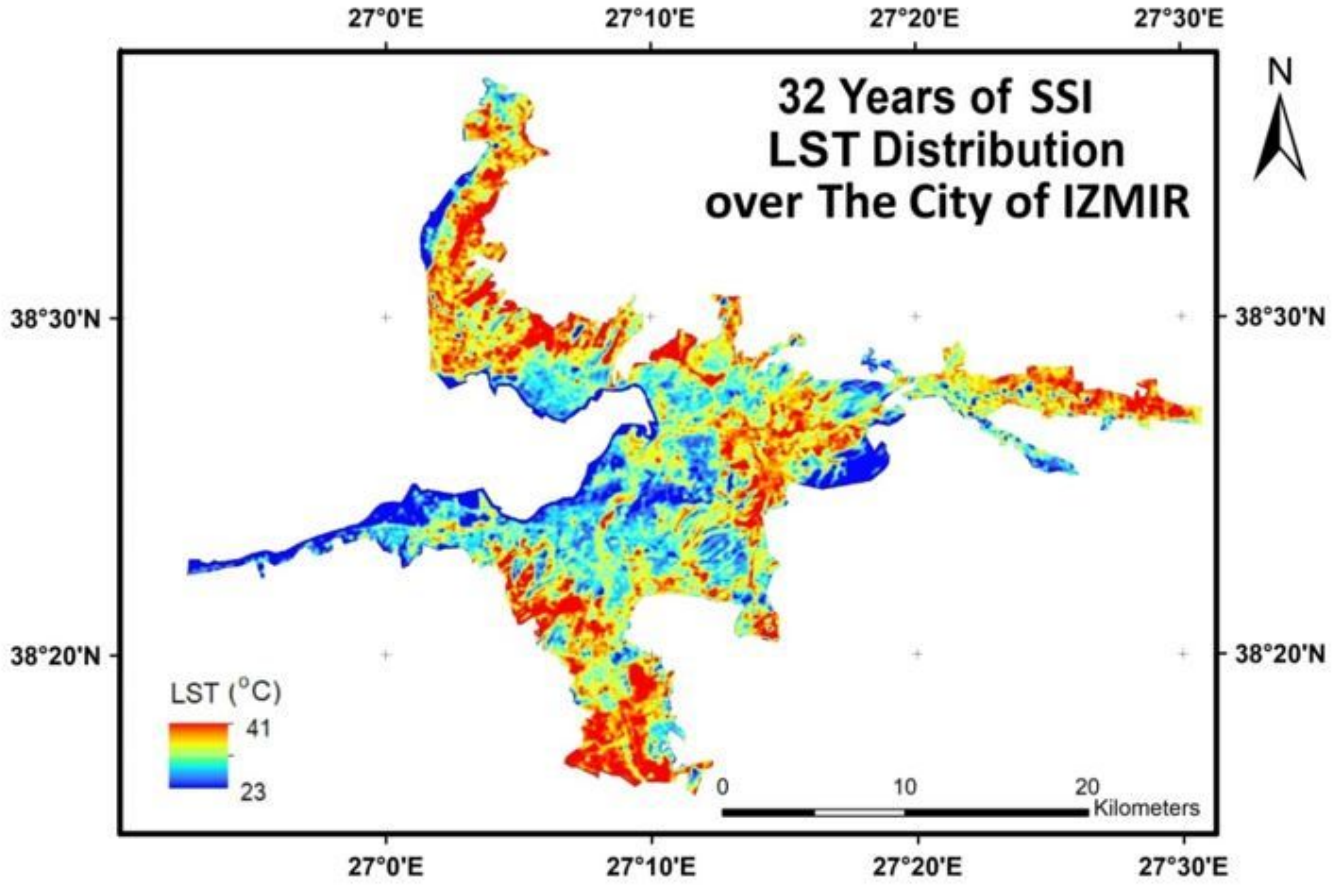

Figure 7

32 years of Simulated Single Image (SSI) LST distribution for the month August over the city of Izmir between 1985 and 2018 Note: The designations employed and the presentation of the material on this map do not imply the expression of any opinion whatsoever on the part of Research Square concerning the legal status of any country, territory, city or area or of its authorities, or concerning the delimitation of its frontiers or boundaries. This map has been provided by the authors.

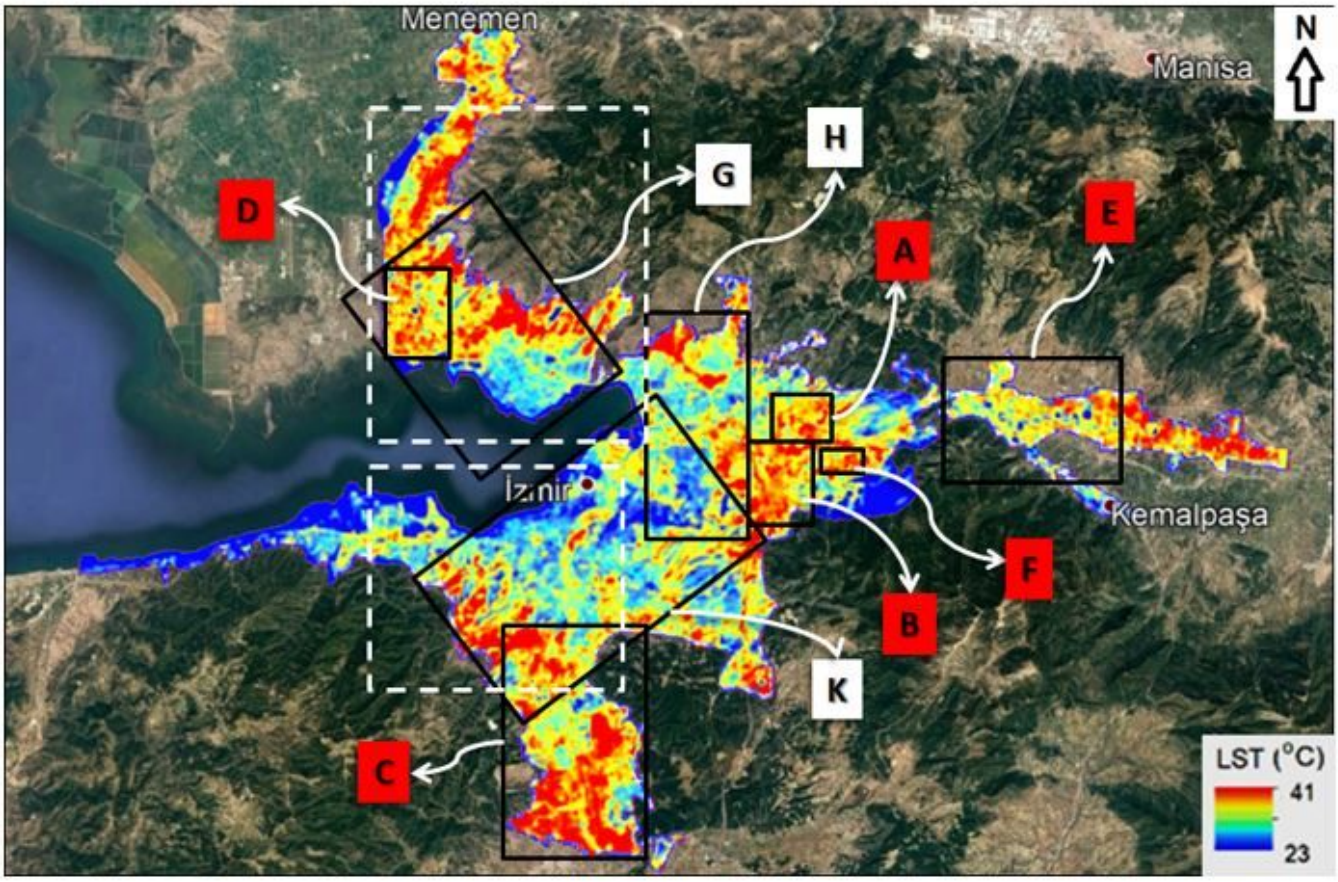

Figure 8

Subsections of the project covering the different urban zones in the city w.r.t. the LST distribution. Note: The designations employed and the presentation of the material on this map do not imply the expression of any opinion whatsoever on the part of Research Square concerning the legal status of any country, territory, city or area or of its authorities, or concerning the delimitation of its frontiers or boundaries. This map has been provided by the authors.

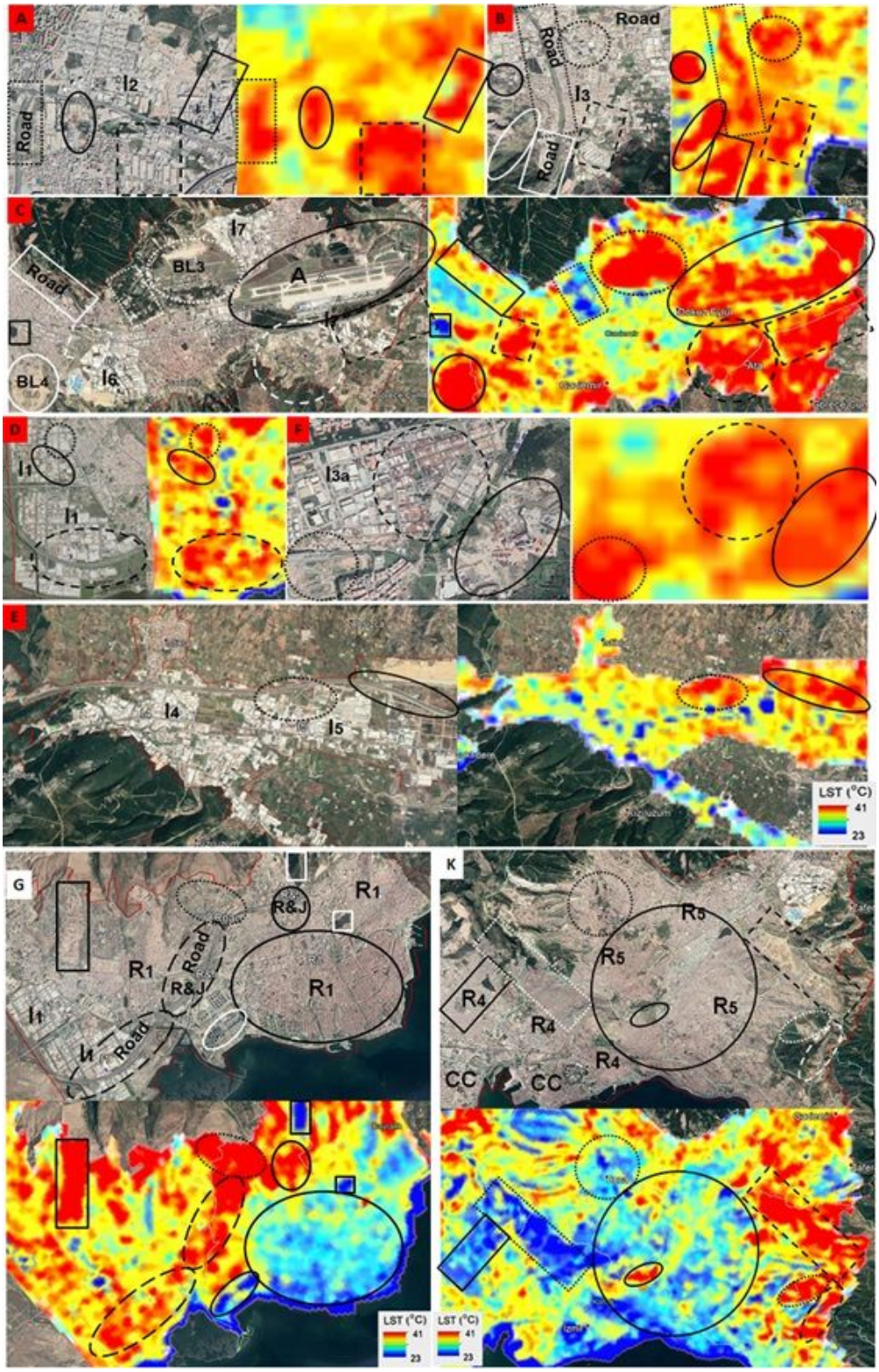

Figure 9

Representation of detailed subsections covering areas with specific urban features shown in different geometrical shapes for the comparison with specific LST distributions in the city. Note: The designations employed and the presentation of the material on this map do not imply the expression of any opinion whatsoever on the part of Research Square concerning the legal status of any country, territory, city or

area or of its authorities, or concerning the delimitation of its frontiers or boundaries. This map has been provided by the authors.

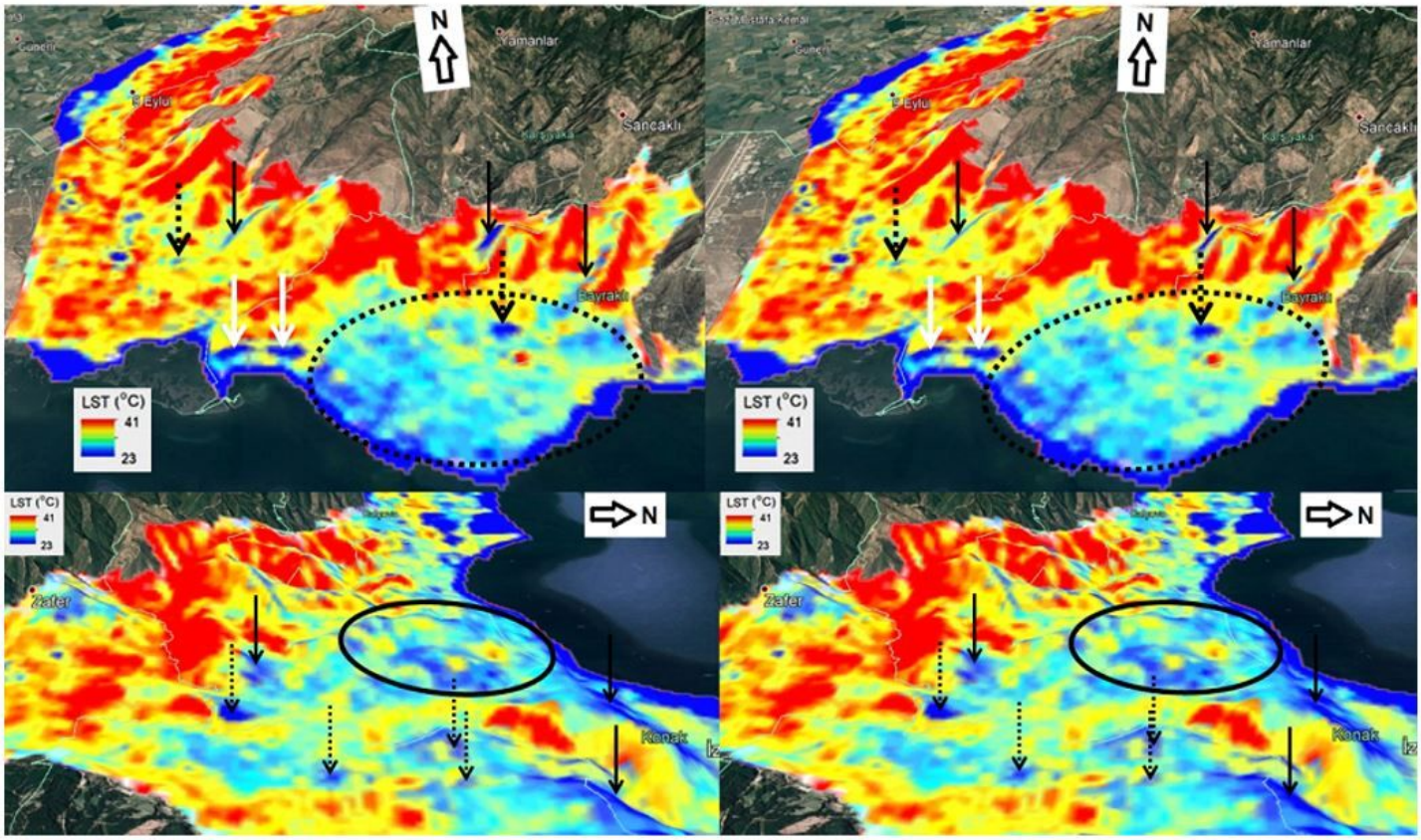

Figure 10

3D illustrations of SSI-LST distribution over the city of Izmir with cool sites marked with arrows and ellipses. Note: The designations employed and the presentation of the material on this map do not imply the expression of any opinion whatsoever on the part of Research Square concerning the legal status of any country, territory, city or area or of its authorities, or concerning the delimitation of its frontiers or boundaries. This map has been provided by the authors.

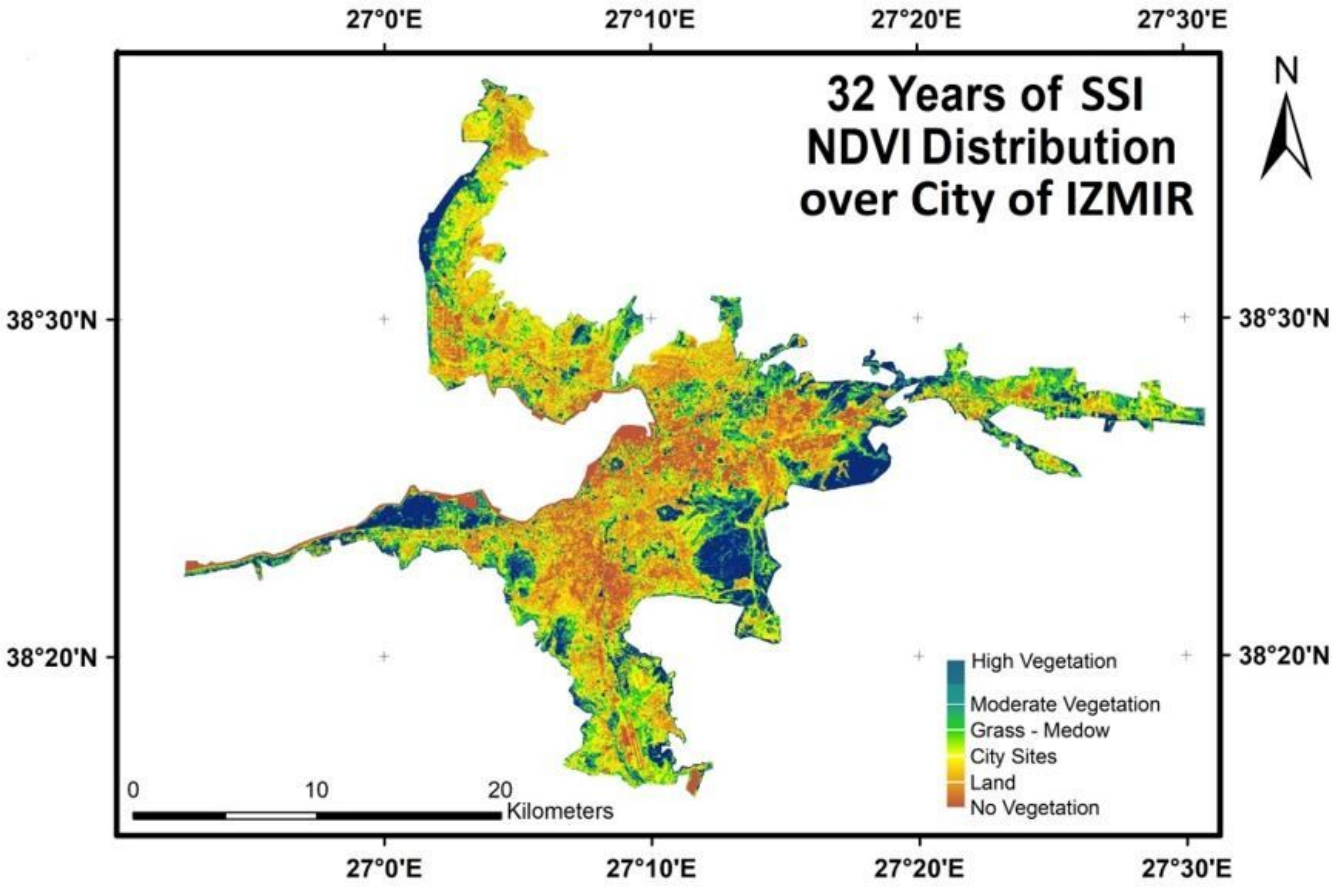

Figure 11

32 years of Simulated Single Image (SSI) NDVI distribution for the month August over the city of Izmir between 1985 and 2018 Note: The designations employed and the presentation of the material on this map do not imply the expression of any opinion whatsoever on the part of Research Square concerning the legal status of any country, territory, city or area or of its authorities, or concerning the delimitation of its frontiers or boundaries. This map has been provided by the authors.

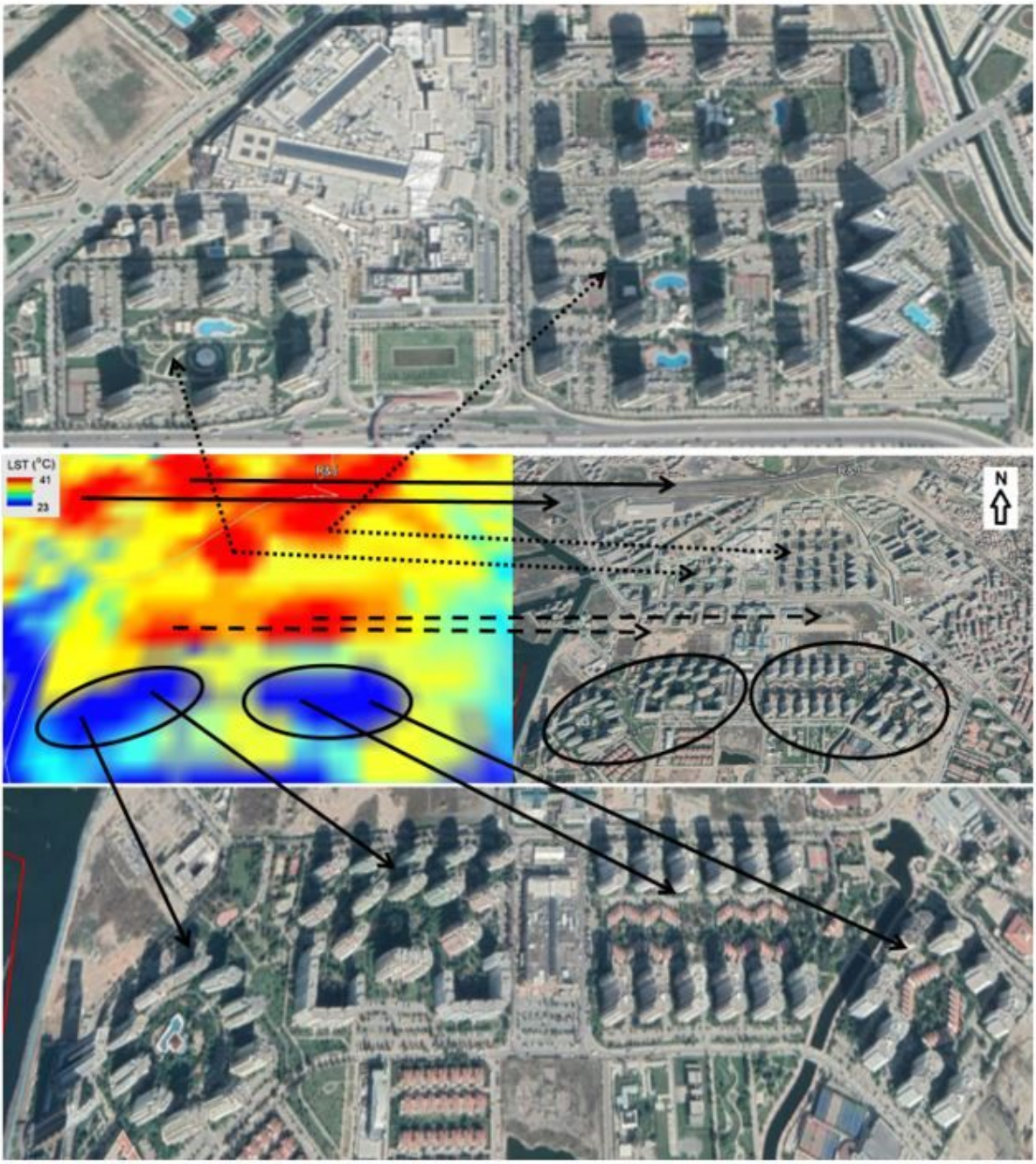

Figure 12

Unique formation of high rise dwelling apartments with specific natural recreation areas for cool site creation in cities. Note: The designations employed and the presentation of the material on this map do not imply the expression of any opinion whatsoever on the part of Research Square concerning the legal status of any country, territory, city or area or of its authorities, or concerning the delimitation of its frontiers or boundaries. This map has been provided by the authors.

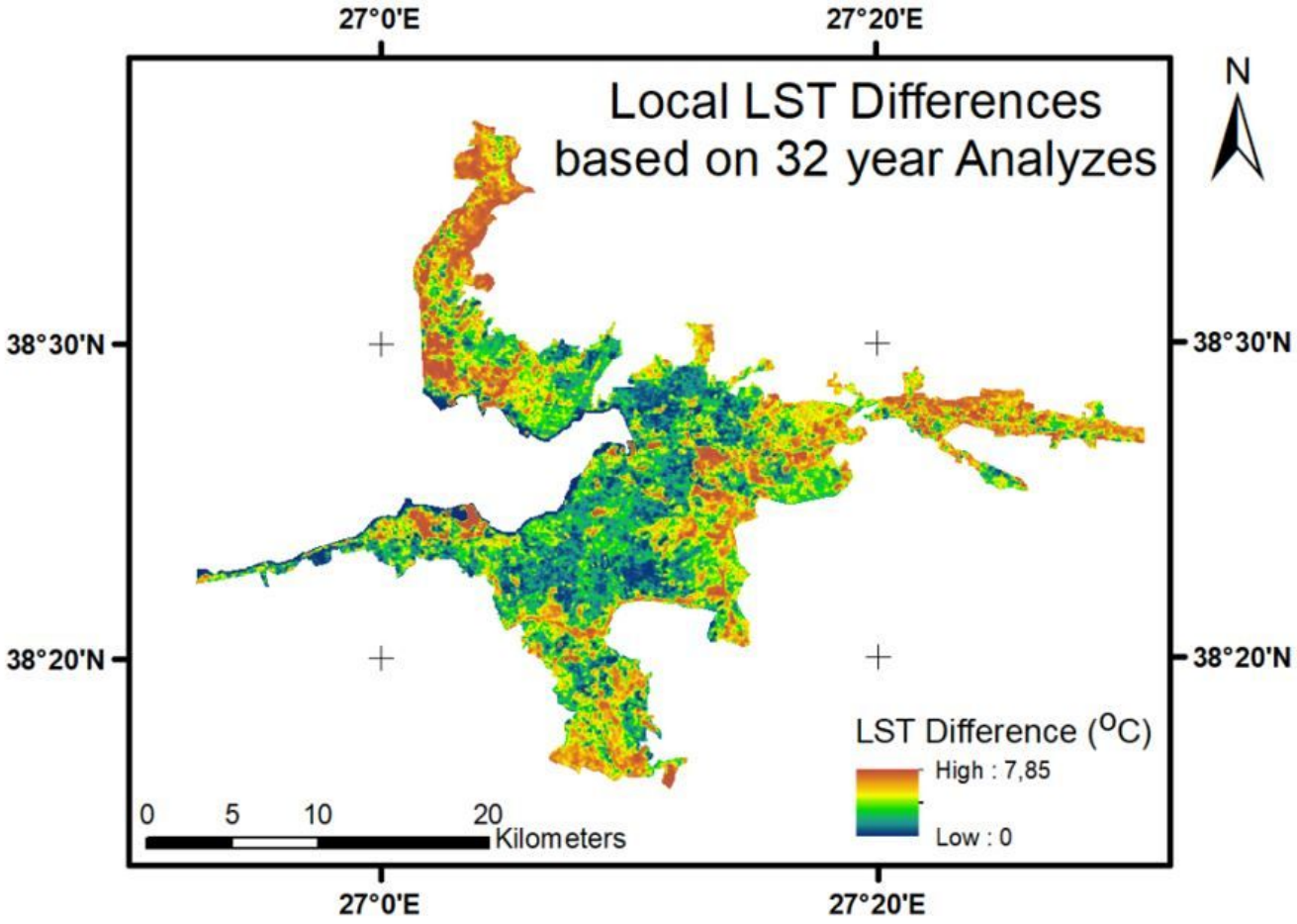

Figure 13

Distribution of Local LST Differences for the entire city of Izmir. Note: The designations employed and the presentation of the material on this map do not imply the expression of any opinion whatsoever on the part of Research Square concerning the legal status of any country, territory, city or area or of its authorities, or concerning the delimitation of its frontiers or boundaries. This map has been provided by the authors.